Unconventional Resources 11 (2026) 100337

Contents lists available at ScienceDirect

Unconventional Resources

journal homepage: www.keaipublishing.com/en/journals/unconventional-resources/

Assessment of risk, safety, hazard, and economic challenges of CCS pipeline and wellbore implementation: Exploring emerging achievements in 2010–2025

Aprianur Fajri [a,b,c], Aditya Rio Prabowo [a,*], Nurul Muhayat [a], Ristiyanto Adiputra [d,**], Sören Ehlers [e,f], Moritz Braun [f]

[a] Department of Mechanical Engineering, Universitas Sebelas Maret, Surakarta, Indonesia
[b] Laboratory of Design and Computational Mechanics, Faculty of Engineering, Universitas Sebelas Maret, Surakarta, Indonesia
[c] Department of Manufacturing Engineering Technology, Akademi Inovasi Indonesia, Salatiga, Indonesia
[d] Research Center for Hydrodynamics Technology, National Research and Innovation Agency (BRIN), Surabaya, Indonesia
[e] Institute for Ship Structural Design and Analysis, Hamburg University of Technology, Hamburg, Germany
[f] Institute of Maritime Energy Systems, German Aerospace Center (DLR), Geesthacht, Germany

ARTICLE INFO

Keywords:
Carbon capture and storage
CCS risk and safety analysis
CCS hazard identification
CCS economic evaluation
CO_2 transportation and storage

ABSTRACT

Carbon capture and storage (CCS) is widely regarded as a strategic mitigation option for reducing CO_2 emissions from fossil fuel–based industries and the energy sector, in line with global efforts to limit the rise in average temperature to below 1.5 °C. Despite its potential to deliver substantial carbon reductions, CCS deployment remains challenged by a range of technical, economic, and operational risks that must be systematically addressed. These risks arise across nearly all stages of the CCS value chain, including CO_2 capture, transportation, and storage. Over the past decade, research on CCS has expanded rapidly, and several review studies have attempted to map emerging research trends in this field. However, existing reviews have generally concentrated on individual components of CCS technologies, such as carbon capture processes or the safety of geological storage. These studies have not adequately examined the interdependencies across the entire system. In contrast, the present study provides a more comprehensive perspective by assessing the whole CCS chain, thereby offering a systemic understanding of its performance and implementation challenges. The novelty of this work lies in its integrative approach, combining risk and safety analysis, hazard identification, and economic evaluation, with particular emphasis on the transportation and storage stages. In addition, recent advances involving modern technologies aimed at enhancing CCS safety and sustainability are discussed to highlight potential directions for future research.

1. Introduction

Global energy demand continues to increase in line with population growth and the expansion of the global economy [1]. To date, the fulfillment of energy needs remains predominantly dependent on fossil resources such as coal, petroleum, and natural gas (Fig. 1a). This reliance on fossil-based energy sources is closely associated with emissions, particularly carbon dioxide (CO_2) produced during combustion [2,3]. In 2024, annual CO_2 emissions from the energy sector exceeded 35 $GtCO_2e$ (Fig. 1b), making it the most significant contributor to total global carbon emissions. The high level of carbon emissions will directly trigger global warming and extreme climate change [4,5]. Conversely, efforts to meet energy demand through cleaner sources continue to face substantial challenges. The development of renewable energy requires a high initial investment and is constrained by supply stability issues, thereby limiting its large-scale deployment [6,7].

One strategic approach emerging to address these challenges is the implementation of carbon capture and storage (CCS) technologies. These technologies can capture CO_2 emissions from primary sources and permanently store them in isolated geological formations. CCS holds

Peer review under the responsibility of KeAi Communications Co., Ltd.
* Corresponding author.
** Corresponding author.
E-mail addresses: aditya@ft.uns.ac.id (A.R. Prabowo), ristiyanto.adiputra@brin.go.id (R. Adiputra).

https://doi.org/10.1016/j.uncres.2026.100337
Received 15 June 2025; Received in revised form 8 February 2026; Accepted 8 February 2026
Available online 12 February 2026

significant potential to reduce CO_2 emissions originating from high-emission fossil fuel use while simultaneously supporting the transition toward a cleaner energy system [9–11]. Beyond the energy sector, the transition toward low-carbon and green industries is also critical in other sectors such as metallurgy, chemicals, transportation, and construction materials, which collectively represent the second-largest source of global CO_2 emissions [12]. The integration of CCS with the high-emission sector has therefore become increasingly vital to accelerate progress toward sustainable development targets and global carbon reduction goals. If widely implemented, CCS is projected to capture more than seven gigatons of CO_2 per year by 2050. This projection aligns with the Net Zero Emission (NZE) objective and the commitment to limit global temperature rise to below 1.5 °C, as stipulated in the Paris Agreement [13–16].

Despite its promising potential, CCS technologies still face several significant barriers. The CCS system requires sophisticated infrastructure to ensure the safe and efficient capture, transport, and storage of CO_2. Previous studies have explored various related topics, including carbon utilization [17], cluster and hub strategies [18], storage strategies [19,20], and the global adoption dynamics of CCS [21]. However, technical aspects related to safety and economic risks remain relatively underexplored, despite their crucial role in determining the long-term sustainability of CCS technologies. This article aims to provide a comprehensive review of the technical and economic challenges in CCS implementation. From a financial perspective, the CO_2 capture stage represents the highest risk component due to its technological complexity and associated highest costs. Meanwhile, transportation and storage systems are critical elements from a safety standpoint, given the potential risks of operational failures, such as gas leakage or infrastructure damage, that could endanger human health and cause environmental contamination.

2. Overview of CCS technologies and associated risks

CCS technologies represent a transformative solution for reducing carbon emissions, particularly within the heavy industry and energy sectors. The implementation of CCS technologies is accompanied by both technical and non-technical risks that must be carefully considered. A comprehensive approach to understanding and managing these risks is crucial for the optimal deployment of CCS. This section provides an overview of CCS risk assessment and recent advancements, encompassing the entire process chain from CO_2 capture to post-storage stages, as shown in Fig. 2.

The CO_2 capture can be carried out using various methods, depending on the characteristics of the emission source and specific operational requirements. The captured CO_2 is subsequently purified to remove water and other impurities. This purification step is crucial, as contaminants can alter the thermodynamic and chemical properties of CO_2, making phase transitions difficult to control and potentially increasing its corrosivity [22–24]. Once high purity is achieved, the CO_2 is transported to designated storage sites via pipeline networks, land-based transport, or marine vessels. The CO_2 is then stored in secure geological formations, accompanied by rigorous monitoring systems designed to detect potential leakage and subsurface migration in real time.

2.1. Capturing method from CO_2 source

The CO_2 capture is one of the most critical stages in CCS technologies, as it involves a complex operational cycle. Broadly, CO_2 capture processes can be categorized into two main types: direct capture from the atmosphere and capture directly from emission sources. Direct air capture, a form of carbon removal, aims to reduce the concentration of CO_2 that has already been released into the atmosphere. However, this technology suffers from inherent efficiency limitations due to the extremely low-concentration of CO_2 in ambient air, leading to significantly higher operational costs than capturing CO_2 from emission sources. Despite these limitations, direct air capture is being developed by several advanced economies as part of their efforts to achieve negative-emission targets [25].

In contrast, capture from emission sources typically associated with fuel combustion processes is being extensively developed, as it is considered more efficient and capable of capturing large volumes of CO_2 at relatively lower cost. Several methods are commonly employed in this approach (see Fig. 3), including post-combustion, pre-combustion, and oxyfuel combustion capture [26–29]. Each of these methods has demonstrated its effectiveness across various industrial applications.

Post-combustion methods rely heavily on chemical absorbents such as monoethanolamine (MEA), methyldiethanolamine (MDEA), calcium oxide, sodium hydroxide, and ionic liquids to capture CO_2 from exhaust gases [31–34]. The chemical reaction for capturing CO_2 with MEA is shown in Eq. (1), where the resulting carbamate can be hydrolyzed with water. The hydrolysis reaction to recover MEA (Eq. (2)) requires high temperatures (125–155 °C), significantly challenging energy efficiency [35].

$$2HOCH_2CH_2NH_2(aq) + CO_2(g) \rightarrow HOCH_2CH_2NH_3^+(aq) + HOCH_2CH_2NHCOO^-(aq) \quad \text{(Eq. 1)}$$

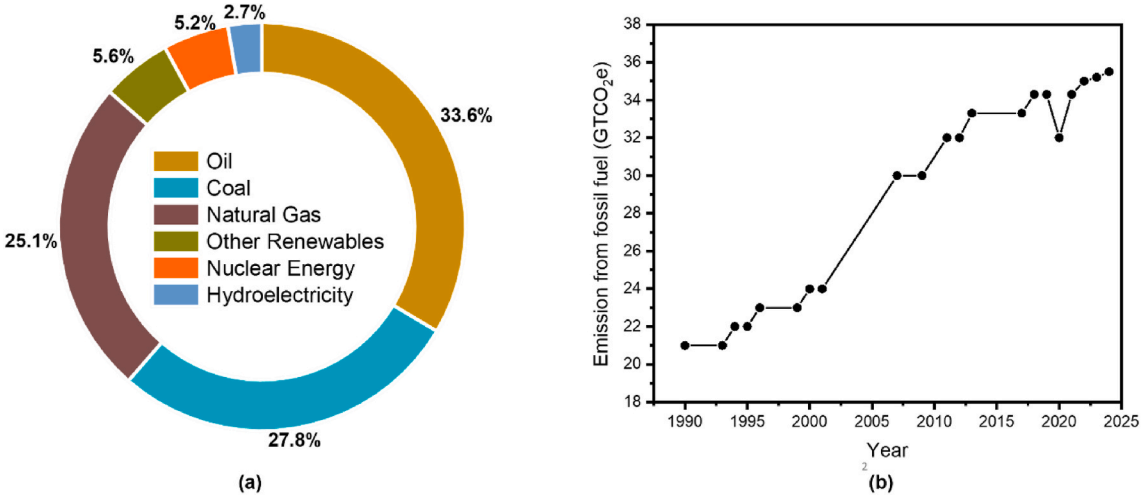

Fig. 1. (a) Global energy source in 2024; (b) Global emission from fossil fuel combustion [8].

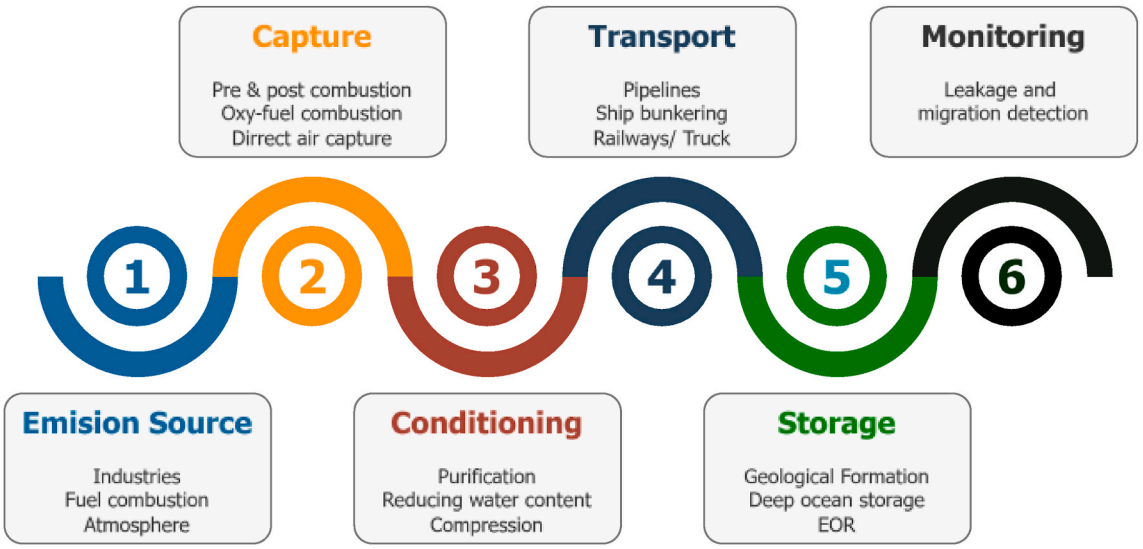

Fig. 2. Carbon capture and storage process.

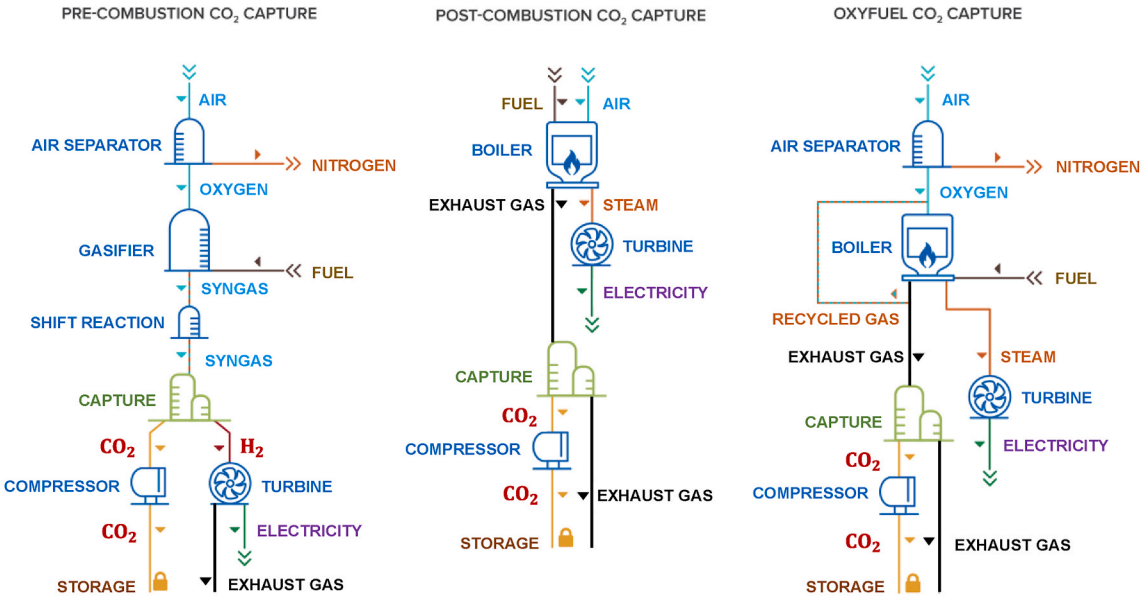

Fig. 3. CO_2 capture method: pre-combustion, post-combustion, and oxy-fuel combustion [30].

$$HOCH_2CH_2NHCOO^-(aq) + H_2O(l) \xrightarrow{\Delta} HOCH_2CH_2NH_2(aq) + CO_2(g)\uparrow + OH^-(aq) \quad \text{(Eq. 2)}$$

The use of MEA in CCS technologies has gained significant popularity in recent years. In addition to MEA, another ingredient that can be used is calcium oxide (Eq. (3)). Once captured, CO_2 and calcium oxide will form a solid calcium carbonate. To facilitate transportation to the storage site, calcium carbonate is heated to a temperature above 840 °C so that a thermal decomposition process occurs (Eq. (4)). The thermal decomposition rate of calcium carbonate ($CaCO_3$) can be calculated using Arrhenius' law (Eq. (5)) by involving an activation energy of more than 160 kJ/mol [36–38].

$$CaO(s) + CO_2(g) \rightarrow CaCO_3(s) \quad \text{(Eq. 3)}$$

$$CaCO_3(s) \xrightarrow{\Delta} CaO(s) + CO_2(g)\ (\Delta H^\circ \approx +178\ kJ/mol) \quad \text{(Eq. 4)}$$

$$k_{react} = N_{exp}\left(-\frac{E_a}{RT}\right) \quad \text{(Eq. 5)}$$

Sodium hydroxide is an alternative CO_2 absorber (Eq. (6)), where the sodium carbonate formed can be regenerated with portlandite to form calcium carbonate (Eq. (7)) [39,40].

$$2NaOH(aq) + CO_2(g) \rightarrow Na_2CO_3(aq) + H_2O(l) \quad \text{(Eq. 6)}$$

$$Na_2CO_3(aq) + Ca(OH)_2(s) \rightarrow 2NaOH(aq) + CaCO_3(s)\downarrow \quad \text{(Eq. 7)}$$

The pre-combustion capture method separates carbon from fossil fuels prior to combustion by converting the fuel into a hydrogen-rich gas stream and CO_2. For example, in a steam methane reforming (SMR) system, methane will be reacted with water vapor at high temperatures to produce syngas (Eq. (8)). Furthermore, the CO in syngas is reacted with water vapor to convert it into CO_2 and H_2 (Eq. (9)). This water-gas shift reaction increases CO_2 levels so that it is easy to separate. The hydrogen gas produced can then be used for fuel with minimal pollution.

However, this capturing method introduces impurities into the captured CO_2, which will be a problem in the next stage. The chemical reactions in the SMR process are endothermic and require nickel catalysts [41–44].

$$CH_4(g) + H_2O(g) \rightarrow CO(g) + 3H_2\ (g)\ (\Delta H^{\circ} = +206\ kJ/mol) \quad \text{(Eq. 8)}$$

$$CO(g) + H_2O(g) \rightarrow CO_2(g) + H_2(g) \quad \text{(Eq. 9)}$$

The oxy-fuel combustion capture method employs pure oxygen instead of air during combustion, producing an exhaust stream primarily composed of CO_2 and H_2O, which facilitates downstream separation [12,26,45]. For example, the chemical reaction in the propane combustion process is shown in Eq. (10).

$$C_3H_8(g) + 5O_2(g) \rightarrow 3CO_2(g) + 4H_2O(g) \quad \text{(Eq. 10)}$$

At the CO_2 capture stage, several risks must be considered. Table 1 provides a comprehensive overview of the various risks and key findings from research on the CO_2 capture process. Risk assessment at the CO_2 capture stage has undergone significant evolution, encompassing technical, environmental, and social aspects. In the early stages, the research focused on operational and technical risks, such as corrosion and mechanical overload [46]. In post-combustion capture using amines and other carbon absorbents, corrosion is a critical risk that must be mitigated. The research conducted by Krzemień et al. [47] revealed that corrosion can be a serious threat as it can degrade the infrastructure components used. Hazard and operability study (HAZOP) and fault tree analysis (FTA) are used to identify system failures.

To assess the efficiency of the process, thermodynamic simulations can be used to compare the advantages of each capturing technology. For example, Gazzani et al. [48] compare the SEWGS process with the MEA/MDEA process. The performance index measured in this study is the specific primary energy consumption for CO_2 avoided (SPECCA), which measures the primary energy costs associated with CO_2 capture. SPECCA is the ratio between the energy used to reduce CO_2 and the amount of CO_2 that is successfully avoided; lower values indicate higher capture efficiency. The SPECCA calculation procedure is presented in Eqs. (11)–(13). The results of this study are presented in Fig. 4, which demonstrates that SEWGS is more efficient than MEA technology.

$$\eta_{el} = \frac{P_{net}}{\dot{m}_f LHV_f} \quad \text{(Eq. 11)}$$

$$CO_{2avoided} = \left(1 - \frac{CO_{2Emission}}{CO_{2Emission\,(Ref)}}\right) \quad \text{(Eq. 12)}$$

$$SPECCA = \frac{HR - HR_{Ref}}{e_{Ref} - e} = \frac{36\left(\frac{1}{\eta} - \frac{1}{\eta_{Ref}}\right)}{e_{Ref} - e} \quad \text{(Eq. 13)}$$

Subsequent studies have focused on optimizing hybrid systems and modeling dynamic risk. Fong et al. [49] and *Ma* et al. [34] highlight the importance of system optimization in improving energy efficiency. Although hybrid technologies can reduce energy consumption, technical risks such as reliability and process control remain significant. Therefore, careful planning and continuous monitoring are necessary to ensure efficient operation without compromising safety. This view aligns with Wang et al. [50] and Zhang et al. [51], who emphasize the importance of systemic and multidisciplinary risk assessment.

Innovation in the capture stage, including the use of mixed solvents (MEA + PZ), ANN-optimized MDEA systems, and low-emission solvent selection, must be accompanied by mitigation of technical and environmental risks. While these approaches can enhance capture efficiency and reduce energy demand, they may also introduce challenges such as increased viscosity, higher pressure requirements or elevated operational costs. Overall, effective risk management at the capture stage requires an integrated evaluation of technical, environmental, and operational factors to ensure long-term system reliability and safety [52–54].

2.2. The risks of CO_2 transport to the storage site

CO_2 transport from capture facilities to storage sites can be achieved via several modes, including pipelines, rail, trucks, and marine transport using dedicated CO_2 carriers. When transported via pipelines, CO_2 is typically maintained in a supercritical state for efficiency. In this phase,

Table 1
Representative studies on CO_2 capture stage.

Year	Ref.	Subject of Observation	Research Object	Research Methods	Finding
2013	[46]	Identification of atypical risks in CCS installations	Integrated gasification combined cycle (IGCC) with pre-combustion capture	Dynamic procedure for atypical scenarios identification (DyPASI) and life cycle assessment (LCA).	IGCC with pre-combustion is safer; Corrosion and mechanical stress are the dominant risks
2015	[47]	Corrosion risk in amine-based installations	Post-combustion capture process using amines	HAZOP, Delphi, and FTA	Degradation of amines and wet acid gases is the leading cause of corrosion; 70 risk scenarios are unacceptable.
2015	[48]	Capture technology performance risk evaluation	The sorption-enhanced water-gas shift (SEWGS) vs. MEA/MDEA	Thermodynamic simulation and exergy analysis	SEWGS exhibits an efficiency of 37.7% and a SPECCA of 2.2 MJ/kg CO_2, surpassing MEA.
2016	[49]	Optimization of energy risk in hybrid capture systems	Pressure-vacuum swing adsorption (PVSA) process and low-temperature separation	Multi-objective optimization (MOO) with genetic algorithms	CO_2 costs avoided minimum 10.4–87.1 €/ton; competitive potential with MEA.
2018	[34]	Ionic liquid-based CO_2 capture	Power plant exhaust system	COSMO-SAC model, energy analysis	Ionic liquids reduce energy consumption and costs.
2023	[50]	Regional-scale CCUS safety risk assessment	CCUS supply chain in Dongying, China	Aspen Plus process modeling, ALOHA simulation, and inherent safety index.	The highest risk in winter is associated with the modules of the riskiest CO_2 emission source.
2024	[51]	Exergy efficiency risks in hybrid systems	Cryogenic separation-liquid air energy storage (CS-LAES) system	Analysis of exergy, energy, and economics	Exergy efficiency is 63.4%, 5.22% higher than the baseline, with a high capital cost risk.
2025	[52]	Energy and performance risks in blended amine solvents	Post-combustion process: MEA, Piperazine (PZ), MEA + PZ, MDEA + PZ	Rate-based Aspen Plus modelling; pilot-scale data validation; scenario analysis	MEA + PZ achieves 90 % CO_2 capture with the lowest specific reboiler duty (4.3–5.4 MJ/kg CO_2); pure PZ faces viscosity and operational constraints that carry energy and operational risk.
2025	[53]	Solvent emission and environmental risk (ammonia vs MEA)	CO_2 absorption from aluminum-electrolysis flue gas	Process-parameter optimization and environmental impact analysis	Aqueous ammonia shows a higher ecological impact due to ammonia slip; solvent selection involves a trade-off between efficiency and emission risk.
2025	[54]	Process intensification and operational risk in MDEA systems	Post-combustion CO_2 capture from residue fluid catalytic cracking (RFCC) flue gas in refineries	Process simulation combined with artificial neural network (ANN) optimization; intercooler integration	Adding an intercooler and employing ANN-based optimization enhances capture efficiency and reduces energy demand, albeit at the cost of increased pressure drop and associated risks.

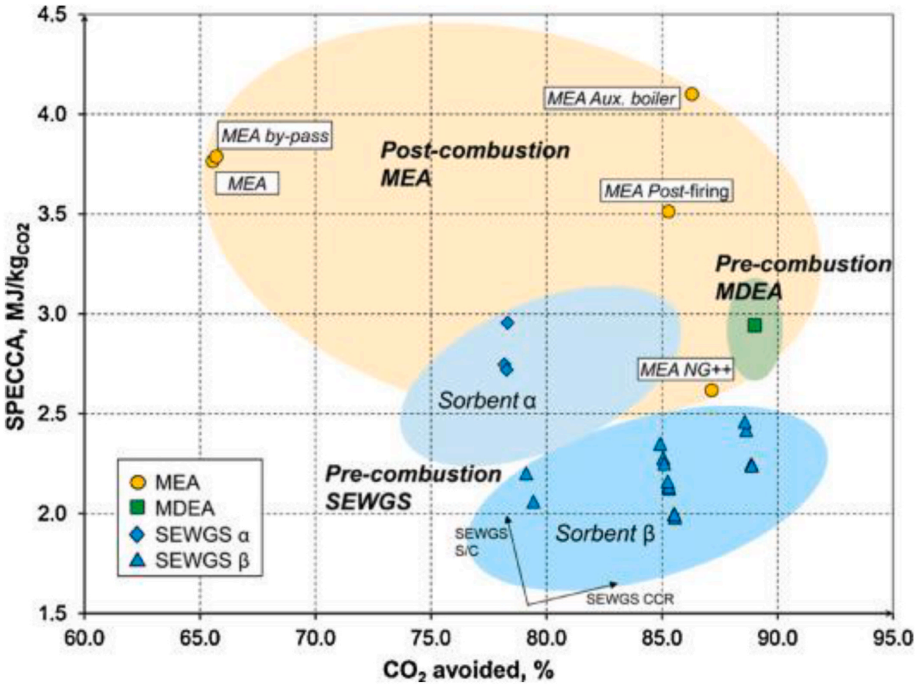

Fig. 4. Comparison of the proposed plant solutions based on CO_2 avoidance and SPECCA [48].

CO_2 exhibits a liquid-like density and gas-like fluidity, enabling the transfer of relatively large volumes. To achieve this state, CO_2 must be compressed to pressures exceeding 7.38 MPa and maintained at temperatures above 31.1 °C [55–57]. These conditions are relatively easier to sustain than those in the liquid phase. For this reason, pipeline systems are commonly used as the primary mode of transport, particularly in large-scale, continuous CCS operations. Although the initial capital investment for pipeline infrastructure is high, it offers lower operational costs for long-distance transportation [58,59].

When transported by rail, truck, or ship, CO_2 is maintained in the liquid phase. This approach is adopted for volumetric efficiency, as the liquid phase has a higher density. Although the required pressure is slightly lower than that of the supercritical phase, liquid-phase transportation necessitates refrigeration systems to maintain temperatures around −50 °C [60,61]. Consequently, transporting CO_2 in liquid form is only suitable under specific conditions, especially for the temporary transfer of relatively small quantities over long distances. In some cases, rail, truck, or ship transport may be more expensive than pipeline transport [62]. Furthermore, extremely low operating temperatures also pose new challenges for structural integrity. Some types of steel exhibit reduced strength at low-temperatures, making them susceptible to failure under excessive loads [63,64].

Each transportation mode presents unique challenges. Nevertheless, the primary safety concern during CO_2 transport is the potential for leakage, which could release gas into the surrounding environment. CO_2 is a colorless and odorless asphyxiant that can cause severe health effects, including hypercapnia and hypoxia, when present at elevated concentrations (Fig. 5). Such leaks can have severe impacts in densely populated areas, as high CO_2 concentrations in the air can cause hypoxia, a life-threatening condition resulting from oxygen deprivation [65]. Therefore, risk mitigation studies are crucial in preventing accidents and minimizing adverse consequences. Table 2 summarizes several studies addressing the CO_2 transportation stage, highlighting associated risks and mitigation strategies across various transport infrastructures, including high-pressure pipelines, ships, and innovative solutions such as subsea shuttles.

CFD modeling has been explored to understand the impact of CO_2 leakage on high-pressure pipelines. Several interrelated similarities exist

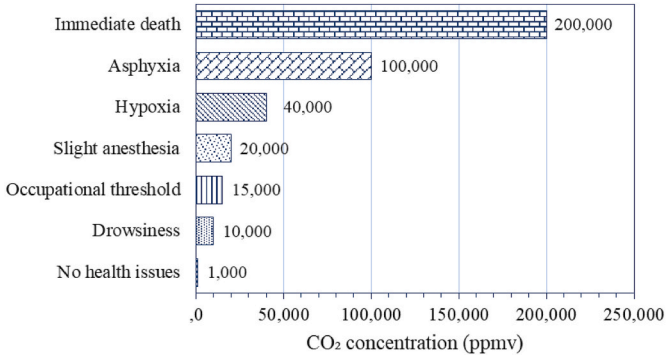

Fig. 5. The effect of CO_2 concentration on human life [66].

in modeling CO_2 leakage risk for CCS transportation systems. The Joule–Thomson effect (Eq. (14)) describes the temperature drop in CO_2 when it undergoes a rapid decrease in pressure. This effect is significant because extreme temperature drops can cause the formation of solid CO_2 (dry ice), thus affecting the dispersion character of CO_2 clouds after leakage [56,77]. The CFD analysis uses the continuity equation (Eq. (15)); the Navier–Stokes momentum equation (Eq. (16)) to calculate changes in fluid momentum due to pressure, external forces, and other sources; and internal energy equations (Eq. (17)) to predict in detail the behavior of the CO_2 plume in various atmospheric conditions and environmental geometry.

$$\Delta T = \varphi \Delta p \quad \text{(Eq. 14)}$$

$$\frac{\partial \rho}{\partial t} + \nabla(\rho \vec{u}) = 0 \quad \text{(Eq. 15)}$$

$$\frac{\partial(\rho \vec{u})}{\partial t} + \nabla(\rho \vec{u}\,\vec{u}\,\sigma_N) = \nabla p + F_s + F_g + F_p \quad \text{(Eq. 16)}$$

$$\frac{\partial(\rho I)}{\partial t} + \nabla(\rho \vec{u} I J) = \nabla \vec{u} + \rho\varepsilon + Q_s + Q_p + Q_h \quad \text{(Eq. 17)}$$

Furthermore, jet-release velocities can be calculated by the Bernoulli

Table 2
Key studies on CO_2 transport stage.

Year	Ref.	Subject of Observation	Research Object	Research Methods	Finding
2011	[67]	Risks of CO_2 transport at high pressures	Gaussian model vs. computational fluid dynamics (CFD).	Model validation with field experiments; CO_2 leakage risk analysis	CFD are more accurate in high-velocity leak simulations, reducing the excessive risk estimation of Gaussian models
2013	[59]	Benchmark transport CO_2 antara pipeline onshore dan shipping	Technical, cost, and climate impact assessment module	Techno-economic analysis, HYSYS® Aspen Simulation, parameter sensitivity analysis	Optimal pipeline for short distances (≤400 km), shipping for long distances; cost and capacity as key factors
2014	[68]	CO_2 cold energy recovery in ship transport	Marine-based CO_2 vessels	Rankine cycle	The main obstacles are the risk of freezing and high pressure in the injection system.
2015	[69]	Impact of leakage from high-pressure CO_2 pipeline	GERG-2008 equation of state (EOS) and CFD models for discharge rate and dispersion prediction	CFD (Fluidyn-PANACHE); validation with experimental data	Impurities (e.g., H_2S) increase the risk; The GERG-2008 model improves prediction accuracy
2016	[70]	Simulation of CO_2 emissions and risks in high-pressure transport	CO_2 transport pipeline	Validation of multiphase flow models (Favre–averaged and k–ε turbulence) with experiments	Changes in the CO_2 phase in the environment, and the effect of impurities in the CO_2 stream.
2018	[71]	CO_2 decompression in the pipeline to prevent material failure	GERG-2008 EOS model and decompression wave speed analysis	Thermodynamic simulations; validation with shock tube data	There is a risk of high pressure on pipe rupture and rapid channel cracking. Impurities reduce the speed of the decompression wave.
2020	[72]	Risks of liquid CO_2 decompression in transport	Transient behavior of high-pressure liquid CO_2 pipeline	Non-equilibrium CFD model with Span-Wagner state equation	The initial density and temperature influence decompression; model validation using experimental data.
2022	[73]	Optimization of ship routes and CO_2 shipping portfolio	CO_2 ship routes with 7-barg and 15-barg technology	Mixed-integer linear programming (MILP) model for cost minimization	Cost and risk efficiencies in CO_2 for ship-based transport over long distances. Collaboration between sources reduces transportation costs by 12%; 7-barg is more economical.
2024	[74]	Subsea shuttle for CO_2 transport	Submarine pipelines and subsea vessels	Techno-economic analysis of subsea shuttle vs conventional methods;	According to CAPEX analysis, underwater shuttles are less competitive compared to 7-bar pressurized ship transport.
2025	[75]	Impurity in CO_2 critical-flow dynamics	High-pressure CO_2 transport pipeline	Numerical modeling and laboratory validation	Impurities significantly alter critical flow behavior; the model enhances the safety and design of CCS transport systems.
2025	[60]	Techno-economic assessment of liquefied CO_2 transport via trucking	Liquefied CO_2 road-transport system	Process simulation; cost modeling; sensitivity analysis	Liquid-phase CO_2 trucking is feasible for small, temporary transfers, with energy costs dominated by refrigeration at −50 °C.
2025	[76]	Effect of double-stage throttling on pressure-relief characteristics in large-scale CO_2 pipelines	Industrial-scale CO_2 transport pipeline	Experimental setup + CFD analysis of depressurization	Double-stage throttling reduces shock intensity and improves safety control during emergency venting.

equation (Eq. (18)) and choked-flow theory (Eq. (19)). These two equations are used to calculate the mass flow rate and jet velocity of CO_2 following a leak in a high-pressure pipeline, which are then used as inputs for CFD simulations. The initial jet velocity determines how quickly and how far CO_2 disperses before the influence of wind and atmospheric turbulence becomes dominant [67,78].

$$\frac{\vec{u}^2}{2}+gh+\frac{p}{\rho}=constant \quad \text{(Eq. 18)}$$

$$\dot{m}=C_D\,A_{choke}\sqrt{\gamma\rho p\left(\frac{2}{\gamma+1}\right)^{\frac{\gamma+1}{\gamma-1}}} \quad \text{(Eq. 19)}$$

After a high-pressure CO_2 leak, fluid flow in the atmosphere is greatly affected by turbulence. Therefore, additional models are needed to predict the characteristics of turbulence that occur. The $k-\varepsilon$ turbulence model is often used for this problem. This model consists of two equations for the turbulent kinetic energy (k) and its dissipation rate (ε). The value of k indicates how much turbulence energy is at a specific point (Eq. (20)). In contrast, ε indicates how quickly that energy is lost due to the effect of small viscosity (Eq. (21)). These two variables are interrelated, where k is generated by the shearing force in the stream and then expended into heat at the ε rate. In the calculation of CFD, k and ε are used to lower the viscosity value (μ), which affects the prediction of velocity distribution patterns and the mixing of pollutants, such as CO_2 [69,79]. The $k-\varepsilon$ equation is key to capturing the effects of turbulence on the dispersion of CO_2 jets in the atmosphere so that predictions of harmful concentrations can be more accurate. Combining thermodynamic effects, jet velocity, and atmospheric dispersion modeling makes risk analysis more realistic. Overall, the integration of these equations provides a more precise estimate of the risk of CO_2 exposure to humans and the environment resulting from transportation system failures in CCS projects.

$$\frac{\partial(\rho k)}{\partial t}+\nabla\left[\rho\vec{u}k-\left(\frac{\mu_t}{\sigma_k}\right)\nabla k\right]=\frac{2}{3}\,\rho k\nabla\vec{u}+G\left(l\frac{Ri}{\sigma_h}\right)\rho\varepsilon+W_p \quad \text{(Eq. 20)}$$

$$\frac{\partial(\rho\varepsilon)}{\partial t}+\nabla\left[\rho\vec{u}\,\varepsilon-\left(\frac{\mu_t}{\sigma_e}\right)\nabla\varepsilon\right]=\frac{\varepsilon}{k}\left[C_1\,G\left(l\frac{Ri}{\sigma_h}\right)-C_2\rho\varepsilon+C_sW_p\right] \quad \text{(Eq. 21)}$$

Mazzoldi et al. [67] investigated the risks associated with CO_2 pipeline leaks using a CFD model, demonstrating elevated concentrations of toxic gases in the vicinity of the leak area. The study also identified the limitations of the Gaussian dispersion model (Eq. (22)) in simulating high-velocity leaks, for which CFD simulations provide more realistic results. These findings support the adoption of CFD-based approaches in quantitative risk assessment (QRA), reducing the overestimation of hazard zones and thereby increasing public acceptability.

$$C\,(x,y,z)=\frac{\dot{m}}{2\pi\,\vec{u}\,\sigma_y\sigma_z}\,exp\left(-\frac{y^2}{2\sigma_y^2}\right)\left[exp\left(-\frac{(z-H)^2}{2\sigma_z^2}\right)+\exp\left(-\frac{(z+H)^2}{2\sigma_z^2}\right)\right] \quad \text{(Eq. 22)}$$

Furthermore, Xiao et al. [72] used a non-equilibrium CFD model to investigate the transient behavior of the CO_2 decompression process during transport to the storage site. This approach employs a multiphase mixture model that accounts for the slip velocity between phases and interphase mass transfer by incorporating a relaxation-time coefficient. The governing equation used is the continuity equation, which ensures

mass conservation in the two-phase mixture during decompression. Subsequently, the change in the mixture momentum is calculated using a modified momentum equation. The mixture density and velocity (Eqs. (23) and (24)) are defined based on the volume fractions and properties of each phase. Meanwhile, the effective viscosity of the mixture is calculated as a linear average (Eq. (25)).

$$\rho = \alpha_l \rho_l + \alpha_v \rho_v \quad \text{(Eq. 23)}$$

$$\vec{u} = \frac{\alpha_l \rho_l \vec{u}_l + \alpha_v \rho_v \vec{u}_v}{\rho} \quad \text{(Eq. 24)}$$

$$\mu = \alpha_l \mu_l + \alpha_v \mu_v \quad \text{(Eq. 25)}$$

The total energy of a two-phase system is calculated using the energy equation (Eq. (26)), which accounts for heat transfer and energy changes due to phase changes, such as latent heat. The mass transfer rate between the liquid and gas phases is formulated using Lee's formulation [80] (Eqs. (27) and (28)), which is essential for capturing non-equilibrium evaporation and condensation during a sudden pressure drop.

$$\frac{\partial}{\partial t}\sum_{k=1}^{n}(\alpha_k \rho_k E_k) + \nabla \sum_{k=1}^{n}\left[\alpha_k \vec{u}_k(\rho_k E_k + p)\right] = \nabla(k_e \nabla T) + S_E \quad \text{(Eq. 26)}$$

If evaporation occurs $(p_l < p_{sat})$, then:

$$\dot{m}_{lv} = \tau_l \alpha_l \rho_l \left(\frac{p_{sat} - p_l}{p_{sat}}\right) \quad \text{(Eq. 27)}$$

If condensation occurs, then: $(p_v > p_{sat})$

$$\dot{m}_{vl} = \tau_v \alpha_v \rho_v \left(\frac{p_{sat} - p_v}{p_{sat}}\right) \quad \text{(Eq. 28)}$$

To elucidate the relationship between pressure, temperature, and density, the Span–Wagner EOS [81] is employed, which is known to be highly precise in predicting the thermodynamic properties of CO_2, particularly at high-pressure and low-temperature conditions relevant to CO_2 transport applications in pipelines. With these equations, this model can predict changes in pressure, temperature, phase distribution, decompression wave speed, and mass outflow rate during the liquid CO_2 decompression process under various initial conditions. Each symbol in the above equation represents a physical parameter commonly encountered in two-phase thermodynamics and fluid mechanics. Sudden changes in pressure and temperature can trigger rapid phase transitions, increasing the risk of structural failure in the pipeline system. These conditions can cause serious and potentially dangerous damage, underscoring the importance of robust handling and system design to mitigate this phenomenon. This approach represents a shift from qualitative to data-driven quantitative risk identification. This research provides strong support for previous findings. Gu et al. [71] also found that fluid decompression can increase the risk of rapidly developing pipeline cracks, especially in ductile pipelines.

You et al. [68] examine the concept of ship-based transport and identify constraints in the risk of CO_2 freezing before injection. This phenomenon requires special attention, particularly when a CO_2 heating system is required before injection to improve fluidity. In contrast, Wareing et al. [70] explore gas-liquid phase transitions in CO_2 streams. CO_2 phase changes (Fig. 6) and the impact of impurities indicate a significant risk of damage to complex pipelines. The behavior of CO_2, which is often in the supercritical phase, can be explained by Peng–Robinson's EOS [82] as shown in Eq. (29). The values of parameters a and b can be searched using the van der Waals mixing rule (Eqs. (30) and (31)).

$$p_{sc} = \frac{RT}{V_m - b} - \frac{\mathrm{a}(\alpha)}{V_m^2 + 2bV_m - b^2} \quad \text{(Eq. 29)}$$

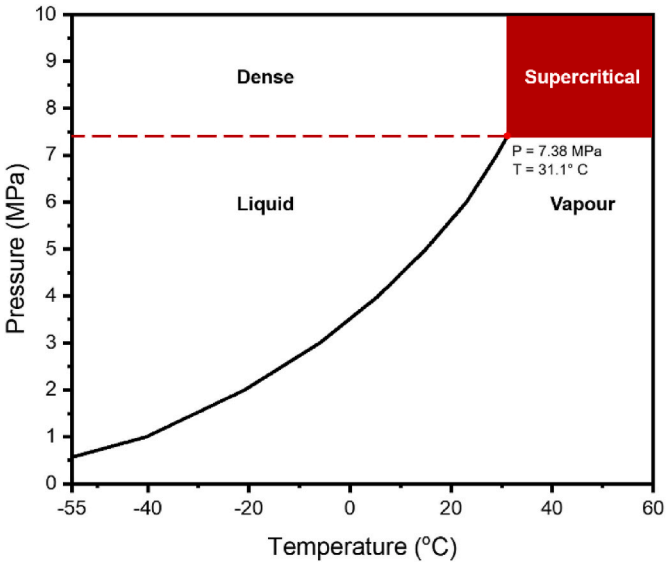

Fig. 6. Phase diagram of CO_2 [71].

$$a = \sum_{i=1}^{N}\sum_{j=1}^{N} x_i x_j \sqrt{a_i a_j}\,(1 - k_{ij}) \quad \text{(Eq. 30)}$$

$$b = \sum_{i=1}^{N} z_i b_i \quad \text{(Eq. 31)}$$

Developments in thermodynamic modeling, such as the integration of the GERG-2008 EOS [69,71], revolutionized the prediction of high-pressure CO_2 behavior. This model can accommodate the effects of impurities and the fluid phase, which are crucial for assessing the risk of pipeline failure and for material design. Real-time risk-monitoring methods using capacitive sensors and data-driven models [83] enable early detection of flow instability, thereby preventing catastrophic failure in CCS structures.

Economic and logistical aspects are explored through the research of Roussanaly et al. [59], which developed a framework for selecting transportation technologies based on distance and capacity. This study compares pipeline technology with ships for CO_2 transport on land. The results show that onshore pipelines dominate for distances of <400 km, while shipping is more flexible for long distances, although it is susceptible to fluctuations in investment costs. Further optimization by Bjerketvedt et al. [73] using the MILP model shows potential savings of 12% through collaboration on ship routes and 7-bar technology. However, the technology's maturity must be taken into consideration. Recent innovations, such as subsea shuttles [74], offer an alternative to underwater transportation but are still limited to specific scenarios due to high CAPEX. For certain distances and volumes, 7-bar low-pressure based vessel hauling is considered more effective than this approach.

Recent studies have demonstrated substantial progress in understanding and optimizing CO_2 transport mechanisms across different phases. Liao et al. [75] investigated impurity-driven variations in CO_2 critical-flow dynamics within high-pressure pipelines using numerical modeling and laboratory validation, showing that impurities significantly alter flow behavior and that improved modeling can enhance CCS transport safety and design. Ashkavand et al. [60] conducted a techno-economic assessment of liquefied CO_2 road transport, concluding that liquid-phase trucking is feasible for small-scale, temporary applications, albeit with high energy penalties due to refrigeration requirements (−50 °C). Similarly, Song et al. [76] demonstrated through experimental and CFD analyses that double-stage throttling in large-scale pipelines can mitigate shock intensity during emergency venting. Collectively, these studies suggest the persistence of technical

risks associated with high pressure, phase transitions, and impurity effects, highlighting the need for integrated transport design strategies. More broadly, recent research reflects a shift from conventional risk-based analyses toward multidisciplinary frameworks integrating thermodynamics, economics, and artificial intelligence. Despite these advances, challenges such as investment uncertainty, increasing model complexity, and limited large-scale field validation remain significant barriers to the widespread deployment of CCS.

2.3. CO_2 storage and monitoring strategies in CCS implementation

The storage and monitoring of CO_2 represent the final and arguably most critical phase in the CCS chain. The long-term viability and sustainability of CCS technologies fundamentally depend on the success of this stage. Considering its large potential storage capacity, CO_2 can be sequestered in either deep-sea sediments or geological formations. Deep-sea sediment storage involves injecting CO_2 directly into the ocean floor at depths exceeding 1000 m. Under such high-pressure and low-temperature conditions, CO_2 can remain in a liquid phase and accumulate as localized CO_2 lakes on the seafloor. The stability of these CO_2 lakes is governed by thermodynamic phase behavior at deep-ocean pressure–temperature conditions, hydrodynamic forcing from bottom currents and local bathymetry, and mass transfer across the CO_2–seawater interface. In some cases, the formation of a hydrate-rich or carbonate crust at the interface may partially inhibit dissolution and diffusion, thereby providing a self-sealing effect. Nevertheless, a fraction of injected CO_2 can dissolve into seawater, which may significantly reduce local pH and impose risks to deep-sea ecosystems. Moreover, strong bottom currents, seafloor slope-driven spreading, or geological discontinuities may compromise containment by enhancing mixing and promoting upward migration, potentially leading to gradual leakage to the water column and the atmosphere [84–86].

In contrast, onshore or offshore geological storage is widely regarded as a safer and more environmentally responsible option compared to direct deep-ocean injection. Nonetheless, this approach is not without risk. CO_2 leakage and gas migration remain significant challenges, particularly when sealing systems fail or degrade over time. Leakage can lead to groundwater contamination by allowing CO_2 to migrate from subsurface formations. The integrity of the caprock, the impermeable rock layer overlying the storage reservoir, is therefore a key determinant of long-term storage security. Ideally, the caprock must exhibit extremely low permeability to contain CO_2 and prevent upward gas migration effectively. Inadequate geomechanical properties of the storage formation may increase the risk of leakage and reduce overall system reliability [87–90].

Risk assessment studies focusing on CO_2 storage have advanced substantially in recent years, encompassing geological, environmental, and operational aspects (Table 3). Polson et al. [91] employed a qualitative expert elicitation approach to identify principal risk factors, including reservoir uncertainty and public resistance to CCS deployment. Their study emphasized the importance of uncertainty reduction through cost-effective methods, such as reprocessing seismic data for preliminary site evaluations. However, limitations in pressure measurements and rock sampling were identified as significant challenges, prompting further research on improved geological characterization. Blackford et al. [92] conducted controlled CO_2 release experiments in marine environments and found that biological impacts were spatially limited, although microbial community shifts persisted over time. These findings underscore the importance of conducting baseline environmental studies to detect and monitor potential leaks. Similarly, Andrew et al. [93] evaluated the geological trapping security of CO_2 using X-ray microtomography and demonstrated that capillary trapping remains effective across diverse rock types, regardless of pore morphology. This discovery alleviates concerns over lithological dependency and expands the range of suitable sites for CCS implementation.

Furthermore, Mitchell and Green [94] examined the risk of induced seismicity that had previously received less attention in CCS risk assessments. They found that an injection-extraction volume imbalance can trigger earthquakes of magnitude greater than 3, especially in large-scale CCS projects. The primary triggering mechanism is

Table 3
Selected studies on CO_2 storage stage.

Year	Ref.	Subject of Observation	Research Object	Research Methods	Finding
2012	[91]	CCS risks related to the uncertainty of geological reservoir evaluation	Two CCS locations: Lincolnshire and the Firth of Forth	Expert elicitation, seismic data reprocessing, and hydrogeological studies	The risk of CO_2 leakage is considered moderate to low. Uncertainty is reduced with inexpensive techniques such as seismic data reprocessing.
2014	[92]	Environmental impact of controlled submarine CO_2 leakage	Controlled CO_2 release on the seabed and its migration	Chemical analysis of sediments, acoustics, and biological samples	Small leaks have a local impact ($\leq$10m). Changes in microbial communities persist 90 days post-injection.
2014	[93]	CO_2 trapping efficiency in carbonate and sandstone rocks	Five samples (2 sandstone, 3 carbonate)	X-ray microtomography at high pressure/temperature	CO_2 trapping is effective on all stones. The distribution of ganglia size follows the theory of percolation.
2017	[94]	Seismicity risk induced by CO_2 injection	Energy technology (CCS, hydraulic fracturing, sewage injection)	Statistical analysis of induced earthquakes, traffic light systems	Large-volume injection increases the risk of earthquakes ($M \leq 6.5$). A mitigation system is required.
2018	[95]	Integrity of the well due to thermal stress during CO_2 injection	Miniature wellbore samples and numerical models	Numerical modelling (elastic stress coupling and heat conduction)	Sub-zero-temperature CO_2 injection is safe if the horizontal stress is at or above 10 MPa. The thermal properties of cement are critical.
2022	[85]	Feasibility and mechanisms of hydrate-based CO_2 sequestration	Gas hydrate formation systems	Literature review and thermodynamic modeling	CO_2 hydrate formation is feasible under high-pressure, low-temperature conditions; kinetics and host sediment properties strongly affect storage efficiency.
2022	[90]	Impact of thermal shock on caprock and reservoir integrity during CO_2 injection	Caprock and reservoir core samples	Laboratory testing of permeability and seismic wave velocity before and after thermal shock	Thermal shock increases rock permeability and reduces seismic velocity, potentially compromising caprock sealing capacity.
2023	[96]	Performance of nanoalumina as an additive in oil well cement under CCS conditions	Oil well cement pastes with nanoalumina	Experimental testing under high-pressure CO_2 environments using dispersive methods	Nanoalumina enhances the durability and microstructural stability of cement under CO_2 exposure, thereby reducing permeability and carbonation effects.
2025	[97]	CO_2 wellbore leakage considering transient flow and phase transition	Numerical simulation of CO_2 injection in inclined formations	Coupled transient multiphase flow modeling and phase transition analysis	Formation dip angle and injection rate significantly affect leakage pathways. Optimized injection strategy reduces leakage risk and enhances storage stability.
2026	[98]	Thermo-mechanical response of the wellbore during CO_2 mixture sequestration	Depleted oil/gas reservoir wellbores	Coupled thermo-mechanical numerical modeling	CO_2 mixtures induce temperature and stress variations that may compromise casing–cement bonds; material optimization is essential for long-term wellbore integrity.

consistent with that observed in brine or wastewater injection: an increase in pore pressure and associated poroelastic stress perturbations. This phenomenon can reduce the effective normal stress on critically stressed faults and may induce slip on the caprock. However, CO_2 injection is not identical to brine injection, because CO_2 is compressible and buoyant. These characteristics can modify pressure diffusion, saturation-dependent permeability, and the spatial–temporal evolution of stress changes compared with single-phase brine injection. Evidence from high-volume subsurface fluid injection in the United States, dominated by brine/wastewater disposal, demonstrates that seismicity rates can increase significantly across multiple states when numerous injection wells operate at high volumes. Pressure perturbations may trigger earthquakes at distances of up to 35 km from the injection well, with effects persisting for months to years after injection ceases. Their recommendations on traffic-light systems provide a practical reference for operational mitigation. Nevertheless, their study also highlights the complexity of seismicity modelling, which requires a multidisciplinary approach integrating multiphase flow, geomechanics, and fault characterization.

Beyond storage formation integrity, wellbore integrity is a crucial factor in ensuring the safe injection and containment of CO_2. Maintaining wellbore integrity is essential to prevent gas migration to the surface or into adjacent aquifers. Investments in enhancing wellbore performance not only mitigate safety risks but also deliver significant economic benefits by minimizing leakage, protecting subsurface assets, and reducing potential environmental liabilities. A proactive approach to wellbore integrity management can yield substantial long-term cost savings by reducing the need for corrective interventions and improving the operational efficiency of CO_2 injection systems [99,100].

Structural defects such as fractures in wellbores induced by thermo-hydro-mechanical-chemical interactions during drilling, completion, production, and abandonment have been identified as major pathways for CO_2 migration [98,101,102]. Engineering studies have demonstrated that fluid leakage along wellbores represents a significant challenge to the integrity of subsurface storage systems. For instance, in British Columbia, Canada, the probability of hydrocarbon leakage from operational oil and gas wells has been reported to reach 10.8%. Similar instances of natural CO_2 leakage through anthropogenic wells have been documented in regions such as the Paradox Basin (Utah), Española Basin (New Mexico), Xining Basin (China), and New Zealand [97,98]. These observations underscore that managing wellbore integrity is a fundamental component for ensuring the long-term safety and success of CCS projects.

Previous studies have revealed several new findings related to wellbore integrity assessment. Roy et al. [95] investigated the integrity of CCS storage wells affected by thermal stresses induced by low-temperature CO_2 injection. The research modeled how temperature variations generate stress and strain within the wellbore structure. Heat transfer was assumed to occur conductively from the well wall to the surrounding formation, and Fourier's Law (Eq. (32)) was applied to determine the temperature distribution. Resulting temperature changes induced thermal expansion or contraction, producing thermal stresses (Eq. (33)) that were combined with mechanical stresses arising from formation and fluid pressures (Eq. (34)). The relationship between stress and strain was expressed using Hooke's law (Eq. (35)). In contrast, the overall mechanical equilibrium was ensured through the stress equilibrium equation (Eq. (36)).

$$\rho C_p \frac{\partial T}{\partial t} = \frac{\partial}{\partial x_j}\left(k_e \frac{\partial T}{\partial x_j}\right) \quad \text{(Eq. 32)}$$

$$\sigma_{ij}^{T} = \frac{E_m \alpha_T}{1-2\nu}\,\Delta T \delta_{ij} \quad \text{(Eq. 33)}$$

$$\sigma_{ij} = \sigma_{ij}^{M} + \sigma_{ij}^{T} \quad \text{(Eq. 34)}$$

$$\sigma_{ij}^{M} = \frac{E_m \nu}{(1+\nu)(1-2\nu)}\varepsilon_{vol}\delta_{ij} + \frac{E_m}{(1+\nu)}\,\varepsilon_{ij} \quad \text{(Eq. 35)}$$

$$\frac{\partial \sigma_{ij}}{\partial x_j} = 0 \quad \text{(Eq. 36)}$$

$$SIF_I = \sqrt{\frac{E_m G_E}{1-\nu^2}} \quad \text{(Eq. 37)}$$

$$G_E = \frac{-1}{2A_{fracture}}\left(f_{closure}\,{}^{\circ}W_t\right) \quad \text{(Eq. 38)}$$

In the presence of pre-existing cracks, the stress concentration near the crack tip was found to be significantly elevated (Fig. 7). The stress intensity factor (SIF) was used to quantify this effect (Eqs. (37) and (38)), and crack propagation was predicted to occur when the SIF exceeded the material's fracture toughness. Consequently, the structural integrity and safety of the well during CO_2 injection can be assessed by comparing simulated SIF values with the mechanical properties of the cement and surrounding rock. In conclusion, Roy et al. [95] demonstrated that thermal stresses induced by low-temperature CO_2 injection can significantly compromise well integrity, emphasizing the importance of temperature control and the selection of materials with high fracture toughness to ensure the long-term safety of CO_2 storage operations.

After the CO_2 injection process, a crucial step in ensuring the long-term security of CO_2 storage within geological formations is the implementation of monitoring activities in accordance with established procedures. The primary objectives of monitoring are to ensure the stability of CO_2 within the geological formation, detect potential leakage, and identify early-stage fluid migration. Commonly employed approaches include geophysical monitoring, geochemical monitoring, and assessment of atmospheric conditions. The implementation of all monitoring stages must comply with applicable standards and regulations, such as ISO 27914:2017 (carbon dioxide capture, transportation and geological storage) and the EU Directive 2009/31/EC [103,104]. A more detailed discussion of the monitoring methods and procedures is presented in Section 4 of this article.

3. Potential accidents in CCS technologies

Some accident risks associated with CCS include overpressure-induced bursts, leaks, and structural failures. A system failure or CO_2 leak would be economically detrimental and have a profound impact on the environment. CO_2 gas released into the atmosphere can cause damage to local ecosystems, for example, in the case of a long-term leak from a carbon storage facility. High concentrations of CO_2 at the soil surface can alter soil pH, affect groundwater quality, and reduce the oxygen available to humans and other living organisms. Underground CO_2 storage requires stable and safe geological formations that can withstand the pressures of trapped CO_2 for many years. Therefore, it is essential to continue researching and developing more sensitive leak detection technologies and reliable security systems to mitigate this risk.

Reviewing milestones (Table 4) reveals how research developments have led to a more comprehensive understanding of the risks associated with bursts caused by overpressure, leakage, and structural failure in CCS technologies. Various approaches, from numerical simulations to predictive models, significantly contribute to understanding these risks and establishing more effective mitigation measures. Kano et al. [105] conducted numerical simulations to estimate changes in pollutant concentrations resulting from CO_2 leakage from the seafloor. In extreme leak scenarios, the simulation results indicate a significant increase in CO_2 around the leak area, posing a high risk to the safety of marine organisms exposed to it. These findings underscore the importance of selecting geological storage locations that are distant from sensitive ecosystems.

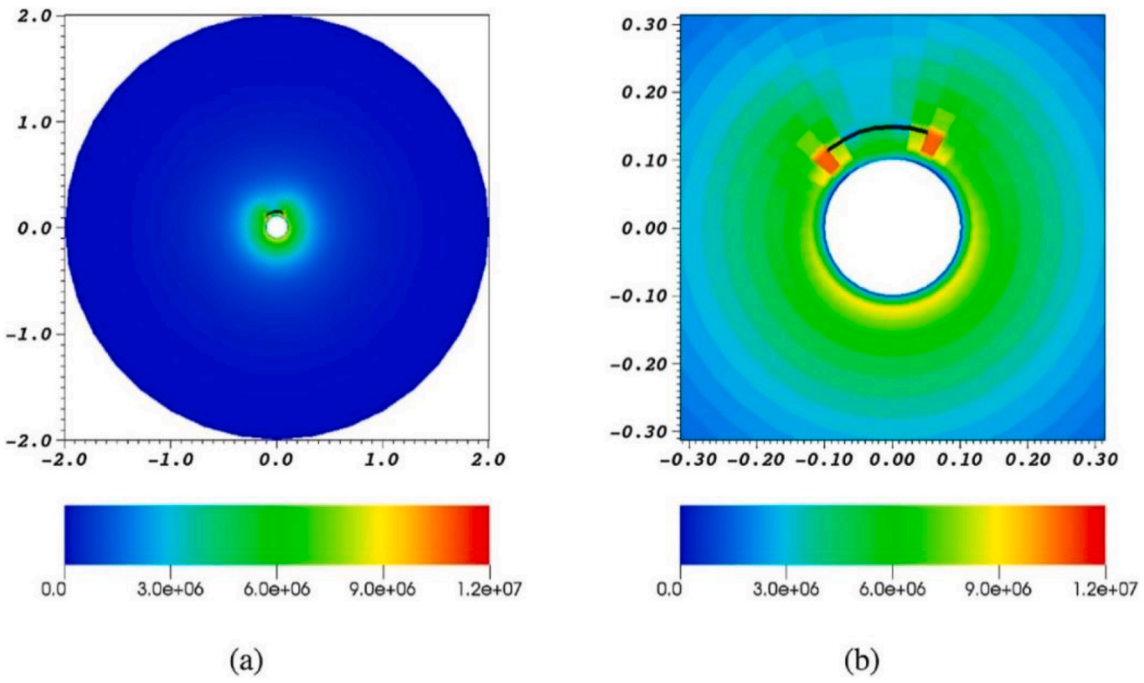

Fig. 7. Radial stress distribution around a single pre-existing fracture caused by wellbore casing cooling: (a) sliced view; (b) detail view on the fracture profile. This profile was captured after 30 min of CO_2 injection at 15 °C (initial temperature: 70 °C). The axis units are in meters, and the color bar indicates stresses in Pa [95]. (For interpretation of the references to color in this figure legend, the reader is referred to the Web version of this article.)

Table 4
Representative studies on the burst due to overpressure, leakage, and failure scenario in CCS.

Year	Ref.	Observational Subject	Research Object	Research Methods	Findings
2010	[105]	Impact of CO_2 leakage under the sea	CO_2 leakage from offshore reservoirs.	Multi-scale numerical simulation of dissolved CO_2 advection-diffusion analysis.	Extreme CO_2 leakage (94,600 t/year) increases CO_2 by up to 300 ppm for floating organisms and >1000 ppm for stationary organisms. The biological impact is minimal in a reasonable leakage scenario (3800 tons per year).
2012	[106]	Estimated maximum CO_2 leakage through old wells	Old wells in the geological formations of Alberta, Canada	Monte Carlo approach to leak simulation	CO_2 leakage remains below 1% per year (95% confidence). Effective wellbore permeability parameters are critical for determining the risk of leakage.
2013	[107]	Atmospheric dispersion of CO_2 from CCS infrastructure leaks	Leakage from pipelines and CO_2 storage tanks	CFD modeling with turbulence (k–ε) and complex field interaction analysis	Complex terrain and obstacles increase the danger zone through the slumping effect of solid gases. Low-momentum leaks form gas clouds concentrated near the surface.
2014	[108]	Comparison of CO_2 vs. natural gas pipeline risks	Natural gas pipeline incident data (USA, 1990–2009) as a proxy for CO_2 pipeline risk	Statistical analysis of incidents and fatality rates	The risk of CO_2 pipelines was previously estimated to be 2 to 3 orders of magnitude higher. The natural gas fatality rate is the upper limit of the risk of CO_2 pipelines.
2014	[109]	Validation of the CFD model for CO_2 dispersion	CO_2 discharge from the high-pressure pipelines	Simulation of CFDs with real EOS gas and SST turbulence model (k–ω)	The CFD model with a real gas, EOS is more accurate than the commercial package (Phast). SST (k–ω) excels at predicting depressed jet flow.
2016	[77]	Dangers of dry ice sublimation post-CCS leak	Establishment of dry ice banks and delayed CO_2 emissions	Comparison of ALOHA, PHAST, and CFD models	A simple model fails to describe near-field hazards. CFDs reveal low-strata CO_2 accumulations that persist for several days.
2016	[110]	Dispersion of CO_2 in complex environments (hilly and urban)	Simulation of CO_2 leakage in flat, hilly, and urban terrain	CFD modeling with variations in wind speeds and building heights	Hills reduce the downstream dispersion of CO_2, while high concentrations can become trapped between buildings. Increased wind speeds reduce the overall impact area.
2018	[111]	CCS well leak prediction using a neural network	500 wells exposed to CO_2 in Texas	Neural network model with wellbore attribute data and operation history	Parameters such as cement placement, cement type, and well age are dominant factors influencing leakage risk. The model's accuracy was validated in the Cranfield field.
2022	[112]	Quantification of uncertainty of CO_2 leakage flux measurement	Volcanic and geothermal areas	Monte Carlo-based (MC-Flux) program with ordinary kriging (OK)	Offset grid sampling results in the most accurate estimate of flux. Integration of high-resolution datasets is necessary to reduce uncertainty.
2024	[113]	Leakage characteristics of high-pressure pipelines	Industrial-scale CO_2 pipelines with N_2 impurities	Experimental study with variation in leakage orifice diameter	N_2 impurities (3%) enlarge the gas-liquid two-phase zone in CO_2, resulting in very low-temperatures near the leak orifice. Impurities also affect dispersed patterns and post-release CO_2 concentrations.

In subsequent studies, Nogues et al. [106] introduced the Monte Carlo method to estimate maximum leakage from old wells, providing regulators with a statistical basis for setting safe leakage limits (<1% per year). This study demonstrates that leakage through existing wells is highly dependent on uncertainty parameters, such as well permeability. The simulation results show that leakage from wells with unknown structural conditions poses a high risk. This study underscores the need for additional mitigation strategies and enhancements to well-construction standards to minimize the risk of future leaks.

The development of CFD modeling has dominated research on gas

dispersion in cases of CO_2 leakage. Hsieh et al. [107] employed CFD simulations to evaluate CO_2 leakage scenarios in topographically complex areas. This study simulates the gas dispersion pattern around CCS storage infrastructure. Due to its higher density relative to air, CO_2 tends to accumulate near the ground, which significantly influences dispersion patterns in complex terrains (Fig. 8). On the other hand, Duncan and Wang [108] corrected common errors in CO_2 pipeline risk assessments by comparing them to natural gas data, reducing risk overestimates by 2–3 orders of magnitude. This study demonstrates that the physical properties of the transported gases differ, thereby affecting the risk of failure. Although CO_2 is not flammable, its toxicity and density require a more in-depth risk analysis, especially in densely populated areas.

Meanwhile, Liu et al. [109] employed a CFD model based on the absolute gas equations, highlighting the risks associated with CO_2 leakage from high-pressure pipelines. The pressure on the pipeline affects the fluid's velocity through the leak orifice (Fig. 9). These jet-release velocities serve as the initial input for the model of CO_2 dispersal into the atmosphere. Research shows that safety measures during CO_2 pipeline construction are crucial due to the potential hazards posed by CO_2 dispersion in the surrounding environment. This research forms the basis for designing safer CCS pipelines.

Mocellin et al. [77] focus on the hazards of forming dry-ice banks due to the rapid release of CO_2 from the CCS pipeline. This study compares various numerical modeling approaches for describing CO_2 dispersion, ranging from simple methods to more complex CFD models. The results of the analysis show that simple models are often insufficient to describe realistic dispersion scenarios nearby, mainly because they are unable to capture the stratification phenomenon that occurs. In contrast, CFDs provide a more accurate representation of gas dispersion patterns under real-world conditions. However, CFDs require considerable computational time, making them more suitable for planning than for emergency response.

In line with this, Liu et al. [110] also developed a CFD simulation to analyze CO_2 dispersion patterns in urban areas with high-rise buildings (Fig. 10). The study aims to investigate the dispersion behavior of CO_2, which is denser than ambient air, in urban environments. The simulations revealed that CO_2 leakage in urban areas poses a significant risk to humans, as this gas can become trapped around buildings or on uneven topography, thereby increasing CO_2 concentrations in certain regions. This study emphasizes the importance of accounting for local conditions when designing CO_2 pipelines, especially in densely populated areas. Thus, the potential danger of CO_2 leakage can be minimized through a design approach that is adaptive to the characteristics of the surrounding area.

Research by Cao et al. [113] has made a significant contribution to process safety in high-pressure CO_2 transport. This study addresses the need for empirical data on the risk of CO_2 pipeline leakage, which has been based primarily on simulations or small-scale experiments with pure CO_2. Through an industrial-scale experiment on a 258-m-long CO_2 pipe with 3% N_2 added, this study systematically examined leakage characteristics from thermodynamic, diffusion, and temperature-change perspectives, as well as concentrations around the leak point. One of the strengths of this research is the experimental approach, which closely approximates real operating conditions (Fig. 11). Hence, the data obtained is relevant for validating risk prediction models and developing CO_2 pipeline safety standards. Using a virtual-source theory model to predict CO_2 concentrations along the leak axis provides a novel solution for estimating danger zones (Fig. 12), which has often been overlooked in simulation-based studies. This study presents significant findings, including a minimum safe distance of 25 m and a distribution of dangerous concentrations extending up to 210 m from the leak area.

Li et al. [111] used machine learning to develop a predictive model that estimates the risk of leakage from wells used for CO_2 storage. This study collected data from ±500 wells in oil and gas fields in Texas, United States. Some of the data analyzed included the wells' ages, types, and operational histories. The results showed that this neural network model could accurately estimate the likelihood of leakage based on specific conditions. This study identifies wells that require special attention and provides recommendations to prevent future leakage risks. A similar study was also conducted by Beaubien et al. [112], who used a Monte Carlo-based approach to overcome the uncertainty in measuring CO_2 leakage flux from storage sites. The results showed that a denser

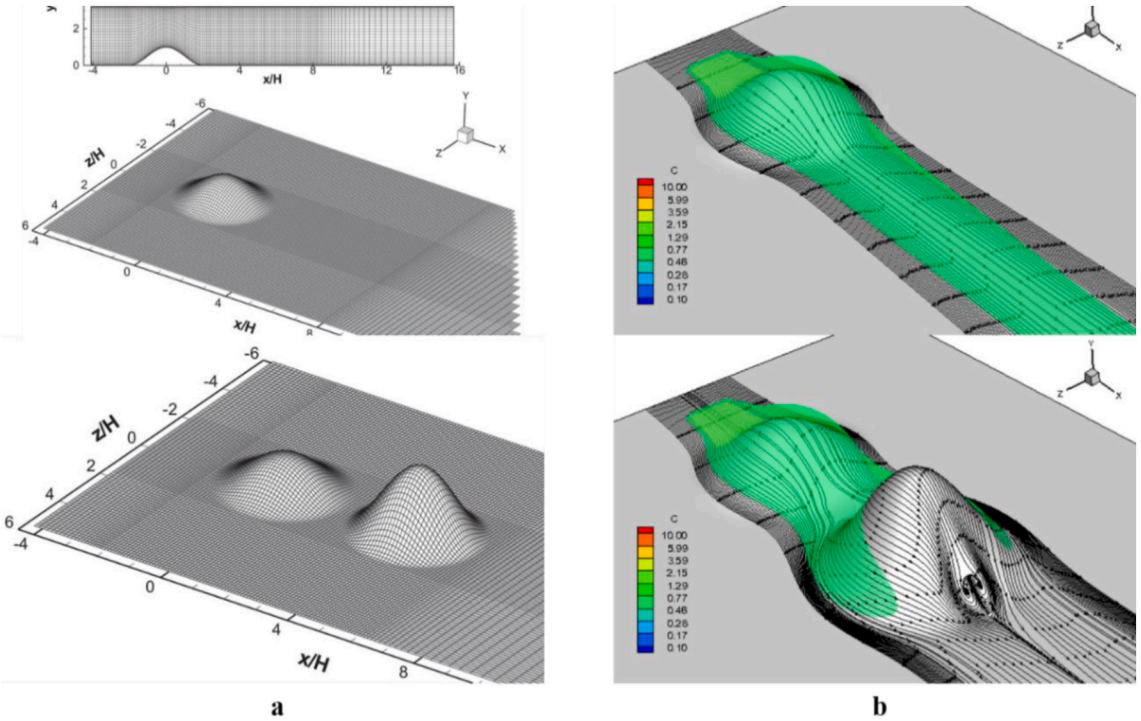

Fig. 8. CFD analysis and result: (a) computational mesh of obstacle model, (b) contour of CO_2 flow with 4% concentration (bright green) and 0.5% (dark green) [107]. (For interpretation of the references to color in this figure legend, the reader is referred to the Web version of this article.)

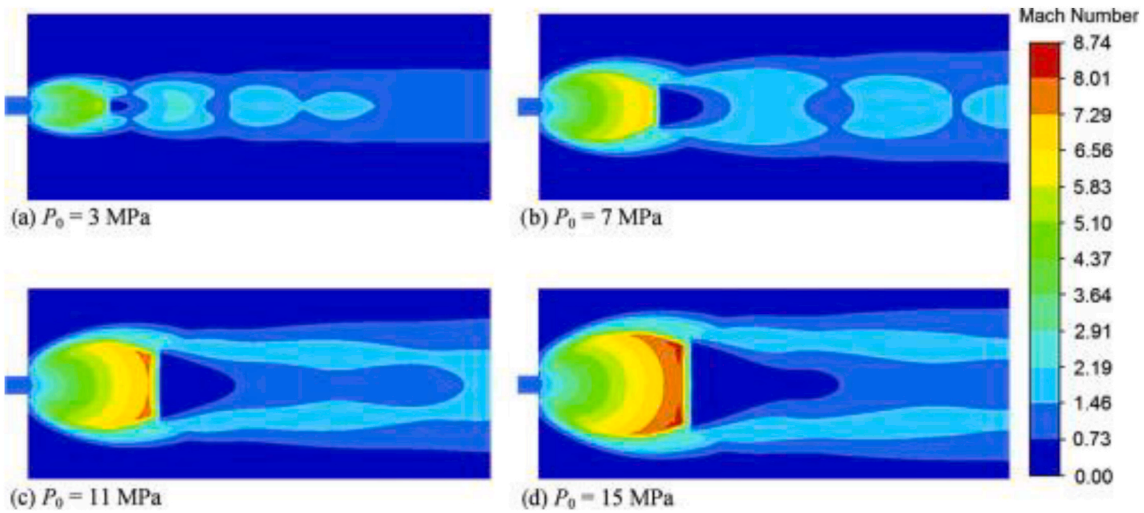

Fig. 9. Mach number distribution profiles for CO_2 jets formed at different stagnation pressures, with a fixed stagnation temperature of 380 K [109].

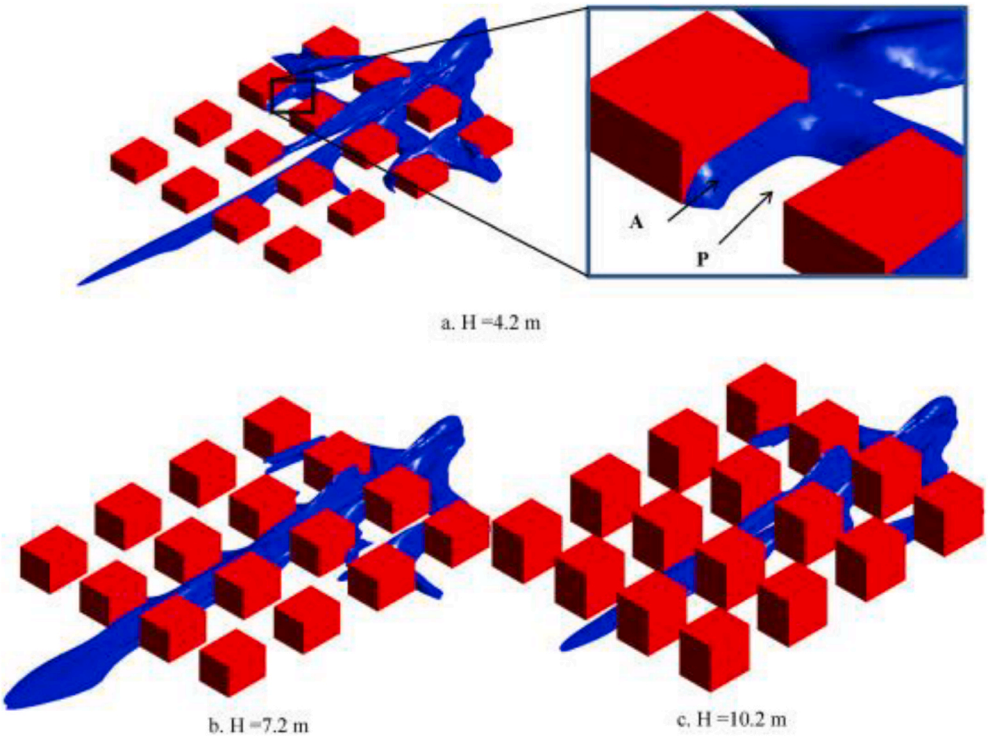

Fig. 10. CO_2 concentration levels were observed 300 s post-release [110].

sampling strategy and geostatistical interpolation (regular kriging) could provide more accurate estimates of leakage. Several previous studies examining the risks of CO_2 transportation have been reviewed. In general, CCS technologies face risks of leakage, overpressure-related bursts, and structural failure in pipelines, wells, and geological storage. Various methods and approaches have been used to map these risks. The study results indicate that the risk of leakage occurring in densely populated areas must be anticipated as much as possible. Strict safety standards and intensive monitoring must be implemented to prevent harmful environmental and human health impacts.

4. Monitoring and leakage detection

Monitoring and leakage detection in CCS technologies are essential to prevent unwanted disasters. Various monitoring methods have been developed over the past few years. Developing a system that delivers fast, accurate, and reliable results at scale is a goal that must be achieved consistently. The essence of research and innovation in monitoring and leak detection is to ensure the sustainability and safety of CCS technologies.

4.1. Offshore geological storage monitoring

Leak detection and monitoring systems for geological storage have undergone significant evolution. Research and innovation have recently focused on developing more efficient and cost-effective monitoring technologies. Seismic monitoring methods using seabed sensors are still under development. This seismic technique can detect changes in pressure, CO_2 concentration, and gas movement in geological formations. Most recently, high-resolution seismic imaging techniques allow

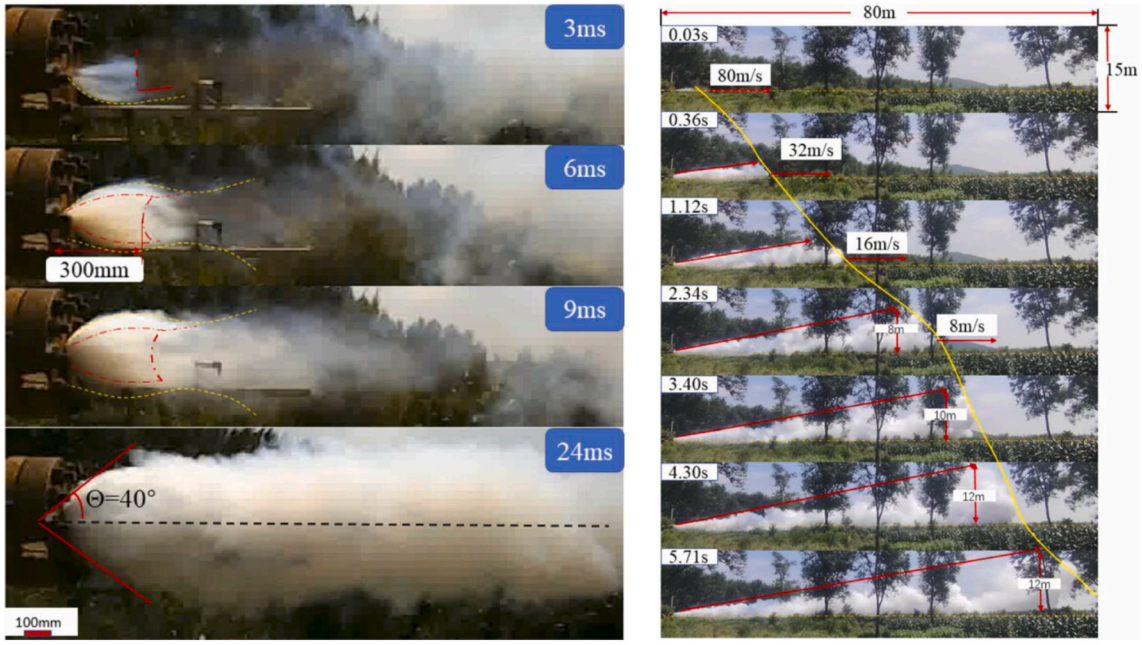

Fig. 11. Evolution of leakage pattern of CO_2 with N_2 impurity after release from high-pressure pipeline (hole diameter 50 mm) [113].

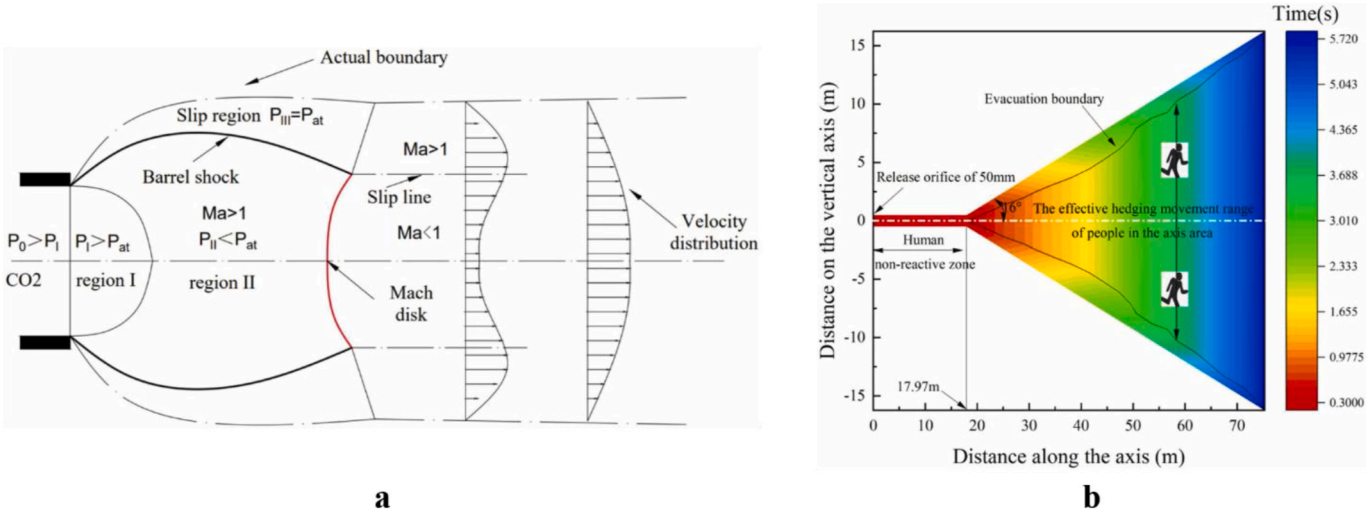

Fig. 12. Experimental result: (a) jet release region scheme; (b) the danger zone of the leak area [113].

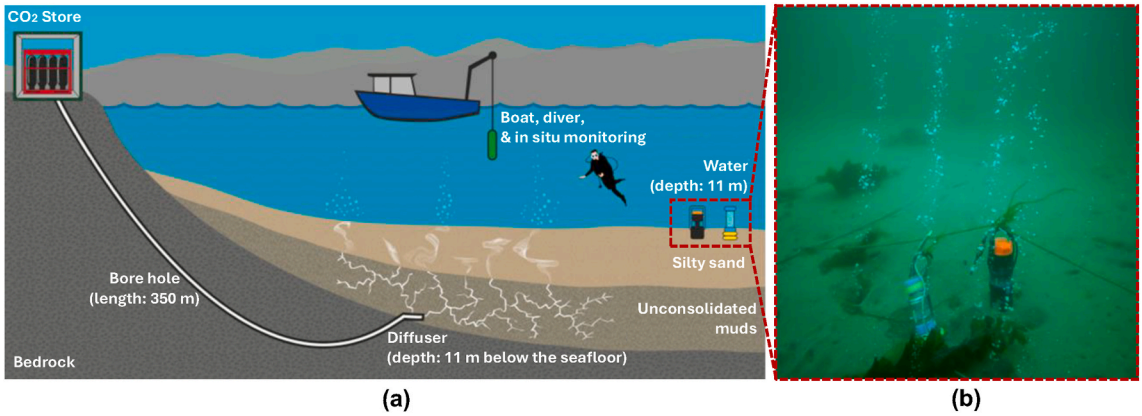

Fig. 13. Subsea CO_2 leakage detection: (a) conceptual diagram; (b) the experimental documentation [116].

operators to visualize changes in CO_2 distribution over time [114]. Further developments include the use of drones and automatic sensors, which are increasingly popular, especially for monitoring onshore and offshore storage sites. Drones equipped with gas sensors and infrared cameras can survey large areas and detect real-time anomalies in CO_2 concentration. Using drones also enables monitoring in hard-to-reach locations without requiring personnel to be directly involved. The advantages of this drone include increased efficiency and safety [115].

Taylor et al. [116] explored and developed CO_2 release experiments under the seabed. This experiment involves releasing CO_2 into the seabed substrate and monitoring its impact on the surrounding environment (Fig. 13). Measurements are taken at various depths and under different environmental conditions to map how CO_2 behaves in the sea and to evaluate monitoring techniques applicable in real-field conditions. The study results indicate that releasing CO_2 into the seabed can alter seawater pH and other chemical conditions, potentially impacting marine life. The experiment also found that although CO_2 leakage from the storage site could be detected using various monitoring methods, the observed leakage under these conditions was relatively low. Proper monitoring and management of environmental impacts are crucial to the successful implementation of CCS at sea. His research also underscores the need to continually develop monitoring methods and technologies to enhance the effectiveness of CO_2 leak detection. Further research is needed to investigate the long-term effects of CO_2 leakage on the broader marine ecosystem. Additionally, developing more sensitive and effective monitoring technologies is necessary to detect leaks more quickly and accurately.

In light of these developments, Hvidevold et al. [117] also focus on monitoring CO_2 leakage in marine geological storage. This study aims to identify the most effective layouts for CCS monitoring infrastructure to detect CO_2 leakage traces in a changing marine environment. This study uses mathematical simulation and probabilistic analysis to develop various design scenarios for the monitoring infrastructure. Factors such as ocean depth, current conditions, and CO_2 distribution in seawater are considered to determine the optimal location for the monitoring device (sensor). The results showed that the layout of the monitoring infrastructure, precisely positioned within the predicted area, has a higher potential for leaks, thereby increasing the likelihood of detecting CO_2 footprints. Further research is recommended to investigate the application of advanced sensor technologies to enhance detection accuracy and reliability, and to evaluate proposed layouts in more realistic, complex field scenarios.

The use of an unmanned surface vehicle (USV) with acoustic sensors (Fig. 14) to detect CO_2 gas leaks in shallow coastal waters has been explored by Scoulding et al. [118]. The research method involves experimentally releasing CO_2 bubbles at depths below 20 m. The results show that acoustic sensors can reliably detect CO_2 leakage at flow rates well below the IPCC's climate-mitigation limits. Nevertheless, the variation in size, gas release rate, and real-current conditions in the bubble model needs to be explored further. Further research for episodic leak cases or a single significant point will complement these findings.

4.2. Soil gas monitoring

Soil gas monitoring methods have been developed over the past few years. Vermeul et al. [119] provide an overview of the design of the monitoring program for the FutureGen 2.0 project, which aims to store CO_2 on a commercial scale in reservoirs. The project is part of an effort to develop a near-zero-emission coal-fired power plant that incorporates CCS technologies. This study describes how the monitoring design is applied to ensure that the CO_2 storage process complies with regulatory requirements. This study successfully designed a monitoring system to address various risks associated with CO_2 storage (Figs. 15 and 16). Timely and accurate monitoring is critical to the success of CCS technologies.

Schroder et al. [120] explored the role of soil flux and groundwater gas monitoring for CO_2 leak detection in a case study conducted in Qinghai, China (Fig. 17). This study emphasizes the use of soil gas measurements to describe CO_2 leakage at the surface, employing techniques such as soil flux measurement and gas migration quantification. This study identified and mapped two CO_2 leak points at the investigated storage sites (Fig. 18). Integrating this method with other methods can enhance leak-detection accuracy, particularly in areas prone to seismic activity and soil variability, which influence gas migration patterns. CO_2 migration in geological formations can be simulated using the Darcy flow equation (Eq. (39)). It can also be written in differential form (Eq. (40)). The Darcy equation is widely used to predict underground CO_2 migration, particularly to ensure the long-term security of storage.

$$Q = -KA_{flow}\frac{\Delta h}{L} \quad \text{(Eq. 39)}$$

$$\vec{u} = -\frac{K}{\mu}\nabla p \quad \text{(Eq. 40)}$$

Shao et al. [121] present a monitoring, verification, and accounting program implemented at the Illinois Basin–Decatur project in the United States. This research focuses explicitly on monitoring groundwater as part of CCS operations. The study results demonstrate the utility of fixed-ground gas and carbon isotopes in identifying CO_2 leaks from underground storage. By tracking temporal changes in gas

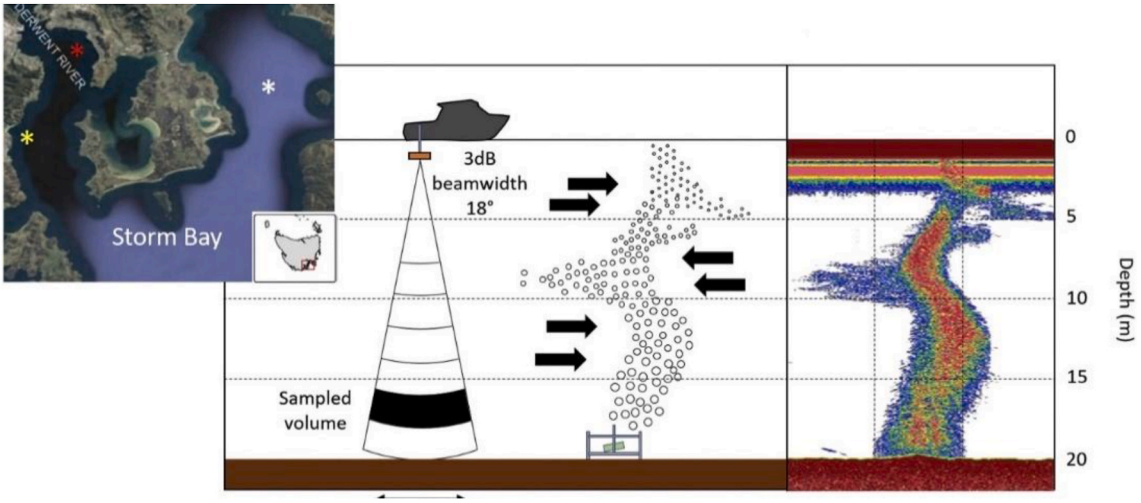

Fig. 14. Illustration of the experimental setup and example of an echogram of the bubble plume [118].

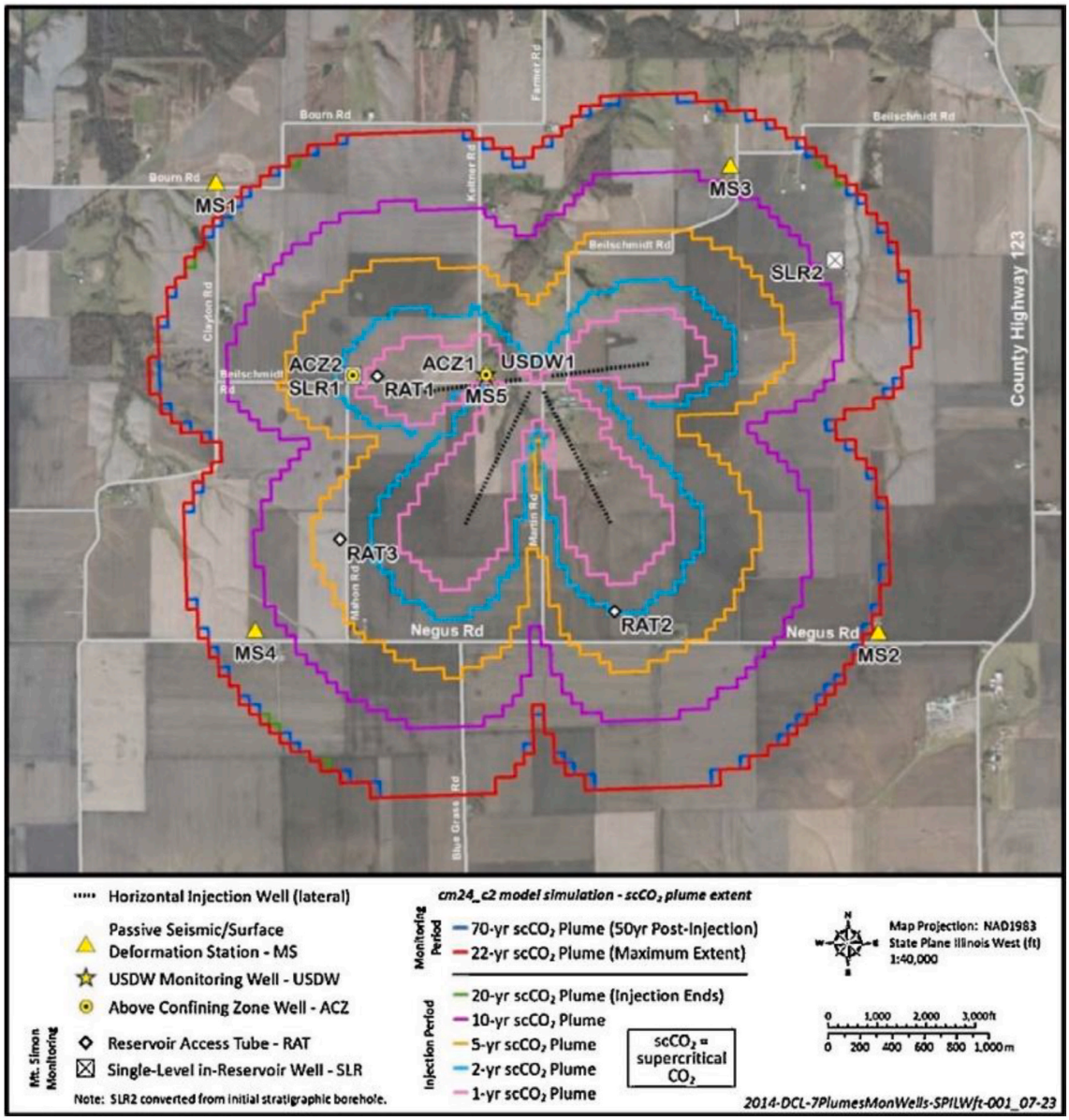

Fig. 15. Monitoring network layout and prediction of supercritical CO_2 (sc-CO_2) plume extent [119].

concentrations, the study provides a detailed picture of CO_2 movement in the soil. The study also examined how various environmental factors, including seasonal fluctuations in temperature and humidity, influence CO_2 flux through the soil. This study suggests that integrating groundwater measurements with other geophysical methods may offer a more comprehensive monitoring strategy for CCS sites. The soil gas monitoring method has proven effective in detecting and measuring CO_2 leakage from CCS sites. Understanding soil gas flux is crucial for enhancing this monitoring technique. Further research should focus on increasing sensitivity and cost efficiency. Integration with other detection methods must be further explored to provide a more comprehensive monitoring framework.

4.3. Geochemical tracer

Geochemical tracers have been investigated for several decades as a monitoring approach for CO_2 storage, with tracer selection commonly influenced by safety, cost, and detection efficiency. The use of noble gases as tracers has received increasing attention in recent years [122–126]. Roberts et al. [127] reviewed the application of geochemical tracers for detecting and quantifying CO_2 leakage from offshore geological storage sites. They highlighted the high investment cost required for tracer deployment and monitoring. Based on cost comparison, artificial tracers (e.g., SF_6, PFCs, and esters) generally exhibit lower implementation costs than natural tracers and noble gas isotopes, making them attractive from an operational perspective (Fig. 19).

In addition to tracer type, the sampling environment plays a significant role in determining monitoring cost. In marine settings, tracer monitoring may require more complex field operations (e.g., vessel-based sampling and underwater deployment) and is affected by tracer dilution and mixing in seawater, which can increase the number of samples and analytical sensitivity required. In contrast, atmospheric monitoring is often associated with simpler sampling logistics and may reduce operational costs for specific tracers. Nevertheless, environmental considerations limit the feasibility of some artificial tracers in offshore applications. Roberts et al. [127] reported that helium and xenon isotopes (e.g., ^{124}Xe and ^{129}Xe) show stable behavior and relatively low environmental impact, supporting their suitability for marine leakage monitoring, whereas SF_6 and ^{14}C were considered less feasible due to environmental concerns. SF_6 is often regarded as unsuitable as a

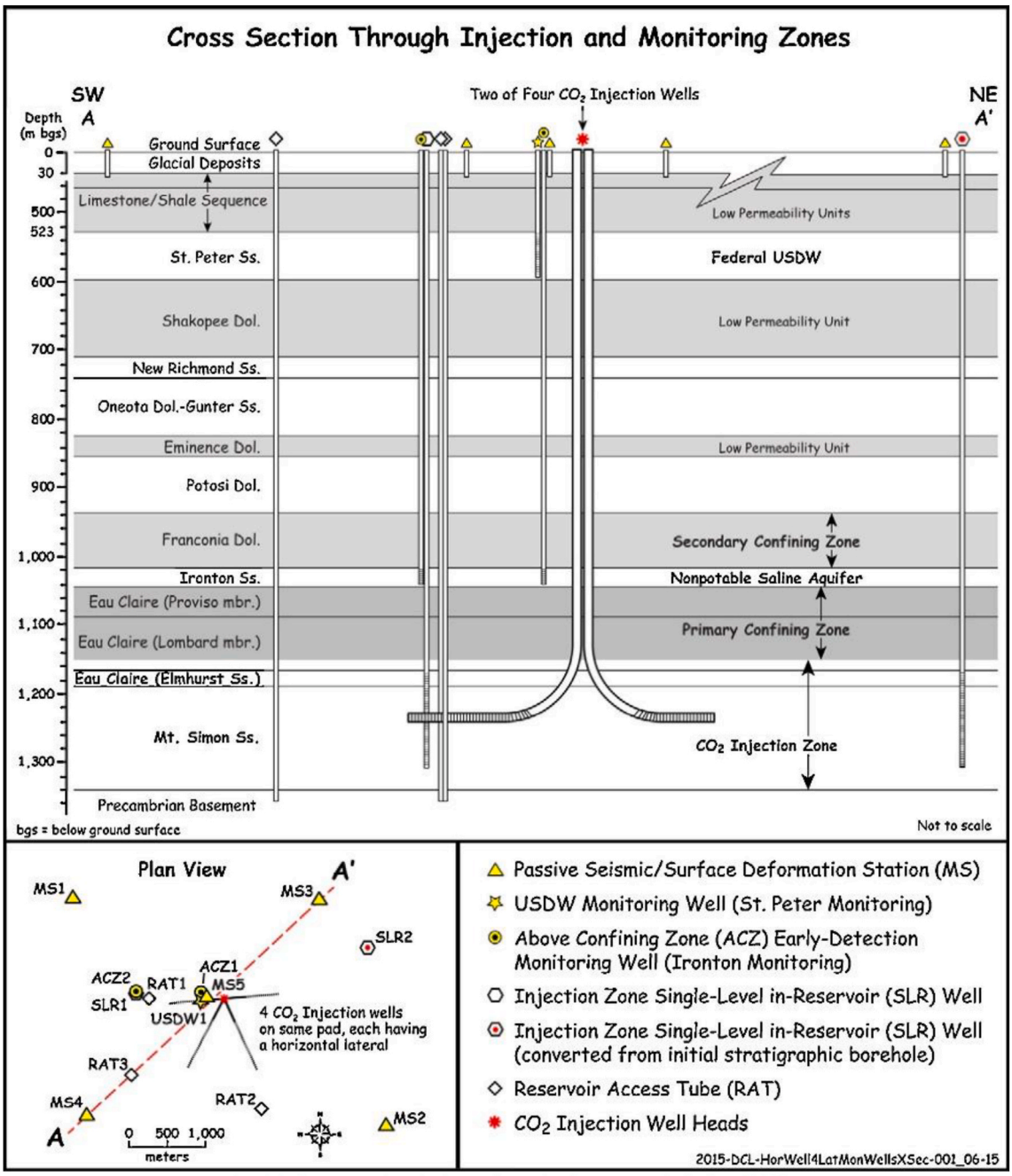

Fig. 16. Cross-sectional view of monitoring network design [119].

tracer for CCS monitoring due to its extremely high global warming potential and long atmospheric lifetime, which raise environmental and regulatory concerns. Similarly, ^{14}C is a radiotracer and may involve additional safety, licensing, and public acceptance challenges, particularly for offshore applications.

A similar study by Flohr et al. [128] evaluated both natural tracers (^{13}C and ^{18}O) and non-toxic gas tracers for offshore leakage detection. The study results indicated that all tested tracers except ^{18}O were able to identify the leakage source, demonstrating the applicability of tracer-based methodologies for large-scale marine monitoring. More recently, Weber et al. [129] investigated noble gases as potential tracers for monitoring CO_2 storage in Norway using on-site mass spectrometry and laboratory analysis. This study's results show that noble gases can be used to track temporal variations and support leakage detection. Further research is required to optimize noble gas tracer monitoring under diverse storage conditions and to improve detection sensitivity using advanced analytical techniques.

4.4. Atmospheric monitoring

The development of atmospheric monitoring methods to detect CO_2 leaks is becoming very important in CCS technologies. Jenkins et al. [130] developed a simple but effective atmospheric monitoring method to detect CO_2 leaks from storage facilities. The developed atmospheric monitoring method is sensor-based and easy to apply for detecting CO_2 leaks (Fig. 20). It provides quick, efficient results without the need for complex or expensive equipment. The study involves testing various atmospheric measurement techniques under multiple conditions to identify the most suitable method. The study results show that the developed atmospheric monitoring method has proven effective at

Fig. 17. Aerial view of the field site and monitoring location of soil gas migration in Qinghai, China [120].

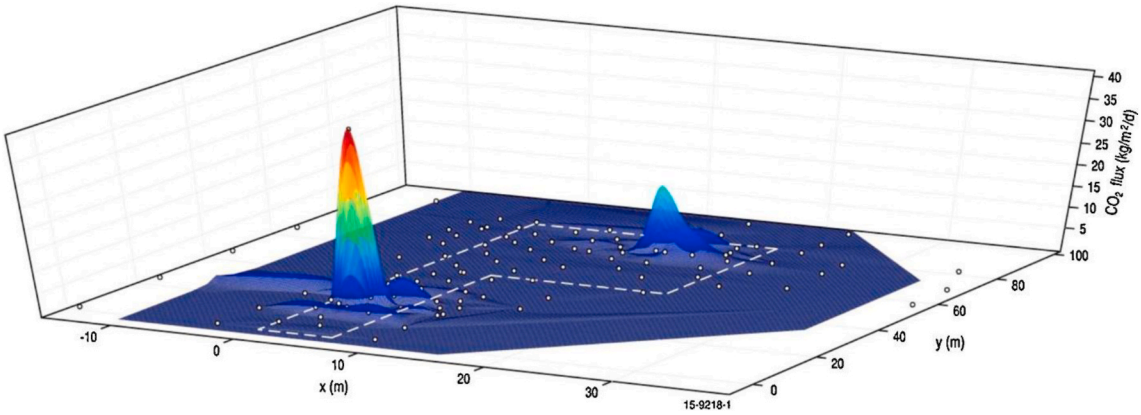

Fig. 18. A 3D surface depicting the distribution of the two principal leak centres based on the measured locations. The white dots indicate the soil flux sampling points [120].

detecting CO_2 leakage at very low concentrations. This technique is instrumental in hard-to-reach areas due to its ease of use and relatively low cost.

Furthermore, atmospheric monitoring in the vicinity of CO_2 storage sites can be conducted using a carbon-isotope approach, which characterizes CO_2 based on the relative abundance of ^{12}C and ^{13}C [131]. The workflow begins with the establishment of a baseline dataset before CO_2 injection, obtained through periodic measurements of atmospheric CO_2 concentrations and their isotopic compositions at multiple monitoring stations. Following the commencement of storage operations, the exact measurements are repeated and subsequently evaluated against both the baseline conditions and the isotopic signature of the injected CO_2. In essence, this method tracks changes in the isotopic fingerprint of atmospheric CO_2. The carbon-isotopic composition of CO_2 is commonly reported as $\delta^{13}C$ calculated using Eq. (41).

$$\delta^{13}C\ (‰) = \left(\frac{R_{sample}}{R_{standard}} - 1\right) \times 1000 \qquad \text{(Eq. 41)}$$

where R_{sample} is the isotopic ratio ($^{13}C/^{12}C$) of the sample, and $R_{standard}$ is the corresponding isotopic ratio of an internationally accepted reference standard. In many CCS applications, captured CO_2 is produced from the combustion of fossil fuels and therefore often exhibits more negative $\delta^{13}C$ values (approximately −25‰ to −35‰) than atmospheric CO_2 (approximately −8‰).

In the event of leakage, near-surface CO_2 concentrations typically increase, and the measured $\delta^{13}C$ values usually shift toward the characteristic signature of reservoir-derived CO_2. Such deviations from baseline conditions may thus provide evidence for additional CO_2 contributions originating from the storage formation. In particular, a sustained progressive departure of measured $\delta^{13}C$ from baseline values,

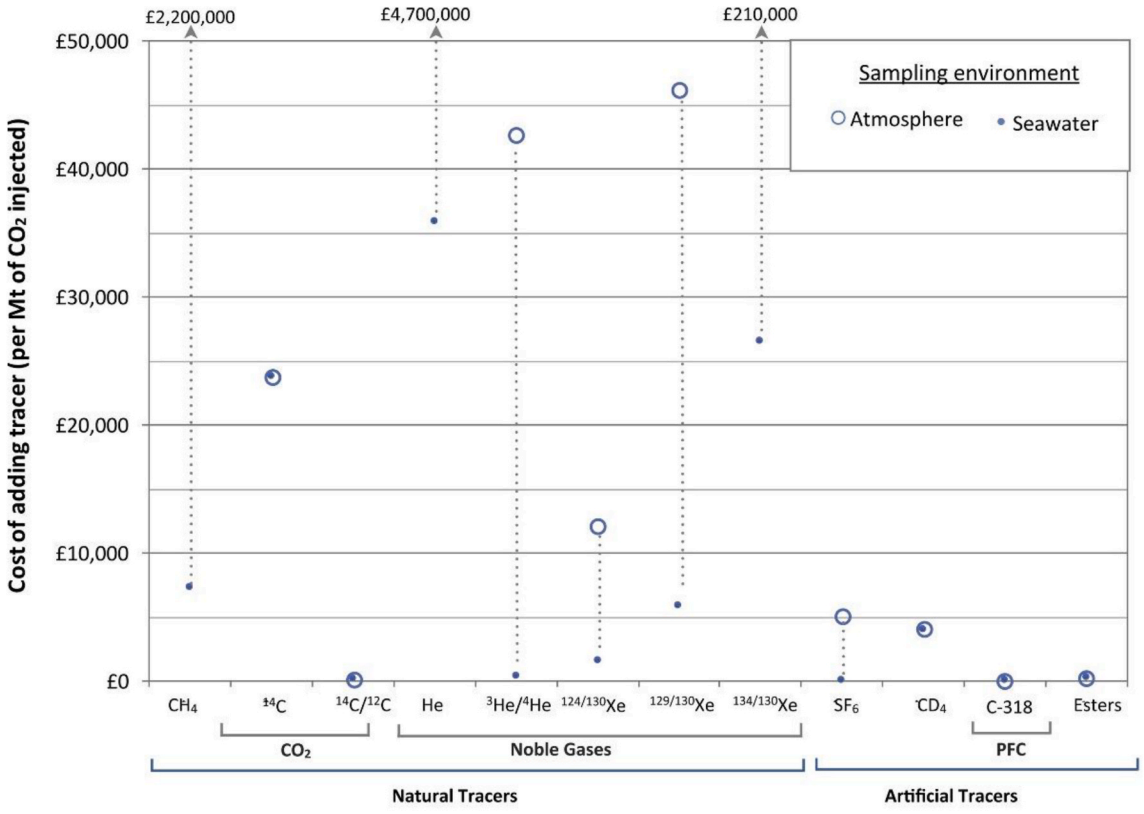

Cost per Mt(CO_2)	Marine environment (seawater)	Terrestrial environment (atmosphere)
£1-100	$^{14}C/^{12}C$ in CO_2, PFCs, SF_6	$^{14}C/^{12}C$ in CO_2, PFCs
£100-1,000	Esters, $^{3}He/^{4}He$	Esters
£1,000-10,000	$^{124,129}Xe/^{130}Xe$, CD_4, CH_4	CD_4, SF_6
£10,000 - 100,000	^{14}C in CO_2, He, $^{134}Xe/^{130}Xe$	^{14}C in CO_2, $^{124,129}Xe/^{130}Xe$, $^{3}He/^{4}He$
£100,000 - 1,000,000	$^{80,83,86}Kr/^{84}Kr$, $^{132}Xe/^{130}Xe$, $^{13}C/^{12}C$	$^{134,132}Xe/^{130}Xe$

Fig. 19. Estimated cost of adding different tracers per Mt of injected CO_2, comparing sampling environments (atmosphere vs seawater) [127].

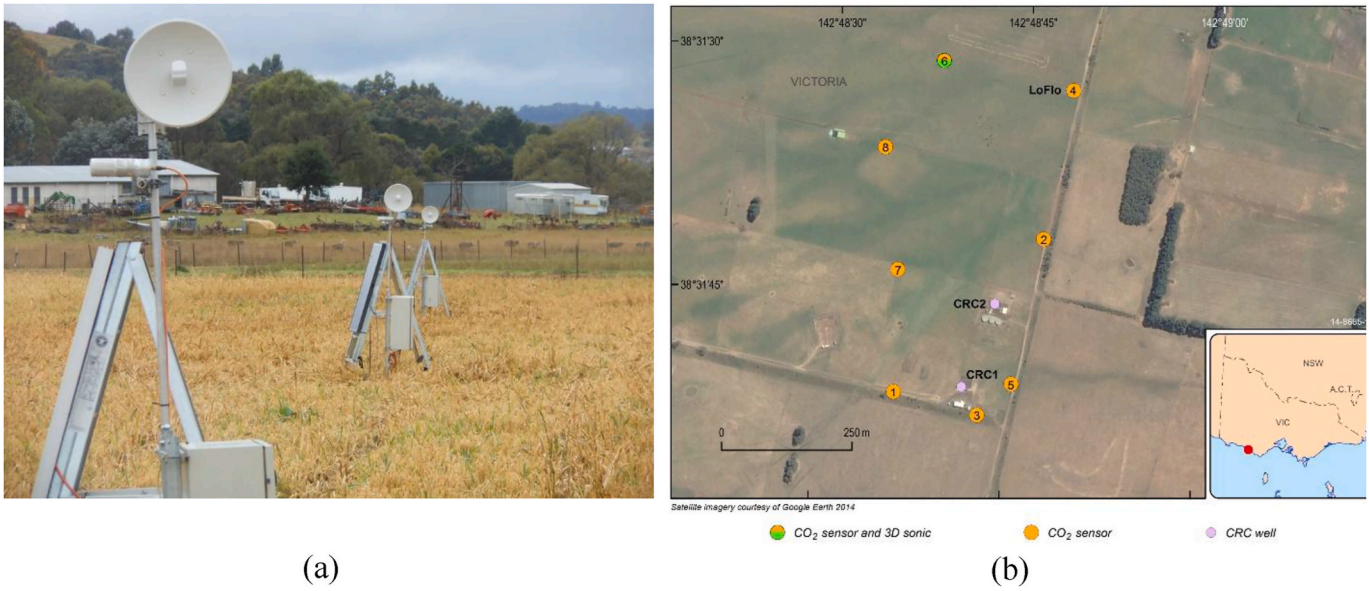

Fig. 20. (a) Three monitoring platforms are operational at Australia's Ginninderra test site; (b) aerial view of the test location captured via Google Earth satellite mapping [130].

accompanied by convergence toward the isotopic composition of the injected CO_2, can be interpreted as an indicator that CO_2 from the storage system is likely emerging into the near-surface environment.

Meanwhile, Turnbull et al. [132] focus on using radiocarbon to detect CO_2 leakage, specifically distinguishing between CO_2 derived from fossils and other sources. By measuring the concentration of radiocarbon (^{14}C) in CO_2 released into the atmosphere, it is possible to determine the source of the leak. This method is more complex but more accurate at identifying the source of leaking CO_2. Radiocarbon measurements in CO_2 enable precise leak detection, as radiocarbon is only found in CO_2 derived from fossil fuels. These results suggest that using radiocarbon as an indicator of leakage can greatly benefit long-term monitoring.

New methods, such as drones, IoT, and satellite monitoring, offer more cost-effective and flexible solutions. Satellite-based tracking, for example, is being considered an alternative to monitoring leaks from large-scale CCS facilities. With hyperspectral sensors that detect atmospheric CO_2, satellites can help monitor large areas and provide macro perspectives on carbon emissions and storage dynamics. However, this method still needs refinement to deliver high-accuracy data to various weather conditions. Improving monitoring efficiency will be key to scaling up CCS implementation in the long run. Further study is needed to develop a more sensitive monitoring method to generate real-time data.

5. Advances in corrosion control and structural integrity for long-term CCS operation

CCS infrastructure must be carefully designed to ensure safety against potential failures. Various factors can contribute to failures in CCS technologies, including inappropriate material selection and inadequate structural design under extreme operating conditions. Materials used in CCS infrastructure are therefore required to exhibit adequate mechanical, thermal, and chemical properties. Failures may occur at different stages of operation, from CO_2 capture to transport and storage. Pipelines are among the most widely used components in CCS systems, and corrosion and erosion in pipelines represent critical and urgent challenges, as they can significantly compromise structural integrity [133,134]. Various solutions have been developed to address this challenge, including coating materials that can extend their lifespan and increase their corrosion resistance. Coating materials, when applied correctly, can provide an effective protective layer against corrosion, enhance structural integrity, and reduce the frequency of component maintenance or replacement.

Additionally, the challenge at the storage stage is that components must directly address mechanical and thermal loads. This component is an interesting object to study. This study will review the development of research related to the above issues, providing an overview of how material innovation can play a crucial role in ensuring the long-term success of CCS technologies implementation.

5.1. Corrosion challenges

Corrosion phenomena are the leading cause of frequent failures in the CCS piping system [135,136]. CO_2 dissolved in water forms carbonic acid (H_2CO_3) as in Eq. (42), which correlates carbon steel (Fe) to form iron carbonate ($FeCO_3$) (Eq. (43)). The $FeCO_3$ layer is porous and unstable at high pressures, increasing the risk of infrastructure failure. The CO_2 corrosion rate in steel pipeline can be predicted using the De Waard–Milliams semi-empirical model (Eq. (44)). For example, Table 5 presents the corrosion rate of several types of materials that can be used for CCS technologies.

$$CO_2(g) + H_2O(l) \leftrightarrow H_2CO_3(aq) \quad \text{(Eq. 42)}$$

$$Fe(s) + H_2CO_3(aq) \rightarrow FeCO_3(s) + H_2(g) \quad \text{(Eq. 43)}$$

Table 5
Corrosion rates of various materials (mm/year) [47].

Material	Solution with 20% wt MEA	Solution with 20% wt MEA
Monel	0.025	0.076
302 and 304 Stainless steel	<0.025	0
316 Stainless steel	0.025	<0.025
410 Stainless steel	0.025	0
Carbon steel	0.025	3.302

$$CR = M \times f_{CO_2}^{0.67} e^{\left(\frac{E_a}{RT}\right)} \quad \text{(Eq. 44)}$$

Selecting appropriate material for corrosive environments is a crucial aspect to avoid structural failure. Pfennig and Kranzmann [137] investigated the corrosion resistance of steel pipelines used in the CO_2 injection process (Fig. 21). The primary method employed was a long-term laboratory experiment in which steel samples were exposed to CO_2-saturated synthetic aquifer water at 60 °C for periods of up to two years. The materials tested in this study were 42CrMo4, X46Cr13, X20Cr13, and X35CrMo17 steels, which differ in their chromium (Cr) and carbon (C) content (Table 6).

After heat treatment and exposure, the sample is analyzed using light microscopy, scanning electron microscopy (SEM), and X-ray diffraction (XRD) to identify the phases that form and measure the corrosion rate. This study examines onshore CO_2 storage conditions in the field, particularly the simulation of interactions between the liquid and gaseous phases of CO_2 (Fig. 22). The results show that steels with higher Cr and lower C content exhibit better corrosion resistance than those with low Cr and high C content. This result was due to the formation of a more stable passivation layer during the experiment. The observed corrosion rate ranged from 0.1 to 0.8 mm/year, depending on the exposure phase, with the most severe corrosion occurring in the water-saturated vapor phase. The corrosion layer primarily consists of siderite ($FeCO_3$), goethite (FeOOH), iron oxides, and sulfides. After 1 year of exposure, the corrosion rate tends to stabilize because the dense corrosion layer limits ion diffusion; therefore, 1 year is sufficient to estimate long-term behavior.

Furthermore, Tang et al. [139] investigated the corrosion behavior of X65-type carbon steel in the sc-CO_2 phase, which contains water vapor (H_2O) and oxygen (O_2). This study uses a combination of weight-loss test methods and electrochemical measurements to understand the corrosion mechanism and rate. Furthermore, surface analysis using a SEM, XRD, an energy-dispersive spectrometer (EDS), and X-ray photoelectron spectroscopy (XPS) was employed to identify the morphology and composition of the corrosion products. The results showed that corrosion of X65 steel in saturated sc-CO_2, free of oxygen, was relatively low, with a corrosion rate of about 0.25 mm/year. A dense and homogeneous protective layer of ferrocarbonate ($FeCO_3$) forms on the surface of the steel under these conditions. Adding oxygen in small amounts (95–475 mg/L) increases the corrosion rate to 0.9–1.5 mm/year. SEM and EDS analysis revealed that oxygen can inhibit the formation of $FeCO_3$ protective layers and promote the formation of a looser and less effective Fe-oxide layer that protects steel surfaces (Fig. 23).

Most recently, Huang et al. [140] developed a predictive model for erosion–corrosion damage in carbon steel pipelines under CO_2 environment. The proposed approach integrates a multiphase flow model, an erosion model, and a CO_2 corrosion model into a unified prediction framework, accounting for the synergistic interaction between erosion and corrosion. The multiphase flow was simulated using CFD based on the Eulerian–Lagrangian discrete particle method (DPM) approach, which enables realistic prediction of solid particle trajectories within the fluid. The numerical simulations were conducted using a three-dimensional elbow geometry (Fig. 24). The CO_2 corrosion model

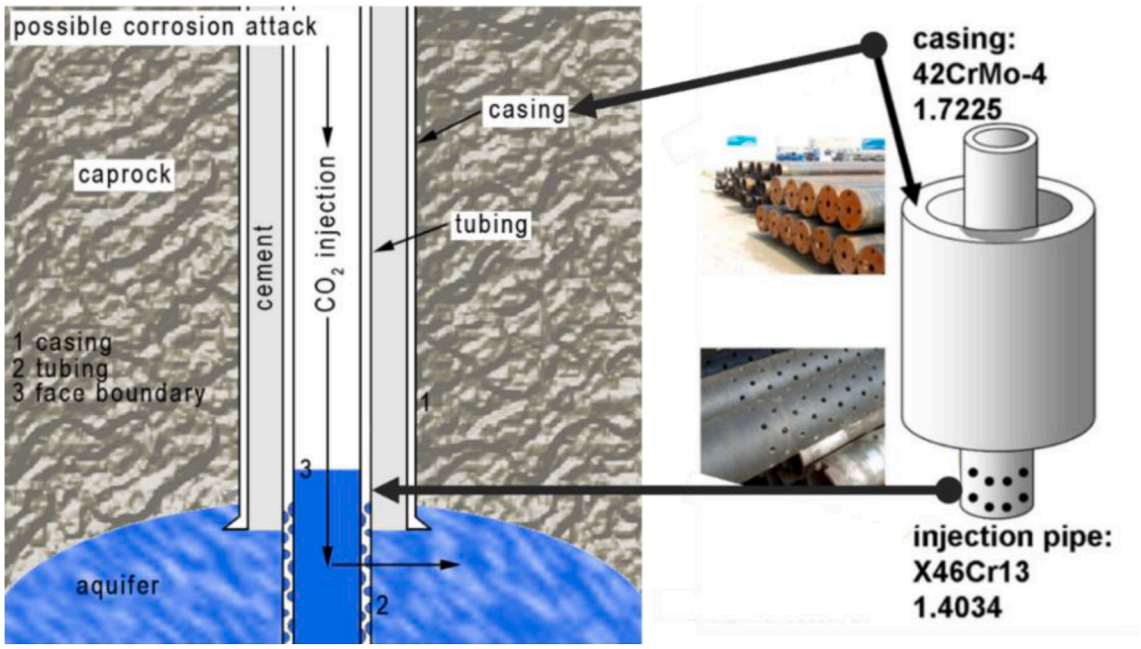

Fig. 21. Casing and tubing of the CCS wellbore [137].

Table 6
Chemical composition of pipeline materials commonly used in CCS (mass %) [137,138].

Element	42CrMo4 (AISI 4140)	X35CrMo17 (AISI 4140)	X20Cr13 (AISI 420J)	X46Cr13 (AISI 420C)	X5CrNiMoCuNb16-4 (AISI 630)
C	0.38–0.45	0.33–0.45	0.17-0.25	0.42–0.50	<0.07
Si	<0.40	≤1.00	≤1.00	<1.00	<0.70
Mn	0.60–0.90	≤1.00	≤1.00	<1.00	<1.50
P	<0.035	≤0.045	≤0.045	<0.045	<0.04
S	<0.035	≤0.030	≤0.030	<0.030	<0.015
Cr	0.90–1.20	15.50–17.50	12.0–14.0	12.5–14.5	15.0-17.0
Mo	0.15–0.30	0.80–1.30		0.03	<0.60
Ni	0.04	≤1.00	0.123	0.13	3.00-5.00
Co	<0.01			0.03	
Fe	97.1			85.4	
Cu					3.00-5.00
Nb					0.20-0.45

adopted was the empirical NORSOK M − 506 model, which was modified and validated through experimental tests on N80 carbon steel material. The results indicated that the maximum erosion rate occurred on the outer wall of the elbow, due to inertial and centrifugal forces acting on the solid particles. In contrast, the highest corrosion rate was observed on the inner wall of the elbow due to the influence of fluid velocity, which damaged the protective $FeCO_3$ layer (Fig. 25). Both erosion and corrosion were found to contribute significantly to damage in CO_2 pipelines. Erosion reduces wall thickness, thereby increasing the likelihood of structural failure.

5.2. *Material protection against the erosion-corrosion problem*

Recent studies aimed at improving the corrosion resistance of materials used in CCS technologies have led to the development of various protection strategies. Wu et al. [141] proposed an intelligent protective concept based on a magnesium metal anode to mitigate corrosion of concrete-encased carbon steel in CO_2 storage facilities (Fig. 26a). The study highlights the carbonation of concrete induced by CO_2 exposure, which reduces the alkalinity of the pore solution and subsequently decreases its pH level. Electrochemical tests were performed to compare the corrosion behavior of metallic Mg(s), Al(s), and Zn(s) anodes in simulated concrete pore solutions (SCPS) with varying pH values, representing different degrees of carbonation (Fig. 26b).

After exposure, surface morphology and corrosion products were analyzed using optical microscopy and SEM. The results demonstrated that the Mg(s) anode provided more effective cathodic protection than Al(s) and Zn(s). Furthermore, the Mg-based anode system can indirectly indicate the carbonation level of concrete, as its electrochemical activity increases with decreasing pH. This behavior is attributed to the unique electrochemical response of magnesium: Mg is relatively passive at high pH due to the stability of surface films, but becomes activated when the pH drops, promoting magnesium dissolution (Eq. (45)) and producing sufficient protective current to reduce steel corrosion (Fig. 27). In contrast, conventional anode materials such as Al(s) and Zn(s) do not exhibit the same pH-sensitive activation behavior, limiting their effectiveness under carbonation-induced low-pH conditions.

$$Mg(s) \rightarrow Mg^{2+} + 2e^{-} \quad \text{(Eq. 45)}$$

Another solution to facing corrosion challenges is to develop coating materials. The function of this coating material is to minimize contact with component surfaces with corrosive substances. Sun et al. [142] investigated composite coatings that offer greater resistance to the corrosive effects of CO_2 and impurities. This research develops an epoxy resin (EP)-based anticorrosive protective layer reinforced with graphene-C_3N_4 (g-C_3N_4-EP) and epoxy silane oligomer (ESO) nanosheets to deal with corrosive CCS environments. The g-C_3N_4-EP coating material improves corrosion resistance by absorbing CO_2 gas and preventing the

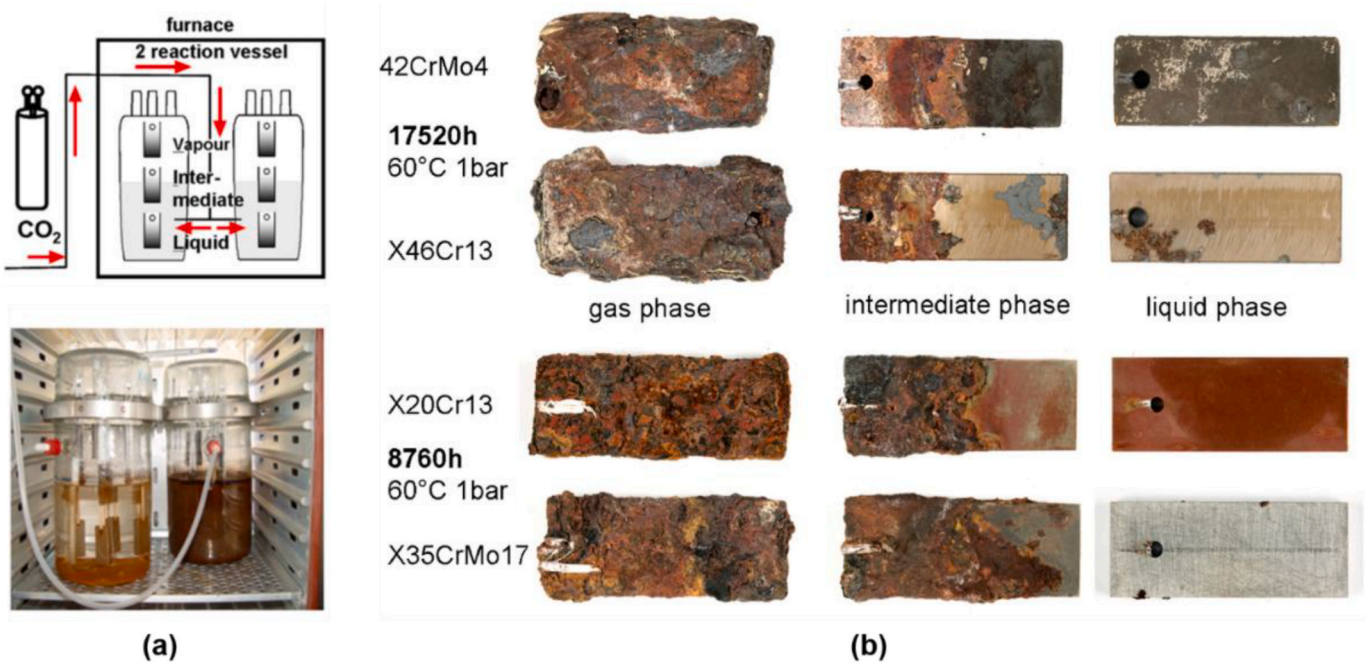

Fig. 22. (a) Experimental setup, and (b) experiment result on corrosion after long-term exposure in a CCS environment [137].

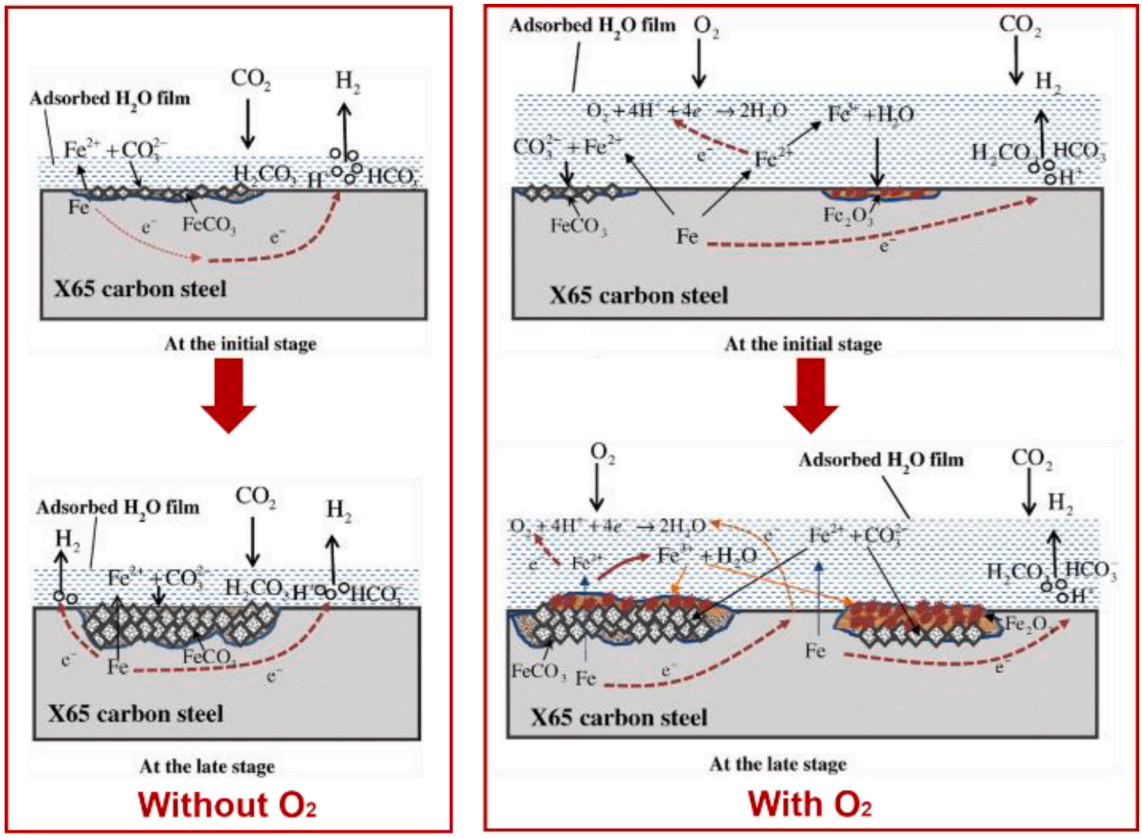

Fig. 23. Schematic X65 carbon steel corrosion mechanism diagram in H_2O-saturated sc-CO_2 phase [139].

diffusion of corrosive ions. The addition of ESO enhances adhesion between the resin and the nanosheet via bonding, thereby reducing surface defects in the coating. The g-C_3N_4-ESO-EP coating demonstrates 99.99% protection efficiency in acidic environments and exhibits long-term corrosion resistance (Fig. 28), offering a novel solution for protecting metal materials.

Pfennig et al. [138] explored the potential of alumina-isolated-based or Boehmit coatings to improve the corrosion resistance of high alloy steels in CCS environments. The X20Cr13 and X5CrNiMoCuNb16-4 steel grades are coated with a water-based alumina and ethanol solution by

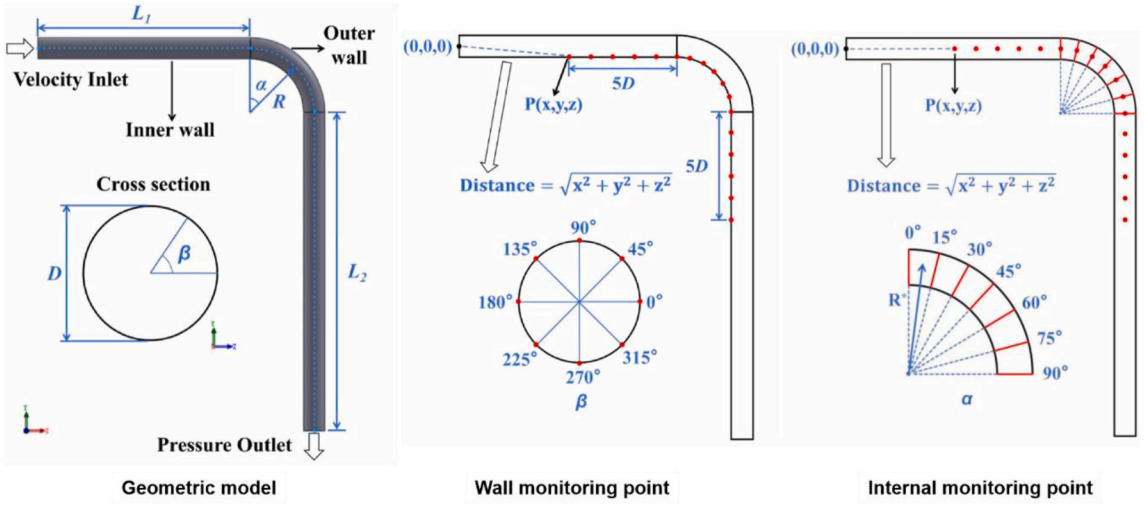

Fig. 24. Model geometry and monitoring point [140].

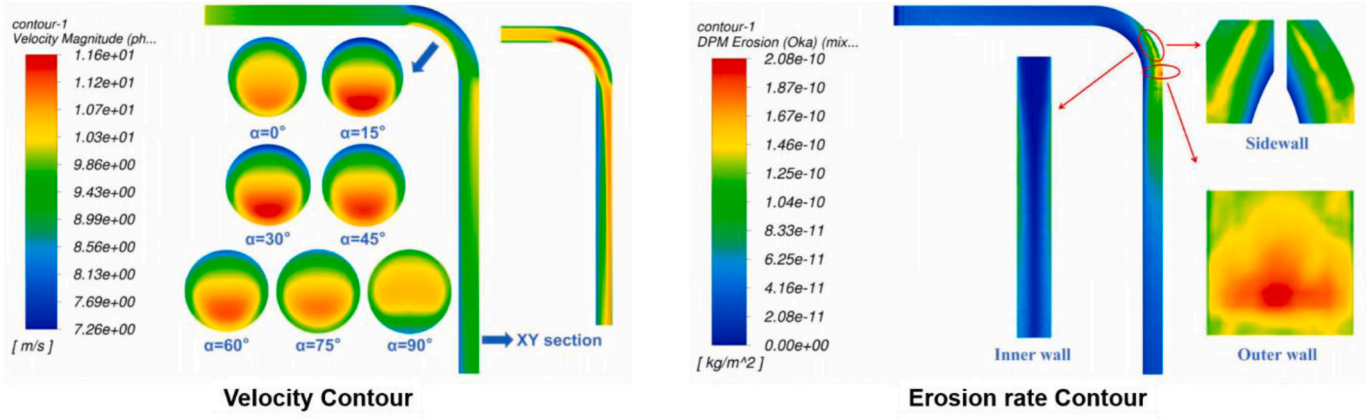

Fig. 25. Simulation result: velocity and erosion rate distribution [140].

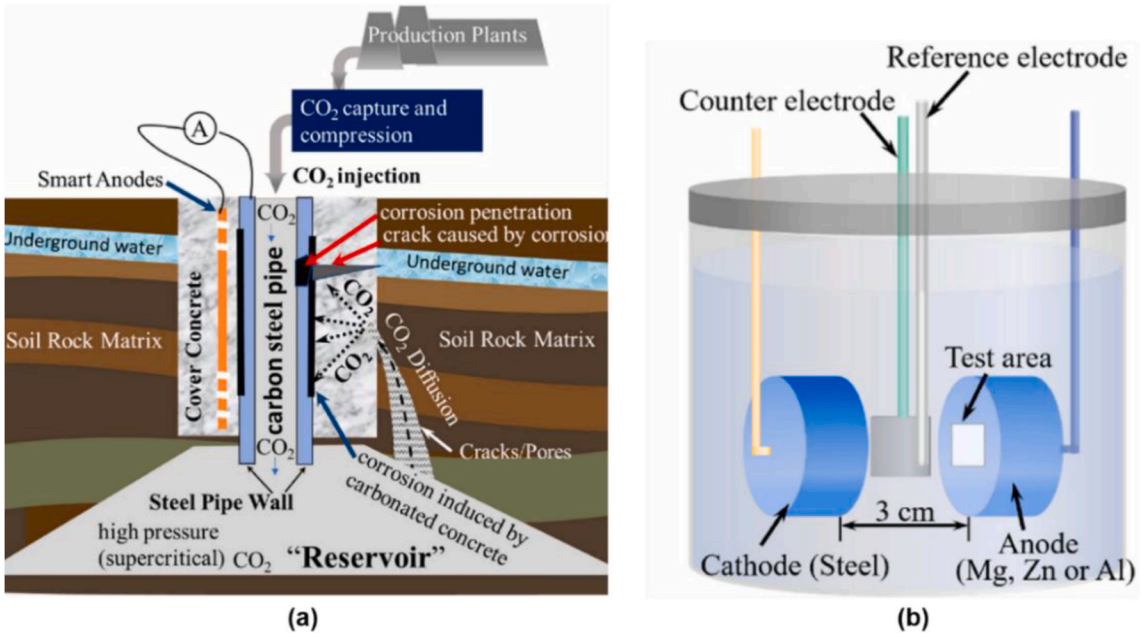

Fig. 26. Illustration of: (a) magnesium (Mg) innovative anode system for corrosion monitoring and prevention in CO_2 Storage, and (b) galvanic corrosion test [141].

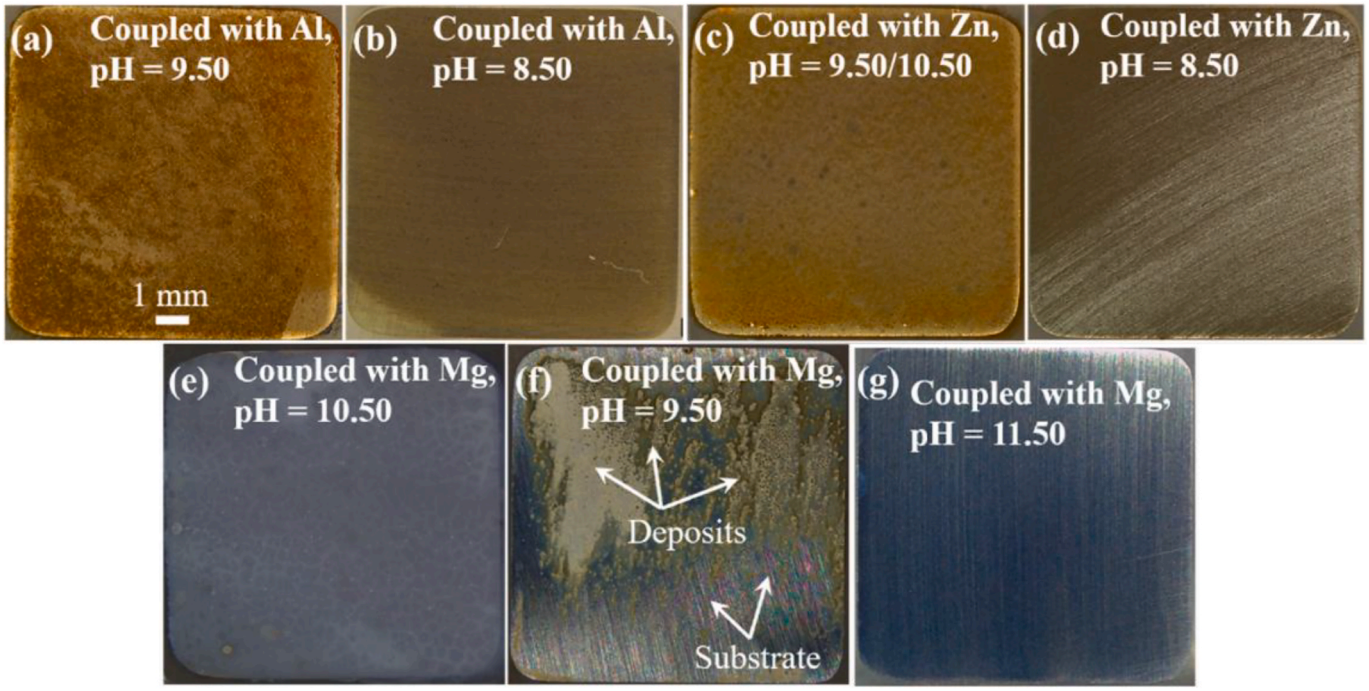

Fig. 27. Surface morphology of specimens after galvanic corrosion tests [141].

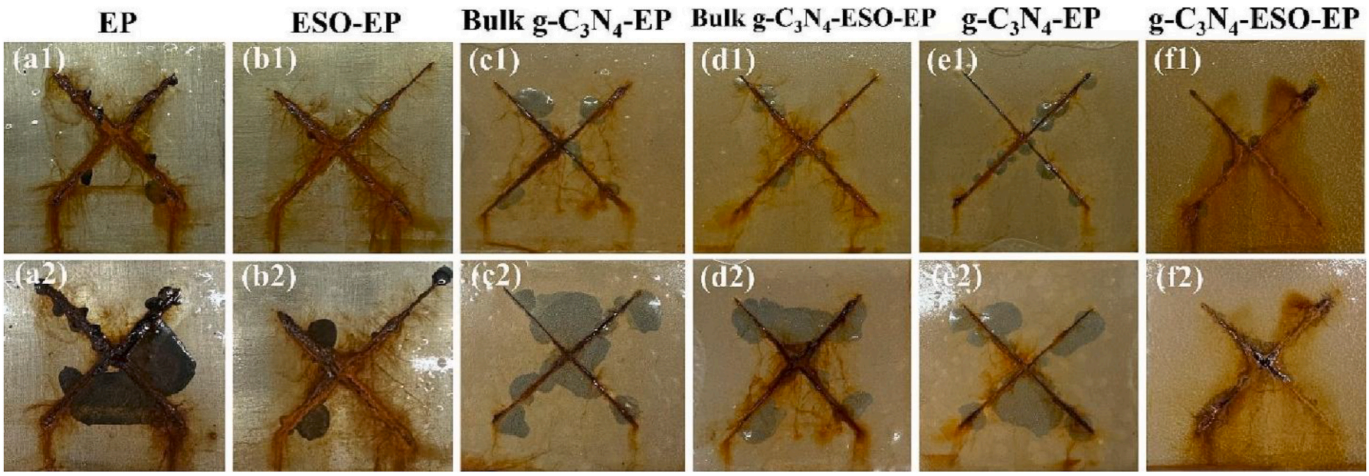

Fig. 28. Visual comparison of salt-spray corrosion progression: (a1–f1) after 200 h and (a2–f2) after 1000 h of exposure [142].

dip coating, followed by heat treatment in an inert atmosphere at 500 °C. After that, the sample was immersed in CO_2-saturated saline aquifer water for 1000 h at atmospheric pressure and 60 °C. Corrosion fatigue behavior was tested on specimens using a resonance machine at various stress amplitudes. The results showed that the alumina layer underwent premature spallation (Fig. 29), rendering the coating ineffective in providing protection. The coating is inhomogeneous and prone to cracking, allowing CO_2-saturated saline aquifer water to enter and initiate corrosion beneath it. The alumina coating also does not improve the specimen's corrosion fatigue resistance. Due to the peeling layer, corrosion pitting can turn into fatigue cracks. Sol-gel alumina coatings are effective at high temperatures and in water-free atmospheres. However, this study shows that this type of coating is unsuitable for wet, corrosive CCS applications. Therefore, further research is not recommended.

Furthermore, Li et al. [143] investigated the effect of laser cladding using a 431M2 coating material on the corrosion resistance of stainless steel pipes. The experiment was conducted to simulate an O_2-containing CO_2 environment with a pH ranging from 2.0 to 4.0. Two coating methods were studied: extreme high-speed laser cladding (EHLC) and conventional laser cladding (CL) (Fig. 30), with the corresponding manufacturing process parameters listed in Table 7.

The results showed that EHLC coating provides better corrosion resistance than CL coating. The superior corrosion resistance of EHLC coatings is attributed to their finer dendrite size, increased grain boundaries, and reduced element segregation (Fig. 31). Decreasing pH reduces corrosion resistance by increasing defects in the passivation layer. However, the high Cr_2O_3 content in the passivation layer maintains corrosion resistance even at low pH.

A review of various corrosion protection methods for CCS technologies has been presented. The cathodic protection method using an intelligent Mg anode offers advantages and is feasible for CO_2 wellbore applications. Furthermore, the coating protection method also provides several benefits. Composite coatings offer several advantages over

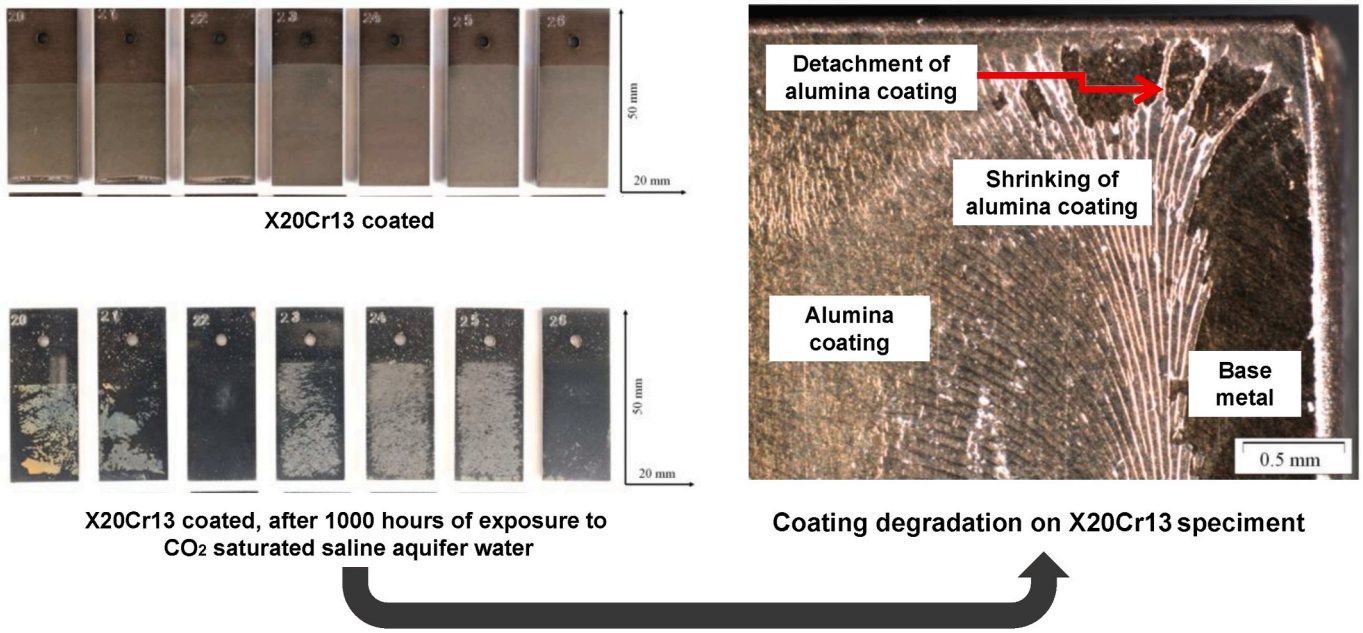

Fig. 29. Coating degradation on X20Cr13 martensitic stainless steel after 1000-h exposure to CO_2-saturated saline aquifer water at 60 °C and atmospheric pressure [138].

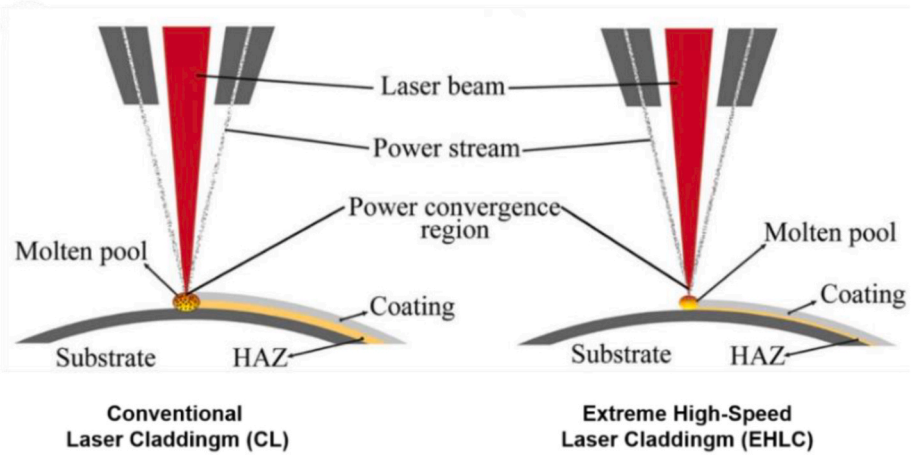

Fig. 30. Conceptual diagram of CL and EHLC [143].

Table 7
Coatings parameter [143].

Parameter	Unit	Optimized value	
		CL	EHLC
Laser power	W	1900	5100
Deposited Speed	m/min	1.5	22
Overlapping ratio	(%)	40	80
Powder flow rate	g/min	14.8	37
Avg. single thickness	mm	0.9	0.4
Laser focus	mm	0	2
Powder focus	mm	0	2
Shielding gas flow rate	L/min	9	9

traditional metal coatings for CCS applications, particularly in terms of long-term durability and dual protection. Traditional metal coatings are more commonly used due to their ease of application and lower cost, though they tend to offer less resistance to extreme conditions. The use of alumina-sole coatings on alloy steels shows significant potential to improve their corrosion resistance. However, it is worth noting that the environmental impact of the chemicals used should be considered in future research. Laser cladding also offers significant advantages. However, further investigation is needed regarding its economic feasibility and long-term durability if used for CCS applications under varying conditions.

5.3. Research on cement material to improve the wellbore integrity

The integrity of CO_2 storage wells is greatly influenced by the quality of the materials and structural design used. Storage wells, which serve as pathways for CO_2 injection into geological formations, can leak if not designed appropriately. The most critical part lies in the well casing, which experiences extreme pressure and is susceptible to chemical reactions. Research on the wellbore's ability to withstand long-term operating loads is of significant concern. This aspect is crucial as it concerns the sustainability of CO_2 storage facilities. The development of cement materials to enhance wellbore integrity in CCS technologies has shown significant progress in recent years. A high-quality cement

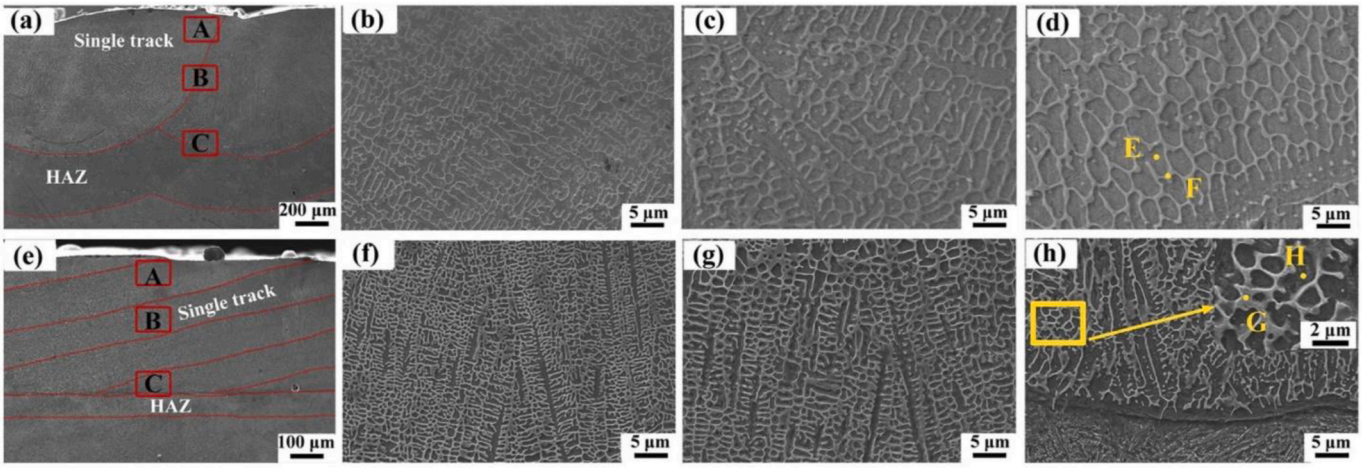

Fig. 31. The cross-sectional macroscopic and microscopic view of the coatings: (a–d) CL, (e–h) EHLC [143].

material will improve the ability to maintain waterproofing and prevent gas leakage at geological storage sites.

Research on stress corrosion in cement exposed to CO_2 by Gu et al. [144] revealed that the reaction between cement and CO_2-saturated brine can dissolve portlandite, the main component in cement. This phenomenon can increase porosity and decrease pressure resistance. This study introduces a novel approach to enhance cement formulations, thereby improving their resistance to such reactions and maintaining wellbore integrity in CCS applications. The study also investigated the combined effect of carbonation and tensile stress on cement materials for CCS well applications, showing that tensile stress accelerates microcrack formation and corrosion (Fig. 32).

Nasvi et al. [145], discussing the effect of carbonation on cement in CCS applications, suggest that carbonation can increase porosity and permeability, thereby affecting the wellbore stability. This result shows the need to develop cement that is more resistant to extreme, corrosive CO_2 conditions. Further studies by Ozyurtkan and Radonjic [146] have demonstrated that incorporating mineral additives, such as fly ash and slag, can enhance cement's resistance to CO_2 while increasing its mechanical strength. This study highlights the importance of additives that enhance cement's resistance to chemical reactions in CCS. Furthermore, Ponzi et al. [147] suggested that better cement formulations could be achieved by using additives that improve cement's resistance to extreme environmental effects of CO_2. The additive in question is basalt powder with a variation of 0–5 [wt.%]. The study results showed that adding basalt powder at a certain level can significantly increase compressive strength and decrease porosity compared to the control without additives (Table 8).

Most recently, Zheng et al. [148] further investigated the role of mineral composition in cement, providing more stable and durable

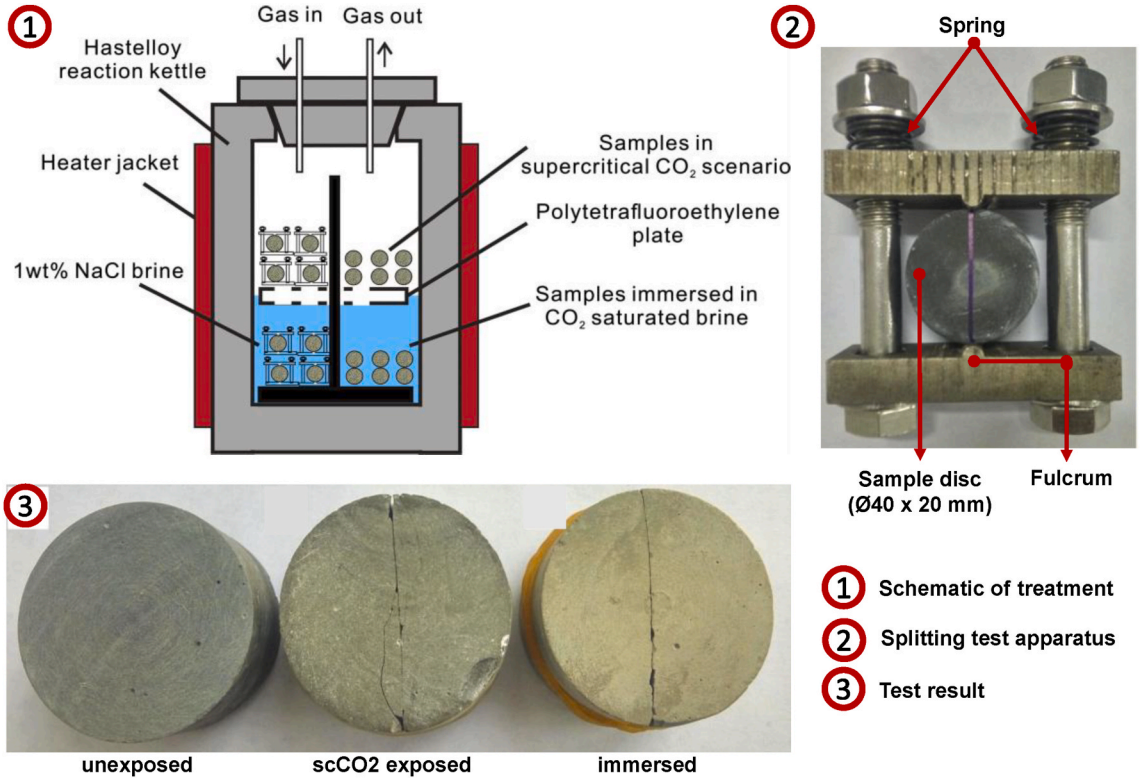

Fig. 32. Experimental procedure for cement stress corrosion study [144].

Table 8
Porosity and compressive strength of cement formulations with basalt powder before (initial) and after (final) carbonation [147].

Basalt Powder [wt.%]	Water-Solid Ratio (W/S)	Porosity [mm^3 %]		Compressive Strength [MPa]	
		Before Carbonation (Initial)	After Carbonation (Final	Before Carbonation (Initial)	After Carbonation (Final
0	0.44	0.49	0.4	28.0 ± 3.6	42.0 ± 8.9
0.25	0.439	0.12	0.08	23.7 ± 3.1	45.3 ± 7.5
0.5	0.438	0.08	0.08	57.7 ± 4.2	52.7 ± 18.8
1	0.436	0.66	0.6	50.7 ± 13.6	40.0 ± 4.0
2.5	0.429	1.06	1.28	42.3 ± 5.0	42.7 ± 2.4
5	0.419	0.35	0.29	45.7 ± 10.2	33.7 ± 11.4

results for CCS applications. This study also demonstrated the potential for additive improvements in cement quality through innovative, more environmentally friendly methods. The study proposes applying a strength calculation model to cement exposed to CCS conditions to obtain more accurate results, thereby enabling more accurate long-term cement strength estimates.

6. Economic challenges: CCS implementation cost

The investment cost of CCS technologies consists of three main components. First, carbon capture is the most expensive component because it requires complex technology and structures. Second, the cost of carbon transport includes the construction of infrastructure such as pipelines to transport CO_2 from emission sources to storage sites. The distance and geographical conditions between the source and the storage location influence these costs. More advanced infrastructure can lower the cost per unit of carbon moved, but it increases the initial investment cost. Third, carbon storage costs are associated with injecting CO_2 into underground geological formations, such as saline aquifers or oil and gas fields that are no longer productive. Assessment of storage locations through geological studies is essential to ensure long-term safety and significantly affects costs. These costs also include long-term monitoring and maintenance to prevent CO_2 leakage, as well as compliance with government regulations and policies governing CCS. Although CCS investment is still high, techno-economic studies continue to be conducted to identify the most efficient financing scenarios. Local case studies can also serve as a reference for broader applications.

6.1. CCS implementation in the heat and energy sector

Research by Rubin et al. [58] examined the cost of CO_2 capture and storage for fossil power plants and compared the assessment results with the costs reported in the 2005 Intergovernmental Panel on Climate Change (IPCC) special report on carbon dioxide capture and storage (SRCCS). The methodology used is similar to that used in SRCCS. Specifically, it reviews and analyzes the latest cost studies for various CCS implementations. Some of the objects studied include (1) post-combustion capture in supercritical pulverized coal (SCPC) power plants and natural gas combined cycle power plants (NGCC); (2) pre-combustion capture at IGCC coal-fired power plants, and (3) oxy-combustion capture at SCPC power plants. All costs are adjusted to the value of the 2013 U S. dollar using the capital, fuel, and operating cost indices to facilitate valid comparisons with historical data. The results show that although the capital cost of the three main types of power plants (NGCC, SCPC, and IGCC) increased by up to 60%, the levelized cost of electricity (LCOE) for plants with and without CCS was relatively stable compared to the old data after inflation adjustments and fuel price increases. The cost of CO_2 mitigation is also not significantly different, with the potential for substantial cost reductions if CO_2 is sold for enhanced oil recovery (EOR). In addition, the post-combustion capture pathway for coal is now more competitive than the pre-combustion approach at IGCC, and oxy-combustion promises a balanced competition.

Furthermore, Roussanaly et al. [149] present a techno-economic analysis of natural gas-fired offshore power plants that utilize CCS. This concept is referred to as clean electricity production from offshore natural gas (CEPONG), as illustrated in Fig. 33. The study considers two main aspects: onshore and offshore oil and gas installation electricity supply. The technical model involves utilizing offshore gas turbines, MEA-based CO_2 capture units, and CO_2 transport and storage systems to saline aquifers or EOR sites.

$$LCOE = \frac{Annualized\ investment + Annual\ OPEX}{Anual\ net\ electricity\ output} \quad \text{(Eq. 46)}$$

This study found that in the onshore electricity market, the CEPONG concept has an LCOE (Eq. (46)) of 178–258 USD/MWh. This value is higher than that of onshore power plants with CCS technologies, which typically range from 94 to 97 USD/MWh. However, CEPONG is more competitive in the electricity market in offshore oil and gas platforms. The LCOE of the CEPONG concept can be reduced to 137 USD/MWh, which is lower than that of onshore plants, which range from 133 to 166 USD/MWh. The technical analysis results indicate that the CCS process's energy consumption results in a decrease in net electricity power of approximately 95 MW, from a total capacity of 733 MW. This result is due to the study also identifying significant cost reduction opportunities through the use of more advanced CO_2 capture technologies, the

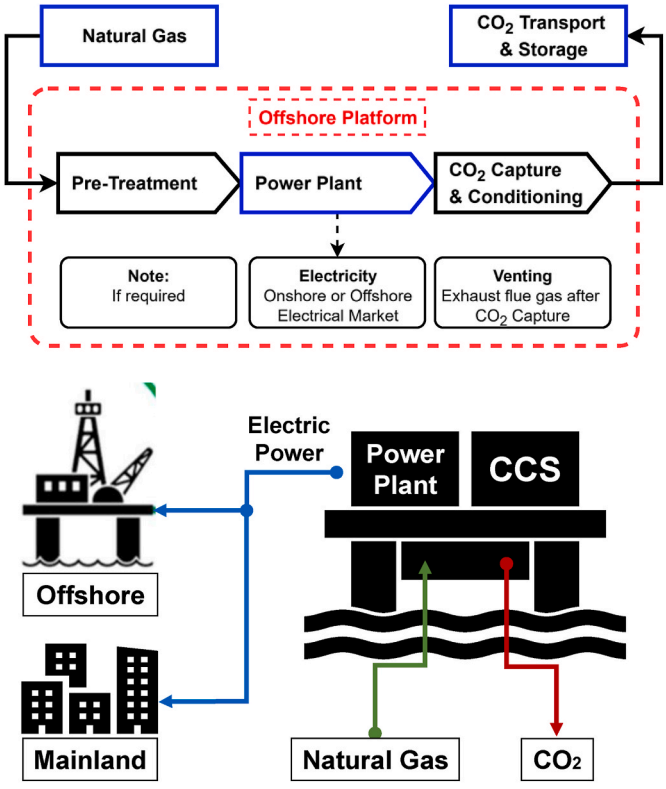

Fig. 33. The CEPONG concept for decarbonizing offshore oil & gas platforms and mainland electricity [149].

utilization of existing infrastructure, and case development with associated or stranded gases.

A techno-economic assessment of the application of CCS in 110 combined heat and power plants fueled by biomass and waste in Sweden has also been conducted by Beiron et al. [150]. This research is motivated by the urgency of achieving Sweden's NZE target by 2045, for which bioenergy-CCS (BECCS) is an essential strategy. The method used in this study models the steam cycle in combined heat and power plants to assess the impact of integrating MEA-based carbon capture on electricity and heat production. Furthermore, the estimated capital expenditure (CAPEX) and operational expenditure (OPEX) for BECCS are calculated based on the obtained data. The results show that by applying CCS to biomass and waste CHP plants in Sweden, the potential CO_2 that can be captured reaches 10–16 Mt CO_2 per year, with the cost of capturing and transporting CO_2 to the intermediate storage hub ranging from 52.72 to 146.43 USD/ton CO_2. This data accounts for approximately 25–40% of Sweden's total CO_2 emissions across all sectors. The lowest costs are obtained in large plants with high operating hours. The study also found that implementing CCS could significantly reduce electricity and heat production without the use of heat recovery technology.

Titus et al. [151] discuss the technical and economic analysis of integrating geothermal energy with two carbon dioxide removal (CDR) technologies: bioenergy with carbon capture and storage (BECCS) and direct air carbon capture and storage (DACCS) in high-temperature geothermal hydrothermal systems (Fig. 34). The uniqueness of this study lies in the comprehensive comparison between three configurations: conventional geothermal, geothermal-BECCS, and geothermal-DACCS, particularly in high-temperature and low-gaseous hydrothermal systems. The results show that at a CO_2 market price of 100 USD/ton, the geothermal system-BECCS has a lower levelized cost of energy (LCOE) of 88 USD/MWh, which is lower than that of geothermal-DACCS (181 USD/MWh) and conventional geothermal (89 USD/MWh). Emission abatement costs are also lower on BECCS (122 USD/tCO_2) than on DACCS (187 USD/tCO_2) and could drop to 45 USD/tCO_2 if BECCS is applied to retrofit existing infrastructure. Another important finding is that geothermal-BECCS generates 20% more electricity than conventional geothermal power for the same number of geothermal fluids; however, it also produces significant harmful emissions. On the other hand, DACCS can remove large amounts of CO_2; however, the high internal energy load also increases the overall cost of decarbonization. Case studies in New Zealand show that BECCS development is more economically and logistically feasible due to the availability of forestry residues as biomass feedstock.

Zhou et al. [152] discussed the effectiveness and potential cost reduction of implementing CCS retrofitting in fossil-fuel power plants in China. The primary method used in this study is the power system optimization model (PSOM), a cost-minimizing mixed-integer linear planning model. This model considers various constraints, including installed capacity, retrofitted capacity, operational capacity, electricity production, carbon emissions, backup needs, and system inertia. The study results show that implementing CCS retrofit can significantly lower the cost of decarbonizing China's electric power system. The cumulative cost of decarbonization systems decreased by 6.2–8.2%, and the cost of electricity supply decreased by 2.1–2.6% by 2060. The study also found that CCS retrofit can reduce the risk of electricity supply shortages by 37.8–48.4% by 2060. In addition, implementing CCS retrofits can help avoid the formation of stranded assets in coal- and gas-fired power plants compared to the no-retrofit scenario.

Overall, the cost evidence from previous studies suggests that CCS should not be judged solely by its cost. Its real value depends on whether the cost fits the technical and economic context of deployment. When cost comparisons are made using consistent assumptions and the same price basis, the increase in CCS-related expenses is not always as significant as commonly perceived. In several cases, the LCOE and abatement costs remain relatively stable after inflation and fuel-price effects are considered. This result implies that CCS economics is strongly influenced by system integration and policy frameworks.

Competitiveness also differs across applications. In many onshore electricity markets, CCS-equipped power plants may be less attractive than cheaper low-carbon options. However, an offshore power supply can offer a stronger case. Reliability needs are higher, and existing infrastructure may reduce costs. Bioenergy-based CCS shows strong potential for negative emissions at a meaningful scale. The lowest costs are achieved in extensive facilities with high operating hours. Yet energy penalties can reduce heat and electricity output without heat recovery. Hybrid pathways such as geothermal with carbon removal can be promising, but feasibility depends on supply chains and environmental trade-offs. At the system level, CCS retrofitting can support decarbonization while lowering the risk of stranded assets. Therefore, CCS should be deployed selectively. Priority should be given to retrofit-ready assets, storage-linked clusters, and high-utilization facilities.

6.2. *CCS on industry sector*

Jakobsen et al. [153] have conducted technical and economic studies

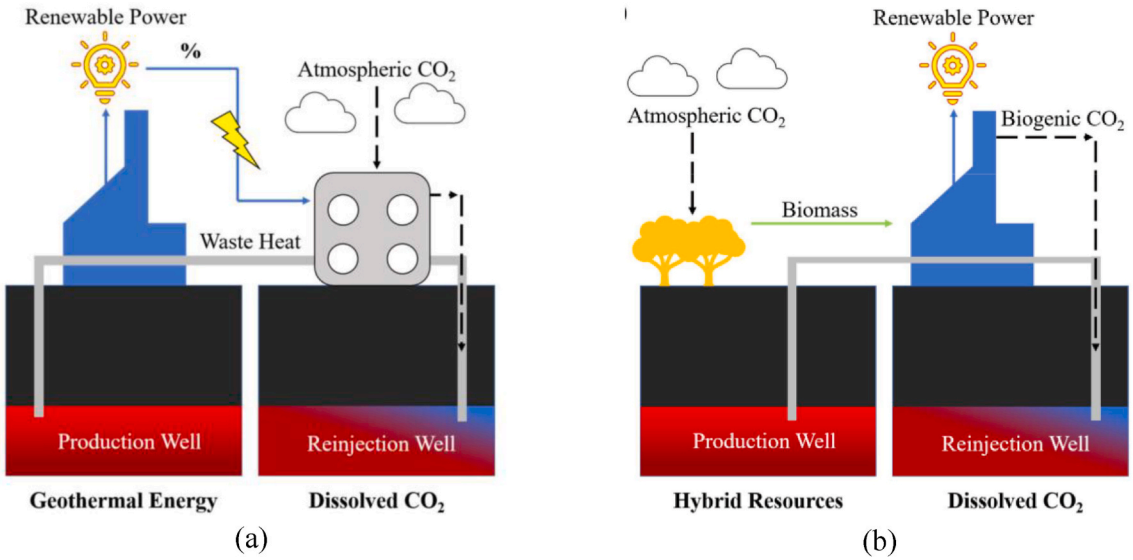

Fig. 34. Conceptual workflow of (a) geothermal-DACCS and (b) geothermal-BECCS [151].

on the application of CCS at the Norcem Brevik cement plant in Norway. This study employs an in-house techno-economic assessment methodology and tool, iCCS. This tool was created to assess the CCS chain in an integrated manner, from CO_2 capture and transportation to storage. Various alternative technologies and CCS scenarios have been investigated for their potential to reduce costs across the CCS chain. Table 9 presents nine alternative CCS chain configurations, each differing in the three main stages: CO_2 capture, transportation, and storage. At the capture stage, most scenarios use MEA-based capture as the reference technology, while others assess advanced solvents and membrane-based technologies as alternatives. For transportation, the dominant mode is shipping, with pipelines applied in selected scenarios to enable cost and infrastructure comparisons. At the storage stage, most scenarios rely on saline aquifers for permanent geological storage, whereas several others incorporate shared EOR storage.

The study results are illustrated in Fig. 35, where the total cost of each scenario is disaggregated into four components: capture, conditioning, transport, and storage. Overall, the figure indicates that capture is the most significant cost contributor across nearly all chains, highlighting capture technology selection as the most influential factor in reducing the total CCS cost. Chain A serves as the reference case and exhibits a relatively high total cost. Several capture technology alternatives demonstrate cost-reduction potential relative to the base case, most notably chain B, which employs improved amine solvents, and membrane-based chains C and D.

From a transportation perspective, differences in transport mode clearly affect total cost. Chain E yields the highest total cost, primarily driven by a substantial transport component associated with the capital investment required for dedicated pipeline construction. In contrast, chain F achieves a considerably lower cost than chain E, underscoring the advantage of shared infrastructure in reducing unit costs per tonne of CO_2. Interestingly, pipeline-based transport in chains E and F also results in lower conditioning costs than ship-based transport. Under pipeline transport, CO_2 is maintained in the supercritical phase, which is generally easier and less costly to sustain. Conversely, CO_2 is transported in the liquid phase during shipping, which increases costs, particularly due to the need for extreme cooling and high pressure.

Regarding storage options, the EOR-based scenarios in chains G and H tend to deliver lower total costs than several saline-aquifer scenarios, suggesting that EOR may offer additional economic value. Furthermore, the full-scale MEA scenario in chain I demonstrates a cost reduction relative to the base case, indicating the role of economies of scale when the system is implemented at a commercial scale. Overall, these findings confirm that CCS cost reductions can be achieved through a combination of more efficient capture technologies, deployment of shared infrastructure, and the selection of optimal transport and storage systems.

Furthermore, Kashyap et al. [154] examined the technical and economic feasibility of utilizing CCS technologies in the Indian cement industry to reduce carbon emissions while producing green urea. The method employed was a multi-criteria analysis (MCA) framework to assess various factors, including technological readiness, capital and operational costs, market demand for green urea, and potential CO_2 emission reduction. The study focused on 32 large cement plants in India, assuming each plant can capture 0.5 million tonnes of CO_2 per year using post-combustion MEA technology. Furthermore, the captured CO_2 is converted into green urea via a specialized chemical reaction. The results indicate that this approach is promising and projects a 12.4% reduction in CO_2 emissions for the cement industry.

Additionally, green urea production is projected to reach 21.82 million tons per year, potentially reducing India's dependence on urea imports. Financially, the study projects a 6-year payback period and a 16.7% return on investment. This analysis demonstrates that applying CCS technologies in Indian cement plants is both technically and economically feasible. However, further investigation is still needed to validate the model and optimize various aspects.

Table 9
Summary of chain design options [153].

Chain	Capture	Transport	Storage
A	MEA-based capture	Shipping	Saline aquifer
B	Advanced solvent-based capture	Shipping	Saline aquifer
C	Membrane-based capture (Polaris)	Shipping	Saline aquifer
D	Membrane-based capture (FSC)	Shipping	Saline aquifer
E	MEA-based capture	Pipeline	Saline aquifer
F	MEA-based capture	Shared pipeline	Shared saline aquifer
G	MEA-based capture	Shipping	Shared EOR storage
H	MEA-based capture	Shipping	Shared EOR storage
I	MEA-based capture at full scale	Shipping	Saline aquifer

6.3. *Cost overruns in certain cases: effect of impurities on operational cost*

In implementing CCS across various emission sources, captured CO_2 often contains impurities that affect transportation efficiency and costs. Skaugen et al. [155] have conducted an in-depth technical and economic evaluation of the effect of impurity content on the conditioning process and CO_2 transportation through a 500 km pipeline with a capacity of 13.1 million tons per year. The method involves simulating the thermophysical properties of mixed CO_2 containing impurities, such as nitrogen, oxygen, and methane, at different concentrations, specifically 5 mol% air and 10 mol% natural gas. The study combined compression calculations from low-pressure after the capture process to a high-pressure of 150 bar.

Additionally, changes in thermophysical properties along the pipeline, as well as heat transfer with the surrounding environment, were also considered. The study evaluated several pipeline diameters ranging from 18 to 28 inches to determine the most economical size for each impurity level. The novelty of this study lies in the integration of simulations of local thermodynamic conditions with a comprehensive cost analysis, which includes material investment, labor, energy consumption, and cooling costs. The study examined in detail the impact of impurities on energy consumption for compression and transportation, a factor that is often overlooked in previous models. The results indicated that CO_2 conditioning and transportation costs increased by 13% to 22% compared to impurity-free conditions, corresponding to an additional cost of approximately 2.69 to 4.45 USD/ton of CO_2 transported. Furthermore, using pipelines designed for pure CO_2 while transporting CO_2 with impurities can result in a 20% to 40% increase in specific costs. This increase is attributed to reduced transport capacity and penalties associated with CO_2 emissions that are not transported.

A similar research by Roussanaly et al. [156] discusses different strategies for conditioning and transporting CO_2 captured from IGCC coal-fired power plants in the Czech Republic. The study also considered the influence of impurities in the captured CO_2 stream. It evaluated various transport options to storage sites in the Czech Republic and European hubs (Fig. 36). The study compared two transportation technologies (pipeline-based and rail-based) to determine the most cost-effective solution. The results of this study indicate that pipelines are the most cost-effective option among the two transport scenarios examined. The cost of conditioning and CO_2 transport by pipeline ranges from 12.30 to 18.04 USD/ton of CO_2. In contrast, with more expensive railways, the price ranges from 21.44 to 29.17 USD/ton of CO_2, primarily due to the longer transport distance and higher conditioning costs associated with handling impurities. Impurities in CO_2 can increase conditioning costs by 1.6% to 11.4%.

7. Concluding remarks

This article presents a comprehensive review of the technological evolution of CCS, with particular emphasis on its technical dimensions, operational risks, economic feasibility, and recent advances in material

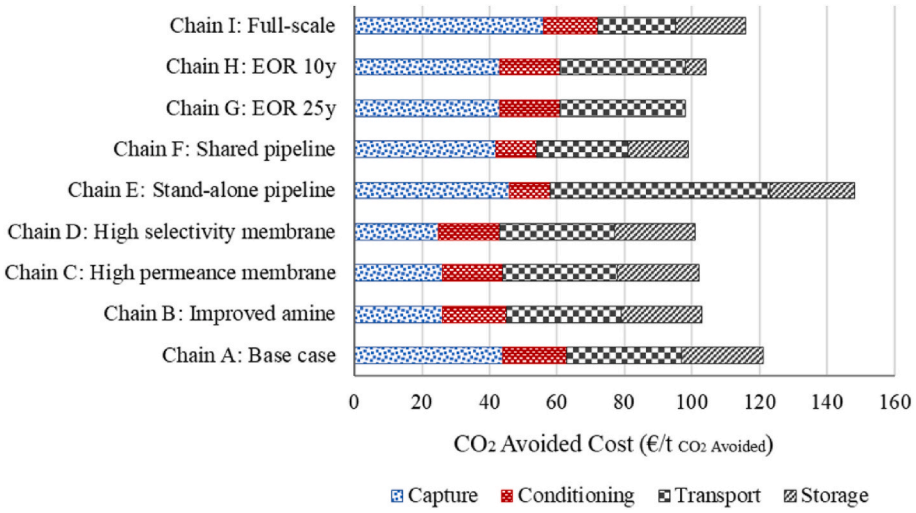

Fig. 35. CO_2 avoided costs for the nine chains are considered [153].

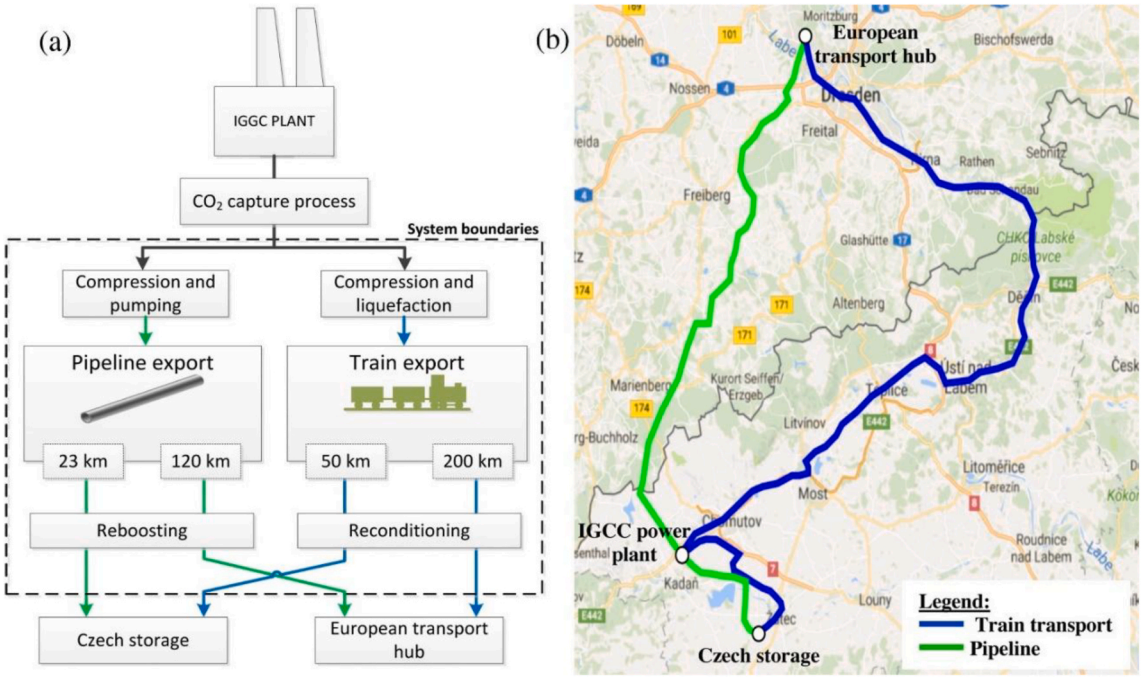

Fig. 36. (a) Conceptual layout, defined system boundaries for the four CO_2 conditioning and transportation configurations, (b) route map highlighting the evaluated pipeline and train logistics pathways [156].

innovation. The synthesis of prior studies yields several key conclusions, outlined below.

1. From the perspective of capture technologies, numerous CO_2 capture methods continue to encounter significant technical barriers. Direct air capture (DAC) has emerged as a promising approach for carbon dioxide removal (CDR); however, it remains constrained by process inefficiencies and elevated operational costs due to the inherently low-concentration of atmospheric CO_2. Post-combustion capture is considered the most suitable method for directly capturing CO_2 from emission sources, as it produces CO_2 of higher purity than pre-combustion and oxy-fuel combustion routes. Conversely, pre-combustion and oxy-fuel systems tend to introduce impurities into the captured CO_2 stream, which can trigger corrosion and abrupt phase transitions. Such phenomena may disrupt fluid dynamics during both transportation and geological injection. Further investigations are required to address these challenges, particularly in developing efficient purification techniques for captured CO_2.
2. Studies on CO_2 transportation reveal that each transport modality possesses distinct technical and economic characteristics. Pipeline transportation enables the continuous conveyance of CO_2 in large quantities, generally in a supercritical phase. This operational condition is relatively stable and cost-effective to maintain compared with the liquid phase. However, the high capital expenditure (CAPEX) associated with pipeline installation, coupled with safety concerns in densely populated areas, poses substantial challenges. Elevated fluid pressure could exacerbate atmospheric gas dispersion in the event of a leak, necessitating complex, robust risk mitigation strategies. Even minor deficiencies in planning or mitigation may result in severe consequences. In contrast, transportation via tank trucks or marine vessels is considered more economical for long-distance transfer of smaller CO_2 volumes. Nevertheless, this

approach requires CO_2 to remain in a liquid state, which demands a high energy input for refrigeration and may introduce structural integrity issues at cryogenic temperatures. Improper tank design or material selection may increase the risk of catastrophic failure. Therefore, additional studies are required to examine the performance and degradation mechanisms of pipeline and tank materials under extreme conditions, including high pressure, corrosive environments, and very low operating temperatures.

3. Geological storage of CO_2 faces several critical technical challenges, notably the risk of fluid migration due to caprock failure and potential leakage through wellbores. Caprocks must exhibit extremely low permeability to ensure long-term containment. The integrity of the wellbore is governed by the ability of casing materials to endure thermal, chemical, and mechanical stresses. Steel casings and cement sheaths must therefore possess high corrosion resistance, tolerance to substantial temperature fluctuations during injection, and sufficient mechanical strength to withstand interactions between the rock and the structure. Recent advances in materials science suggest that corrosion protection of CCS infrastructure through smart anodes, innovative composite coatings, and laser cladding technologies holds considerable potential to enhance long-term operational reliability and safety.
4. The deployment of reliable CO_2 monitoring systems is fundamental to the success of long-term storage operations. From a risk-mitigation standpoint, prior research emphasizes the need for multidisciplinary approaches to facilitate early detection of potential failures, notably through numerical simulations and data-driven predictive modeling. Future research should further advance high-resolution monitoring technologies, such as geochemical tracers and drone- or satellite-based atmospheric surveillance systems, to enable rapid, spatially extensive detection of CO_2 leakage.
5. Despite persistent challenges concerning cost and energy efficiency, CCS remains a pivotal technology for enabling global decarbonization. Previous studies have explored diverse strategies to enhance its economic viability. Although initial investment costs are substantial, retrofitting CCS to existing fossil-fuel power plants has been demonstrated to reduce overall decarbonization expenses while mitigating the risk of electricity supply shortages. Such retrofit mechanisms represent a practical and cost-effective pathway for energy transition, minimizing the occurrence of stranded assets. The integration of CCS, particularly through bioenergy with CCS (BECCS) utilizing biomass and waste-derived feedstocks, offers significant potential for achieving global NZE targets. Moreover, the economic feasibility of CCS can be further improved through CO_2 utilization pathways, such as EOR and industrial feedstock applications.

CRediT authorship contribution statement

Aprianur Fajri: Writing – original draft, Investigation, Funding acquisition, Formal analysis, Data curation. **Aditya Rio Prabowo:** Writing – review & editing, Writing – original draft, Supervision, Project administration, Investigation, Funding acquisition, Conceptualization. **Nurul Muhayat:** Visualization, Supervision, Conceptualization. **Ristiyanto Adiputra:** Writing – review & editing, Supervision, Resources, Methodology, Investigation, Conceptualization. **Sören Ehlers:** Writing – review & editing, Conceptualization. **Moritz Braun:** Writing – review & editing, Conceptualization.

Availability of data and materials

The authors confirm that the data supporting the findings of this study are available within the article.

Declaration of competing interest

The authors declare that they have no known competing financial interests or personal relationships that could have appeared to influence the work reported in this paper.

Acknowledgments

The authors are grateful to the Indonesia Endowment Fund for Education (LPDP), Ministry of Finance, Republic of Indonesia, for the financial support provided for this research.

Appendix A. Supplementary data

Supplementary data to this article can be found online at https://doi.org/10.1016/j.uncres.2026.100337.

Appendix: Nomenclature

Acronym

BECCS	bioenergy with carbon capture and storage
CAPEX	capital expenditure
CCS	carbon capture and storage
CCUS	carbon capture, utilization, and storage
CDR	carbon dioxide removal
CEPONG	clean electricity production from offshore natural gas
CFD	computational fluid dynamics
CL	conventional laser cladding
DACCS	direct air carbon capture and storage
DPM	discrete particle method
EDS	energy-dispersive spectrometer
EHLC	extreme high-speed laser cladding
EOR	enhanced oil recovery
EOS	equation of state
ESO	epoxy silane oligomer
FTA	fault tree analysis
HAZOP	hazard and operability study
IGCC	integrated gasification combined cycle
IPCC	intergovernmental panel on climate change

LCOE	levelized cost of energy
MCA	multi-criteria analysis
MDEA	methyldiethanolamine
MEA	monoethanolamine
MOO	multi-objective optimization
NGCC	natural gas combined cycle
NZE	net zero emission
OPEX	operational expenditure
PSOM	power system optimization model
PVSA	pressure-vacuum swing adsorption
QRA	quantitative risk assessment
sc-CO_2	supercritical CO_2
SEM	scanning electron microscopy
SEWGS	sorption enhanced water gas shift
SMR	steam methane reforming
SCPC	supercritical pulverized coal
SRCCS	special report on carbon dioxide capture and storage
XPS	X-ray photoelectron spectroscopy
XRD	X-ray diffraction

Symbol

A_{choke}	strangulation cross-section area (m^2)
A_{flow}	cross-sectional area of flow (m2)
$A_{fracture}$	new fracture surface area
a, b	gas-specific parameters
C	concentration of pollutants (kg/m^3)
C_1, C_2, C_s	model constant
C_D	discharge coefficient (0.72)
CO_2	carbon dioxide
$CO_{2Emission}$	CO_2 Emission produced (kg/s)
$CO_{2avoided}$	amount of CO_2 avoided
C_p	type heat capacity
CR	corrosion rate (mm/year)
e	specific CO_2 emission rate ($kgCO_2$/MWHel)
E_a	activation energy (kJ/mol)
E_k	phase K-specific total energy
E_m	modulus of elasticity
f_{CO_2}	the fugacity of CO_2 (bar)
$f_{closure}$	the force of the cover at the end of the crack
F_g	force due to gravitational acceleration
F_p	force due to interaction with droplets/particles (N/m2)
F_s	rate of momentum gain per unit volume due to pollutant emissions (N/m^2)
G	turbulence production rate by shear (m^2/s^3)
G_E	fracture release energy rate vector
$GtCO_2e$	gigaton carbon dioxide equivalent
H	emission source height (m)
HR	heat rate of the plant being studied (kJLHV/kWh el)
i, j	represent the different components of the mixture
I	specific internal energy (J/kg)
J	heat flux vector (W/m^2)
K	formation permeability (m^2)
k	turbulent kinetic energy per unit mass (m^2/s^3)
k_e	effective thermal conductivity
k_{ij}	binary interaction parameter between components i and j (value 0, if I j)
k_{react}	constant of reaction rate
L	flow path length (m)
l	turbulent length scale (m)
LHV_f	fuel low heating value (MJ/kg fuel)
M	material constant
$\dot{m}$	mass flow rate (kg/s)
$\dot{m}_f$	fuel mass flow rate (kg/s)
$\dot{m}_{lv}, \dot{m}_{vl}$	the rate of time transfer from liquid to gas or vice versa
N	pre-exponential factors
p	fluid pressure (Pa)
p_l, p_v	liquid and gaseous phase pressure

P_{net}	net power output (MW)
p_{sat}	saturated pressure
p_{sc}	supercritical gas pressure (Pa)
Q	volumetric flow rate (m3/s)
Q_h	rate of specific internal energy gain due to surface energy budget (J/kgs)
Q_p	rate of specific internal energy gain due to interaction with particles
Q_s	rate of specific internal energy gain due to pollutant emissions
R	universal gas constant (8.314 J/(mol· K))
Ref	reference case of energy generation without CCS
Ri	Richardson number for atmospheric stability indicator
S_E	energy sources such as latent heat
SIF	stress intensity Factor
SPECCA	specific primary energy consumption for CO_2 avoided
T	absolute temperature (K)
$\overrightarrow{u}$	fluid velocity vector (m/s)
USV	unmanned surface vehicle
ν	Poisson ratio
V_m	volume molar (m^3/mol)
W_p	turbulence production due to interaction with particles (m^2/s^3)
x	mole fraction of liquid or vapor phase
(x, y, z)	space coordinates (m)
$^{\circ}W_t$	the crack at the node trailing the crack tip, (°) the entrywise product (Hadamard product)

Greek letters

α	correction factor, temperature function, and gas properties
α_T	linear thermal expansion coefficient
α_l, α_v	liquid and gaseous phase volume fraction (αl + αv 1)
γ	specific heat ratio (J/kg. K)
Δh	hydraulic head difference (M)
ΔT	temperature change (K)
Δp	change in pressure (MPa)
δ_{ij}	delta Kronecker
ε	dissipation of turbulent kinetic energy (m^2/s^3)
ε_{ij}	strain tensor
ε_{vol}	volumetric strain
η_{el}	net electric efficiency
μ	viscosity (Pa.s)
μ_l, μ_v	viscosity of liquids and gases
μ_t	turbulence viscosity (kg/ms)
ρ	density of mixed gas (kg/m^3)
ρ_l, ρ_v	density of liquids and gases
σ_h	turbulent Prandtl number
σ_{ij}	a stress tensor that expresses the magnitude and direction of the stress at a point
σ_{ij}^M	mechanical stress
σ_{ij}^T	thermal stress
σ_k, σ_e	model constant for and k and ε
σ_N	Newtonian viscous stress tensor (N/m)
σ_y, σ_z	horizontal and vertical dispersion parameters (m)
τ_l, τ_v	coefficient of relaxation time for evaporation and condensation
φ	Joule-Thomson coefficient (for CO_2 = 13 K/MPa)

References

[1] IEA, World Energy Outlook 2023. https://www.iea.org/reports/world-energy-outlook-2023, 2023.

[2] D. Huisingh, Z. Zhang, J.C. Moore, Q. Qiao, Q. Li, Recent advances in carbon emissions reduction: policies, technologies, monitoring, assessment and modeling, J. Clean. Prod. 103 (2015) 1–12, https://doi.org/10.1016/j.jclepro.2015.04.098.

[3] L. Jiang, A.S. Parry, C.T. White, R. Hartungi, Current development of carbon capture and storage in the UK: a non-technical review, Int. J. Low Carbon Technol. 8 (2013) 225–229, https://doi.org/10.1093/ijlct/cts008.

[4] F. Johnsson, J. Kjärstad, J. Rootzén, The threat to climate change mitigation posed by the abundance of fossil fuels, Clim. Policy 19 (2019) 258–274, https://doi.org/10.1080/14693062.2018.1483885.

[5] K. Jiang, P. Ashworth, The development of Carbon Capture Utilization and Storage (CCUS) research in China: a bibliometric perspective, Renew. Sustain. Energy Rev. 138 (2021), https://doi.org/10.1016/j.rser.2020.110521.

[6] IRENA and CPI, Global landscape of renewable energy finance. https://www.irena.org/Publications/2023/Feb/Global-landscape-of-renewable-energy-finance-2023, 2023.

[7] IRENA, Renewable Capacity Statistics, 2024. Abu Dhabi, 2024, www.irena.org.

[8] EI, Statistical Review of World Energy, 2025. London, 2025.

[9] W. Rohlfs, R. Madlener, Optimal investment strategies in power generation assets: the role of technological choice and existing portfolios in the deployment of low-carbon technologies, Int. J. Greenh. Gas Control 28 (2014) 114–125, https://doi.org/10.1016/j.ijggc.2014.06.012.

[10] X. Wang, L. Du, Study on carbon capture and storage (CCS) investment decision-making based on real options for China's coal-fired power plants, J. Clean. Prod. 112 (2016) 4123–4131, https://doi.org/10.1016/j.jclepro.2015.07.112.

[11] A. González-Díaz, M.O. González-Díaz, A.M. Alcaráz-Calderón, J. Gibbins, M. Lucquiaud, Priority projects for the implementation of CCS power generation with enhanced oil recovery in Mexico, Int. J. Greenh. Gas Control 64 (2017) 119–125, https://doi.org/10.1016/j.ijggc.2017.07.006.

[12] M.H. Islam, S.R. Patlolla, A review on the state-of-the-art and commercial status of carbon capture technologies, Energies 18 (2025) 3937, https://doi.org/10.3390/en18153937.

[13] T. Mikunda, L. Brunner, E. Skylogianni, J. Monteiro, L. Rycroft, J. Kemper, Carbon capture and storage and the sustainable development goals, Int. J. Greenh. Gas Control 108 (2021), https://doi.org/10.1016/j.ijggc.2021.103318.

[14] P.J. Cook, CCS research development and deployment in a clean energy future: lessons from Australia over the past two decades, Engineering 3 (2017) 477–484, https://doi.org/10.1016/J.ENG.2017.04.014.

[15] R. Wennersten, Q. Sun, H. Li, The future potential for carbon capture and storage in climate change mitigation – an overview from perspectives of technology, economy and risk, J. Clean. Prod. 103 (2015) 724–736, https://doi.org/10.1016/j.jclepro.2014.09.023.

[16] UNFCC, The Paris Agreement, United Nations Framework Convention on Climate Change, 2015. Paris.

[17] K. Zhao, C. Jia, Z. Li, X. Du, Y. Wang, J. Li, Z. Yao, J. Yao, Recent advances and future perspectives in Carbon Capture, Transportation, Utilization, and Storage (CCTUS) technologies: a comprehensive review, Fuel 351 (2023) 128913, https://doi.org/10.1016/j.fuel.2023.128913.

[18] R. Wang, Status and perspectives on CCUS clusters and hubs, Unconv. Resour. 4 (2024) 100065, https://doi.org/10.1016/j.uncres.2023.100065.

[19] M.E. Helmi, I. Mohammed, M.G. Rezk, A.O. Gbadamosi, A. Raza, M. Mahmoud, Unlocking the potential of CO_2 storage in saline aquifers: challenges, knowledge gaps, and future directions for large-scale storage, Carbon Capture Sci. Technol. 16 (2025) 100460, https://doi.org/10.1016/j.ccst.2025.100460.

[20] P. Ndlovu, R. Bulannga, L.L. Mguni, Progress in carbon dioxide capture, storage and monitoring in geological landform, Front. Energy Res. 12 (2024) 1–30, https://doi.org/10.3389/fenrg.2024.1450991.

[21] M.M. Ali Awan, F.U. Din Kirmani, Achieving low-carbon future through CO_2 storage: a comprehensive review of global projects and policies, Pet. Res. 10 (2025) 636–658, https://doi.org/10.1016/j.ptlrs.2025.04.004.

[22] Z. Liu, Q. Gao, Y. Zhou, R. Pan, Research progress on major influencing factors of corrosion behavior of pipeline steel in supercritical CO_2 environment, Materials 18 (2025), https://doi.org/10.3390/ma18112424.

[23] S.K. Kairy, S. Zhou, A. Turnbull, G. Hinds, Corrosion of pipeline steel in dense phase CO_2 containing impurities: a critical review of test methodologies, Corros. Sci. 214 (2023) 110986, https://doi.org/10.1016/j.corsci.2023.110986.

[24] J. Liu, D. Yao, K. Chen, C. Wang, C. Sun, H. Pan, F. Meng, B. Chen, L. Wang, Effect of H_2O content on the corrosion behavior of X52 steel in supercritical CO_2 streams containing O_2, H_2S, SO_2 and NO_2 impurities, Energies 16 (2023), https://doi.org/10.3390/en16176119.

[25] D. Casaban, E. Tsalaporta, The impact of direct air capture during the last two decades: a bibliometric analysis of the scientific research Part II, Sustain. Chem. Clim. Action 2 (2023) 100021, https://doi.org/10.1016/j.scca.2023.100021.

[26] R. Stanger, T. Wall, R. Spörl, M. Paneru, S. Grathwohl, M. Weidmann, G. Scheffknecht, D. McDonald, K. Myöhänen, J. Ritvanen, S. Rahiala, T. Hyppänen, J. Mletzko, A. Kather, S. Santos, Oxyfuel combustion for CO_2 capture in power plants, Int. J. Greenh. Gas Control 40 (2015) 55–125, https://doi.org/10.1016/j.ijggc.2015.06.010.

[27] X. Zhang, B. Singh, X. He, T. Gundersen, L. Deng, S. Zhang, Post-combustion carbon capture technologies: energetic analysis and life cycle assessment, Int. J. Greenh. Gas Control 27 (2014) 289–298, https://doi.org/10.1016/j.ijggc.2014.06.016.

[28] M. Healey, K. Mistry, T. Jones, E. Luna-Ortiz, Understanding gas-phase breakout with high H_2 content in CCS pipeline gathering networks, Int. J. Greenh. Gas Control 90 (2019), https://doi.org/10.1016/j.ijggc.2019.102816.

[29] R. Bala, M. Kaur, H. Thakur, P. Kashyap, A. Karnwal, T. Malik, A sociotechnical review of Carbon Capture, Utilization, and Storage (CCUS) technologies for industrial decarbonization: current challenges, emerging solution, and future directions, Int. J. Chem. Eng. 2025 (2025), https://doi.org/10.1155/ijce/7195300.

[30] Global CCS Institute, Understanding CCS: Capture, 2022.

[31] L. Raynal, P.A. Bouillon, A. Gomez, P. Broutin, From MEA to demixing solvents and future steps, a roadmap for lowering the cost of post-combustion carbon capture, Chem. Eng. J. 171 (2011) 742–752, https://doi.org/10.1016/j.cej.2011.01.008.

[32] A. Sanna, M. Dri, M. Maroto-Valer, Carbon dioxide capture and storage by pH swing aqueous mineralisation using a mixture of ammonium salts and antigorite source, Fuel 114 (2013) 153–161, https://doi.org/10.1016/j.fuel.2012.08.014.

[33] A.R. Shaikh, A. Grillo, M.C. D'Alterio, J.J. Pajski, S.I. Amran, H. Karim, M. Chawla, G. Talarico, A. Poater, L. Cavallo, Choline-based amino acid ionic liquids for CO_2 capture, J. Mol. Liq. 424 (2025) 127084, https://doi.org/10.1016/j.molliq.2025.127084.

[34] Y. Ma, J. Gao, Y. Wang, J. Hu, P. Cui, Ionic liquid-based CO_2 capture in power plants for low carbon emissions, Int. J. Greenh. Gas Control 75 (2018) 134–139, https://doi.org/10.1016/j.ijggc.2018.05.025.

[35] M.M.G. Perdana, R. Andika, B.H. Susanto, S. Steven, N. Nishiyama, I.C. Sophiana, Transforming CO_2 emissions into fuel: an energy analysis of dimethyl ether production pathways, Results Eng. 25 (2025) 104330, https://doi.org/10.1016/j.rineng.2025.104330.

[36] J. Blamey, E.J. Anthony, J. Wang, P.S. Fennell, The calcium looping cycle for large-scale CO_2 capture, Prog. Energy Combust. Sci. 36 (2010) 260–279, https://doi.org/10.1016/j.pecs.2009.10.001.

[37] J.R. Fernandez, S. Turrado, J.C. Abanades, Calcination kinetics of cement raw meals under various CO_2 concentrations, React. Chem. Eng. 4 (2019) 2129–2140, https://doi.org/10.1039/C9RE00361D.

[38] P.N.Y.M. Otabir, A. Khanal, F. Nath, Geochemical impacts of CO_2 mineralization in carbonate and basalt formations: a critical review on challenges and future outlook, Energy Fuels 39 (2025) 1226–1251, https://doi.org/10.1021/acs.energyfuels.4c04424.

[39] A. Alqahtani, M. Addassi, H. Hoteit, E. Oelkers, Rapid CO_2 mineralization by zeolite via cation exchange, Sci. Rep. 15 (2025) 1–15, https://doi.org/10.1038/s41598-024-82520-6.

[40] Z. Xu, J. Ma, X. Chen, Z. Song, D. Liu, C. Liang, CO_2 capture performance of ZrO_2-doped Na_2CO_3/γ-Al_2O_3 adsorbent, J. Environ. Sci. (China) 155 (2025) 382–394, https://doi.org/10.1016/j.jes.2024.09.027.

[41] L. Szablowski, M. Wojcik, O. Dybinski, Review of steam methane reforming as a method of hydrogen production, Energy 316 (2025) 134540, https://doi.org/10.1016/j.energy.2025.134540.

[42] K. Bayramoğlu, T. Bayramoğlu, Integrated modeling of steam methane reforming and carbon capture for blue hydrogen production, Hydrogen 6 (2025) 94, https://doi.org/10.3390/hydrogen6040094.

[43] L. Dehimi, O. Alioui, Y. Benguerba, K.K. Yadav, J.K. Bhutto, A.M. Fallatah, T. Shukla, M.A. Alreshidi, M. Balsamo, M. Badawi, A. Erto, Hydrogen production by the water-gas shift reaction: a comprehensive review on catalysts, kinetics, and reaction mechanism, Fuel Process. Technol. 267 (2025) 108163, https://doi.org/10.1016/j.fuproc.2024.108163.

[44] M.Z. Shahid, A.S. Farooqi, K. Fajri, M. El-Adawy, M. Hamdy, A.S. Farooqi, O. Y. Abdelaziz, M.M. Hossain, M.A. Nemitallah, Clean hydrogen production via sorption enhanced water gas shift reaction: a comprehensive review, Int. J. Hydrogen Energy 100 (2025) 1483–1512, https://doi.org/10.1016/j.ijhydene.2024.12.400.

[45] C. Kroumian, J. Maier, K. Peloriadi, G. Scheffknecht, P. Grammelis, Evaluation of 100% alternative fuel combustion under oxyfuel conditions in a pilot-scale burner for application in retrofit oxyfuel cement kiln, Fuel 381 (2025) 133697, https://doi.org/10.1016/j.fuel.2024.133697.

[46] N. Paltrinieri, L. Breedveld, J. Wilday, V. Cozzani, Identification of hazards and environmental impact assessment for an integrated approach to emerging risks of CO_2 capture installations, Energy Proc. 37 (2013) 2811–2818, https://doi.org/10.1016/j.egypro.2013.06.166.

[47] A. Krzemień, A. Więckol-Ryk, A. Smoliński, A. Koteras, L. Więcław-Solny, Assessing the risk of corrosion in amine-based CO_2 capture process, J. Loss Prev. Process. Ind. 43 (2016) 189–197, https://doi.org/10.1016/j.jlp.2016.05.020.

[48] M. Gazzani, M.C. Romano, G. Manzolini, CO_2 capture in integrated steelworks by commercial-ready technologies and SEWGS process, Int. J. Greenh. Gas Control 41 (2015) 249–267, https://doi.org/10.1016/j.ijggc.2015.07.012.

[49] J.C.L.Y. Fong, C.J. Anderson, G. Xiao, P.A. Webley, A.F.A. Hoadley, Multi-objective optimisation of a hybrid vacuum swing adsorption and low-temperature post-combustion CO_2 capture, J. Clean. Prod. 111 (2016) 193–203, https://doi.org/10.1016/j.jclepro.2015.08.033.

[50] F. Wang, J. Cao, Y. Zhang, K.B. Aviso, R.R. Tan, Z. Li, X. Jia, Safety risk assessment of the large-scale carbon capture, utilization, and storage demonstration project in Dongying, China, J. Clean. Prod. 414 (2023), https://doi.org/10.1016/j.jclepro.2023.137699.

[51] L. Zhang, K. Ye, Y. Wang, W. Han, M. Xie, L. Chen, Performance analysis of a hybrid system combining cryogenic separation carbon capture and liquid air energy storage (CS-LAES), Energy 290 (2024) 129867, https://doi.org/10.1016/j.energy.2023.129867.

[52] S. Elmarghni, M. Ansarpour, T.N. Borhani, Effect of different amine solutions on performance of post-combustion CO_2 capture, Processes 13 (2025) 1–28, https://doi.org/10.3390/pr13082521.

[53] H. Li, J. Wang, S. Zhao, H. Wu, Z. Sun, Parameter optimization of solution method of CO_2 capture from aluminum electrolysis flue gas: ammonia versus MEA, J. Environ. Chem. Eng. 13 (2025) 115702, https://doi.org/10.1016/j.jece.2025.115702.

[54] S.M. Hosseini, R.P. Moghadam, A. Afshar Ebrahimi, Boosting CO_2 capture efficiency of the exhausted RFCC flue gas by using intercooler exchangers: leveraging ANN in MDEA-based approach, J. CO_2 Util. 95 (2025) 103091, https://doi.org/10.1016/j.jcou.2025.103091.

[55] R. Brown, G. Chinello, Investigation of the transferability of calibration between alternative fluids for liquid and dense phase carbon dioxide flow measurement, Flow Meas. Instrum. 98 (2024), https://doi.org/10.1016/j.flowmeasinst.2024.102644.

[56] D. Raju, M. Ramdin, T.J.H. Vlugt, Thermophysical properties and phase behavior of CO_2 with impurities: insight from molecular simulations, J. Chem. Eng. Data 69 (2024) 2735–2755, https://doi.org/10.1021/acs.jced.4c00268.

[57] Y. Xiong, B. Qin, Q. Zhang, D. Yuan, Z. Lu, Dynamic characteristics of high-pressure and high-density carbon dioxide leakage process, Appl. Therm. Eng. 256 (2024), https://doi.org/10.1016/j.applthermaleng.2024.124155.

[58] E.S. Rubin, J.E. Davison, H.J. Herzog, The cost of CO_2 capture and storage, Int. J. Greenh. Gas Control 40 (2015) 378–400, https://doi.org/10.1016/j.ijggc.2015.05.018.

[59] S. Roussanaly, J.P. Jakobsen, E.H. Hognes, A.L. Brunsvold, Benchmarking of CO_2 transport technologies: part I-Onshore pipeline and shipping between two onshore areas, Int. J. Greenh. Gas Control 19 (2013) 584–594, https://doi.org/10.1016/j.ijggc.2013.05.031.

[60] M. Ashkavand, M. Scheffler, W. Heineken, M.D. Solomon, T. Birth-Reichert, Techno-economic assessment of liquefied CO_2 transport via trucking, Int. J. Greenh. Gas Control 147 (2025) 104491, https://doi.org/10.1016/j.ijggc.2025.104491.

[61] H. Noh, K. Kang, Techno-economic analysis of large-scale CO_2 ship transport with onboard boil-off gas reliquefaction, Int. J. Greenh. Gas Control 142 (2025) 104337, https://doi.org/10.1016/j.ijggc.2025.104337.

[62] M.M.J. Knoope, A. Ramírez, A.P.C. Faaij, Investing in CO_2 transport infrastructure under uncertainty: a comparison between ships and pipelines, Int. J. Greenh. Gas Control 41 (2015) 174–193, https://doi.org/10.1016/j.ijggc.2015.07.013.

[63] S. Suryanto, A.R. Prabowo, T. Muttaqie, I. Istanto, R. Adiputra, N. Muhayat, A. Fajri, M. Braun, S. Ehlers, Evaluation of high-tensile steel using nonlinear analysis: experiment-FE materials benchmarking of LNG carrier structures under low-temperature conditions, Energy Rep. 9 (2023) 149–161, https://doi.org/10.1016/j.egyr.2023.05.252.

[64] M.F.A. Ahzhan, S. Suryanto, A. Rio Prabowo, T. Muttaqie, Q. Thang Do, B. Santoso, F.B. Laksono, H. Nubli, Mechanical behavior of designed AH32 steel specimens under tensile loading at low temperatures: strength and failure assessments based on experimentally verified FE modeling and analysis, J. Mech. Behav. Mater. 33 (2024), https://doi.org/10.1515/jmbm-2024-0018.

[65] F.H. Hedlund, The extreme carbon dioxide outburst at the Menzengraben potash mine 7 July 1953, Saf. Sci. 50 (2012) 537–553, https://doi.org/10.1016/j.ssci.2011.10.004.

[66] S.K. Mahjour, S.A. Faroughi, Risks and uncertainties in carbon capture, transport, and storage projects: a comprehensive review, Gas Sci. Eng. 119 (2023), https://doi.org/10.1016/j.jgsce.2023.205117.

[67] A. Mazzoldi, T. Hill, J.J. Colls, Assessing the risk for CO_2 transportation within CCS projects, CFD modelling, Int. J. Greenh. Gas Control 5 (2011) 816–825, https://doi.org/10.1016/j.ijggc.2011.01.001.

[68] H. You, Y. Seo, C. Huh, D. Chang, Performance analysis of cold energy recovery from CO_2 injection in ship-based carbon capture and storage (CCS), Energies 7 (2014) 7266–7281, https://doi.org/10.3390/en7117266.

[69] X. Liu, A. Godbole, C. Lu, G. Michal, P. Venton, Study of the consequences of CO_2 released from high-pressure pipelines, Atmos. Environ. 116 (2015) 51–64, https://doi.org/10.1016/j.atmosenv.2015.06.016.

[70] C.J. Wareing, M. Fairweather, S.A.E.G. Falle, R.M. Woolley, A.M.E. Ward, High pressure CO_2 CCS pipelines: comparing dispersion models with multiple experimental datasets, Int. J. Greenh. Gas Control 54 (2016) 716–726, https://doi.org/10.1016/j.ijggc.2016.08.030.

[71] S. Gu, Y. Li, L. Teng, Q. Hu, D. Zhang, X. Ye, C. Wang, J. Wang, S. Iglauer, A new model for predicting the decompression behavior of CO_2 mixtures in various phases, Process Saf. Environ. Prot. 120 (2018) 237–247, https://doi.org/10.1016/j.psep.2018.08.034.

[72] C. Xiao, Z. Lu, L. Yan, S. Yao, Transient behaviour of liquid CO_2 decompression: CFD modelling and effects of initial state parameters, Int. J. Greenh. Gas Control 101 (2020), https://doi.org/10.1016/j.ijggc.2020.103154.

[73] V.S. Bjerketvedt, A. Tomasgard, S. Roussanaly, Deploying a shipping infrastructure to enable carbon capture and storage from Norwegian industries, J. Clean. Prod. 333 (2022), https://doi.org/10.1016/j.jclepro.2021.129586.

[74] S. Roussanaly, S.E. Holm, A. Subramanian, Can subsea shuttles be a cost-competitive solution for CO_2 transport? Carbon Capture Sci. Technol. 13 (2024) https://doi.org/10.1016/j.ccst.2024.100246.

[75] H. Liao, X. Wang, K. Yang, Z. Hou, H. Wang, Impurity-driven variations in CO_2 critical flow dynamics: modeling approaches for enhanced CCS safety, Energy 323 (2025) 135850, https://doi.org/10.1016/j.energy.2025.135850.

[76] H. Song, T. Wang, J. Qi, K. Jin, J. Liu, F. Li, F. Qiao, K. Zhao, B. Yin, J. Yu, Experimental study of the effect by double-stage throttling on the pressure relief characteristics of a large-scale CO_2 transportation pipeline, Energies 18 (2025) 1–21, https://doi.org/10.3390/en18133244.

[77] P. Mocellin, C. Vianello, G. Maschio, Hazard investigation of dry–ice bank induced risks related to rapid depressurization of CCS pipelines: analysis of different numerical modelling approaches, Int. J. Greenh. Gas Control 55 (2016) 82–96, https://doi.org/10.1016/j.ijggc.2016.11.004.

[78] P. Joshi, P. Bikkina, Q. Wang, Consequence analysis of accidental release of supercritical carbon dioxide from high pressure pipelines, Int. J. Greenh. Gas Control 55 (2016) 166–176, https://doi.org/10.1016/j.ijggc.2016.10.010.

[79] X. Liu, A. Godbole, C. Lu, G. Michal, V. Linton, Investigation of the consequence of high-pressure CO_2 pipeline failure through experimental and numerical studies, Appl. Energy 250 (2019) 32–47, https://doi.org/10.1016/j.apenergy.2019.05.017.

[80] W.H. Lee, A pressure iteration scheme for two-phase flow modelling, Multiph. Transp. Fundam. React. Safety, Appl. (1980) 407–431, https://doi.org/10.1017/9781316597392.007.

[81] R. Span, W. Wagner, A new equation of state for carbon dioxide covering the fluid region from the Triple-Point temperature to 1100 K at pressures up to 800 MPa, J. Phys. Chem. Ref. Data 25 (1996) 1509–1596.

[82] D.-Y. Peng, D.B. Robinson, A new two-constant equation of State, Ind. Eng. Chem. Fundam. 15 (1976) 59–64, https://doi.org/10.1021/i160057a011.

[83] D. Shao, Y. Yan, W. Zhang, S. Sun, C. Sun, L. Xu, Dynamic measurement of gas volume fraction in a CO_2 pipeline through capacitive sensing and data driven modelling, Int. J. Greenh. Gas Control 94 (2020) 102950, https://doi.org/10.1016/j.ijggc.2019.102950.

[84] A. Di Giuseppe, A.M. Gambelli, CO_2 storage in deep Oceanic sediments in the form of hydrates: energy evaluation and advantages related to the use of N_2-Containing mixtures, Energies 17 (2024), https://doi.org/10.3390/en17164102.

[85] X. Cao, H. Wang, K. Yang, S. Wu, Q. Chen, J. Bian, Hydrate-based CO_2 sequestration technology: feasibilities, mechanisms, influencing factors, and applications, J. Pet. Sci. Eng. 219 (2022) 111121, https://doi.org/10.1016/j.petrol.2022.111121.

[86] A. Oschlies, L.T. Bach, K. Fennel, J.P. Gattuso, N. Mengis, Perspectives and challenges of marine carbon dioxide removal, Front. Clim. 6 (2024) 1–15, https://doi.org/10.3389/fclim.2024.1506181.

[87] B. Chen, Q. Li, Y. Tan, Y. Zhang, T. Yu, J. Ma, Y. Zhong, X. Li, Caprock sealing integrity and key indicators of CO_2 geological storage considering the effect of hydraulic-mechanical coupling: x field in the Bohai Bay Basin, China, Eng. Geol. 342 (2024), https://doi.org/10.1016/j.enggeo.2024.107741.

[88] L. Skerbisch, D. Misch, M. Drews, K. Arnberger, V. Schuller, A. Zamolyi, T. Hantschel, D. Palmowski, A. Kleine, Caprock integrity: a critical factor for carbon capture and storage in the Vienna Basin, Int. J. Greenh. Gas Control 146 (2025) 104434, https://doi.org/10.1016/j.ijggc.2025.104434.

[89] H. Kim, V. Vilarrasa, R.Y. Makhnenko, Laboratory-Scale assessment of CO_2 sealing potential of heterogeneous caprock, Water Resour. Res. 61 (2025), https://doi.org/10.1029/2025WR040339.

[90] O.O. Blake, D.R. Faulkner, R.H. Worden, P.J. Armitage, A.A. Espie, Effect of thermal shock on the permeability and seismic wave velocity of the caprock and reservoir during CO_2 injection, Int. J. Greenh. Gas Control 118 (2022) 103691, https://doi.org/10.1016/j.ijggc.2022.103691.

[91] D. Polson, A. Curtis, C. Vivalda, The evolving perception of risk during reservoir evaluation projects for geological storage of CO_2, Int. J. Greenh. Gas Control 9 (2012) 10–23, https://doi.org/10.1016/j.ijggc.2012.02.010.

[92] J. Blackford, H. Stahl, J.M. Bull, B.J.P. Bergès, M. Cevatoglu, A. Lichtschlag, D. Connelly, R.H. James, J. Kita, D. Long, M. Naylor, K. Shitashima, D. Smith, P. Taylor, I. Wright, M. Akhurst, B. Chen, T.M. Gernon, C. Hauton, M. Hayashi, H. Kaieda, T.G. Leighton, T. Sato, M.D.J. Sayer, M. Suzumura, K. Tait, M.E. Vardy, P.R. White, S. Widdicombe, Detection and impacts of leakage from sub-seafloor deep geological carbon dioxide storage, Nat. Clim. Change 4 (2014) 1011–1016, https://doi.org/10.1038/nclimate2381.

[93] M. Andrew, B. Bijeljic, M.J. Blunt, Pore-scale imaging of trapped supercritical carbon dioxide in sandstones and carbonates, Int. J. Greenh. Gas Control 22 (2014) 1–14, https://doi.org/10.1016/j.ijggc.2013.12.018.

[94] J.K. Mitchell, R.A. Green, Some induced seismicity considerations in geo-energy resource development, Geomech. Energy Environ. 10 (2017) 3–11, https://doi.org/10.1016/j.gete.2017.01.001.

[95] P. Roy, J.P. Morris, S.D.C. Walsh, J. Iyer, S. Carroll, Effect of thermal stress on wellbore integrity during CO_2 injection, Int. J. Greenh. Gas Control 77 (2018) 14–26, https://doi.org/10.1016/j.ijggc.2018.07.012.

[96] L.B. Schemmer, G. dos S. Batista, J.J. de O. Andrade, E.M. da Costa, Testing the behavior of nanoalumina as a supplementary material to oil well cement pastes by different dispersive methods under CCS conditions, Geoenergy Sci. Eng. 224 (2023), https://doi.org/10.1016/j.geoen.2023.211602.

[97] Y. Cai, D. Yang, H. Lei, G. Feng, Influence of formation dip angle and injection strategy on CO_2 wellbore leakage with consideration of CO_2 transient flow and phase transition, Energy 330 (2025), https://doi.org/10.1016/j.energy.2025.136889.

[98] H. Li, J. Li, W. Lian, H. Zhang, J. Liu, Wellbore thermo-mechanical response during CO_2 mixture geological sequestration in depleted reservoirs, Geoenergy Sci. Eng. 257 (2026), https://doi.org/10.1016/j.geoen.2025.214244.

[99] F. Ahammad, S. Azadbakht, A comprehensive review of factors affecting wellbore integrity in CO_2 injection wells, Energy Geosci. 6 (2025), https://doi.org/10.1016/j.engeos.2025.100401.

[100] B. Pullen, A. Cahill, D. Arnold, Differentiating legacy wellbores in the scottish north sea using multi-criteria decision analysis with a view to minimising containment risk for carbon capture and storage, Int. J. Greenh. Gas Control 142 (2025) 104336, https://doi.org/10.1016/j.ijggc.2025.104336.

[101] K. Li, A.M.H. Pluymakers, Effects of thermal shocks on integrity of existing and newly-designed sealants for CCS applications, Int. J. Greenh. Gas Control 133 (2024), https://doi.org/10.1016/j.ijggc.2024.104103.

[102] J. Iyer, M.M. Smith, Impact of cement composition, brine concentration, diffusion rate, reaction rate and boundary condition on self-sealing predictions for cement-CO_2 systems, Int. J. Greenh. Gas Control 134 (2024) 104126, https://doi.org/10.1016/j.ijggc.2024.104126.

[103] K. Bishop, K.L. English, Policies and other factors influencing deployment of CO_2 geostorage: learnings from early mover nations in Europe, Int. J. Greenh. Gas Control 146 (2025) 104445, https://doi.org/10.1016/j.ijggc.2025.104445.

[104] G. Petho, D. Bason, S. De Morton, H. Nourollah, M. Watson, Shaping the future of MMV in CO_2 storage: a look at established and emerging technologies, Aust. Energy Prod. J. 65 (2025) EP24196, https://doi.org/10.1071/EP24196.

[105] Y. Kano, T. Sato, J. Kita, S. Hirabayashi, S. Tabeta, Multi-scale modeling of CO_2 dispersion leaked from seafloor off the Japanese coast, Mar. Pollut. Bull. 60 (2010) 215–224, https://doi.org/10.1016/j.marpolbul.2009.09.024.

[106] J.P. Nogues, B. Court, M. Dobossy, J.M. Nordbotten, M.A. Celia, A methodology to estimate maximum probable leakage along old wells in a geological sequestration operation, Int. J. Greenh. Gas Control 7 (2012) 39–47, https://doi.org/10.1016/j.ijggc.2011.12.003.

[107] K.J. Hsieh, F.S. Lien, E. Yee, Dense gas dispersion modeling of CO_2 released from carbon capture and storage infrastructure into a complex environment, Int. J. Greenh. Gas Control 17 (2013) 127–139, https://doi.org/10.1016/j.ijggc.2013.05.003.

[108] I.J. Duncan, H. Wang, Estimating the likelihood of pipeline failure in CO_2 transmission pipelines: new insights on risks of carbon capture and storage, Int. J.

Greenh. Gas Control 21 (2014) 49–60, https://doi.org/10.1016/j.ijggc.2013.11.005.
[109] X. Liu, A. Godbole, C. Lu, G. Michal, P. Venton, Source strength and dispersion of CO_2 releases from high-pressure pipelines: CFD model using real gas equation of state, Appl. Energy 126 (2014) 56–68, https://doi.org/10.1016/j.apenergy.2014.03.073.
[110] B. Liu, X. Liu, C. Lu, A. Godbole, G. Michal, A.K. Tieu, Computational fluid dynamics simulation of carbon dioxide dispersion in a complex environment, J. Loss Prev. Process. Ind. 40 (2016) 419–432, https://doi.org/10.1016/j.jlp.2016.01.017.
[111] B. Li, F. Zhou, H. Li, A. Duguid, L. Que, Y. Xue, Y. Tan, Prediction of CO_2 leakage risk for wells in carbon sequestration fields with an optimal artificial neural network, Int. J. Greenh. Gas Control 68 (2018) 276–286, https://doi.org/10.1016/j.ijggc.2017.11.004.
[112] S.E. Beaubien, G. Ciotoli, M.G. Finoia, S. Lombardi, S. Bigi, Monte Carlo simulations to assess the uncertainty of locating and quantifying CO_2 leakage flux from deep geological or anthropogenic sources, Stoch. Environ. Res. Risk Assess. 36 (2022) 609–627, https://doi.org/10.1007/s00477-021-02123-9.
[113] Z. Cao, Y. Hu, L. Chen, X. Yan, S. Yu, J. Yu, Experimental study of leakage characteristics and risk prediction of N_2-containing dense-phase CO_2 pipelines in real transportation conditions, Process Saf. Environ. Prot. 187 (2024) 1112–1125, https://doi.org/10.1016/j.psep.2024.05.045.
[114] I. Falcon-Suarez, G. Papageorgiou, A. Chadwick, L. North, A.I. Best, M. Chapman, CO_2-brine flow-through on an Utsira Sand core sample: experimental and modelling. Implications for the Sleipner storage field, Int. J. Greenh. Gas Control 68 (2018) 236–246, https://doi.org/10.1016/j.ijggc.2017.11.019.
[115] C. Sun, Y. Yan, W. Zhang, D. Shao, Measurement of CO_2 leakage from pipelines under CCS conditions through acoustic emission detection and data driven modeling, Meas. J. Int. Meas. Confed. 237 (2024), https://doi.org/10.1016/j.measurement.2024.115164.
[116] P. Taylor, H. Stahl, M.E. Vardy, J.M. Bull, M. Akhurst, C. Hauton, R.H. James, A. Lichtschlag, D. Long, D. Aleynik, M. Toberman, M. Naylor, D. Connelly, D. Smith, M.D.J. Sayer, S. Widdicombe, I.C. Wright, J. Blackford, A novel sub-seabed CO_2 release experiment informing monitoring and impact assessment for geological carbon storage, Int. J. Greenh. Gas Control 38 (2014) 3–17, https://doi.org/10.1016/j.ijggc.2014.09.007.
[117] H.K. Hvidevold, G. Alendal, T. Johannessen, A. Ali, T. Mannseth, H. Avlesen, Layout of CCS monitoring infrastructure with highest probability of detecting a footprint of a CO_2 leak in a varying marine environment, Int. J. Greenh. Gas Control 37 (2015) 274–279, https://doi.org/10.1016/j.ijggc.2015.03.013.
[118] B. Scoulding, R. Kloser, S. Gastauer, Evaluation of unmanned surface vehicle acoustics for gas seep detection in shallow coastal waters, Int. J. Greenh. Gas Control 102 (2020) 103158, https://doi.org/10.1016/j.ijggc.2020.103158.
[119] V.R. Vermeul, J.E. Amonette, C.E. Strickland, M.D. Williams, A. Bonneville, An overview of the monitoring program design for the FutureGen 2.0 CO_2 storage site, Int. J. Greenh. Gas Control 51 (2016) 193–206, https://doi.org/10.1016/j.ijggc.2016.05.023.
[120] I.F. Schroder, H. Zhang, C. Zhang, A.J. Feitz, The role of soil flux and soil gas monitoring in the characterisation of a CO_2 surface leak: a case study in Qinghai, China, Int. J. Greenh. Gas Control 54 (2016) 84–95, https://doi.org/10.1016/j.ijggc.2016.07.030.
[121] H. Shao, D.A.N. Ussiri, C.G. Patterson, R.A. Locke, H. Wang, A.H. Taylor, H. F. Cohen, Soil gas monitoring at the Illinois Basin – decatur Project carbon sequestration site, Int. J. Greenh. Gas Control 86 (2019) 112–124, https://doi.org/10.1016/j.ijggc.2019.04.012.
[122] J.E. Amonette, L. Zhong, T.H. Darrah, B.S. Grove, D.R. Cole, Noble and major gases released from rock core materials as intrinsic tracers for detecting carbon dioxide leakage – laboratory evaluation, Int. J. Greenh. Gas Control 89 (2019) 76–88, https://doi.org/10.1016/j.ijggc.2019.05.010.
[123] S.M.V. Gilfillan, M. Wilkinson, R.S. Haszeldine, Z.K. Shipton, S.T. Nelson, R. J. Poreda, He and Ne as tracers of natural CO_2 migration up a fault from a deep reservoir, Int. J. Greenh. Gas Control 5 (2011) 1507–1516, https://doi.org/10.1016/j.ijggc.2011.08.008.
[124] D. Györe, F.M. Stuart, S.M.V. Gilfillan, S. Waldron, Tracing injected CO_2 in the Cranfield enhanced oil recovery field (MS, USA) using He, Ne and Ar isotopes, Int. J. Greenh. Gas Control 42 (2015) 554–561, https://doi.org/10.1016/j.ijggc.2015.09.009.
[125] U.W. Weber, N. Kampman, A. Sundal, Techno-economic aspects of noble gases as monitoring tracers, Energies 14 (2021), https://doi.org/10.3390/en14123433.
[126] Y.J. Ju, S.M.V. Gilfillan, S.S. Lee, D. Kaown, D. Hahm, S. Lee, I.W. Park, S.W. Ha, K. Park, H.K. Do, S.T. Yun, K.K. Lee, Application of noble gas tracers to identify the retention mechanisms of CO_2 migrated from a deep reservoir into shallow groundwater, Int. J. Greenh. Gas Control 97 (2020), https://doi.org/10.1016/j.ijggc.2020.103041.
[127] J.J. Roberts, S.M.V. Gilfillan, L. Stalker, M. Naylor, Geochemical tracers for monitoring offshore CO_2 stores, Int. J. Greenh. Gas Control 65 (2017) 218–234, https://doi.org/10.1016/j.ijggc.2017.07.021.
[128] A. Flohr, J.M. Matter, R.H. James, K. Saw, R. Brown, J. Gros, S. Flude, C. Day, K. Peel, D. Connelly, C.R. Pearce, J.A. Strong, A. Lichtschlag, D.J. Hillegonds, C. J. Ballentine, R.L. Tyne, Utility of natural and artificial geochemical tracers for leakage monitoring and quantification during an offshore controlled CO_2 release experiment, Int. J. Greenh. Gas Control 111 (2021), https://doi.org/10.1016/j.ijggc.2021.103421.
[129] U.W. Weber, R. Kipfer, E. Horstmann, P. Ringrose, N. Kampman, Y. Tomonaga, M. S. Brennwald, A. Sundal, Noble gas tracers in gas streams at Norwegian CO_2 capture plants, Int. J. Greenh. Gas Control 106 (2021) 103238, https://doi.org/10.1016/j.ijggc.2020.103238.
[130] C. Jenkins, T. Kuske, S. Zegelin, Simple and effective atmospheric monitoring for CO_2 leakage, Int. J. Greenh. Gas Control 46 (2016) 158–174, https://doi.org/10.1016/j.ijggc.2016.01.001.
[131] S.M.V. Gilfillan, G.W. Sherk, R.J. Poreda, R.S. Haszeldine, Using noble gas fingerprints at the Kerr Farm to assess CO_2 leakage allegations linked to the Weyburn-Midale CO_2 monitoring and storage project, Int. J. Greenh. Gas Control 63 (2017) 215–225, https://doi.org/10.1016/j.ijggc.2017.05.015.
[132] J.C. Turnbull, E.D. Keller, M.W. Norris, R.M. Wiltshire, Atmospheric monitoring of carbon capture and storage leakage using radiocarbon, Int. J. Greenh. Gas Control 56 (2017) 93–101, https://doi.org/10.1016/j.ijggc.2016.11.017.
[133] A.A. Pratama, A.R. Prabowo, T. Muttaqie, N. Muhayat, R. Ridwan, B. Cao, F. B. Laksono, Hollow tube structures subjected to compressive loading: implementation of the pitting corrosion effect in nonlinear FE analysis, J. Brazilian Soc. Mech. Sci. Eng. 45 (2023) 1–23, https://doi.org/10.1007/s40430-023-04067-3.
[134] D.P. Islami, R. Adiputra, A.R. Prabowo, S. Ehlers, M. Braun, M. Jurkovič, B. F. Riyalda, W. Wibowo, Effects of crevice corrosion induced by biofouling on the mechanical response of engineered plate designs as an idealization of naval and marine structures, Ocean. Eng. 340 (2025) 122406, https://doi.org/10.1016/j.oceaneng.2025.122406.
[135] M. Vitali, C. Zuliani, F. Corvaro, B. Marchetti, F. Tallone, Statistical analysis of incidents on onshore CO_2 pipelines based on PHMSA database, J. Loss Prev. Process. Ind. 77 (2022), https://doi.org/10.1016/j.jlp.2022.104799.
[136] D. Xi, H. Lu, Y. Fu, S. Dong, X. Jiang, J. Matthews, Carbon dioxide pipelines: a statistical analysis of historical accidents, J. Loss Prev. Process. Ind. 84 (2023), https://doi.org/10.1016/j.jlp.2023.105129.
[137] A. Pfennig, A. Kranzmann, Reliability of pipe steels with different amounts of C and Cr during onshore carbon dioxide injection, Int. J. Greenh. Gas Control 5 (2011) 757–769, https://doi.org/10.1016/j.ijggc.2011.03.006.
[138] A. Pfennig, W. Mohring, M. Wolf, The insignificant improvement of corrosion and corrosion fatigue behavior in geothermal environment applying boehmit coatings on high alloyed steels, Appl. Sci. 14 (2024), https://doi.org/10.3390/app14041575.
[139] Y. Tang, X.P. Guo, G.A. Zhang, Corrosion behaviour of X65 carbon steel in supercritical-CO_2 containing H_2O and O_2 in carbon capture and storage (CCS) technology, Corros. Sci. 118 (2017) 118–128, https://doi.org/10.1016/j.corsci.2017.01.028.
[140] Y. Huang, X. Wang, K. Lu, J. Hu, Carbon steel pipeline CO_2 erosion-corrosion damage prediction model and numerical simulation research, Geoenergy Sci. Eng. 246 (2025) 213558, https://doi.org/10.1016/j.geoen.2024.213558.
[141] P.P. Wu, G.L. Song, Y.X. Zhu, Y.J. Deng, D.J. Zheng, An intelligent Mg anode for protection of the concrete-covered steel tubing in carbon capture and storage, Compos. Part B Eng. 243 (2022), https://doi.org/10.1016/j.compositesb.2022.110165.
[142] Y. Sun, S. Yuan, Z. Bai, B. Liang, D. Fu, H. Hu, L. Pei, R. Wang, Y. Zhu, H. Wang, A unique anti-corrosion composite coating with CO_2 gas barrier and acid resistance suitable for CCUS environment, Chem. Eng. J. 472 (2023), https://doi.org/10.1016/j.cej.2023.144879.
[143] C. Li, Z. Liu, F. Huang, J. Dong, C. Wang, J. Yuan, Q. Fu, Experimental study of corrosion resistance of 431M2 stainless steel coatings in a CO_2-saturated NaCl solution deposited by extreme high-speed laser cladding, Mater. Today Commun. 38 (2024), https://doi.org/10.1016/j.mtcomm.2024.108202.
[144] T. Gu, X. Guo, Z. Li, X. Cheng, X. Fan, A. Korayem, W.H. Duan, Coupled effect of CO_2 attack and tensile stress on well cement under CO_2 storage conditions, Constr. Build. Mater. 130 (2017) 92–102, https://doi.org/10.1016/j.conbuildmat.2016.10.117.
[145] M.C.M. Nasvi, P.G. Ranjith, J. Sanjayan, A. Haque, Sub- and super-critical carbon dioxide permeability of wellbore materials under geological sequestration conditions: an experimental study, Energy 54 (2013) 231–239, https://doi.org/10.1016/j.energy.2013.01.049.
[146] M.H. Ozyurtkan, M. Radonjic, An experimental study of the effect of CO_2 rich brine on artificially fractured well-cement, Cem. Concr. Compos. 45 (2014) 201–208, https://doi.org/10.1016/j.cemconcomp.2013.10.007.
[147] G.G.D. Ponzi, V.H.J.M. dos Santos, R.B. Martel, D. Pontin, A.S. de G.e. Stepanha, M.K. Schütz, S.C. Menezes, S.M.O. Einloft, F.D. Vecchia, Basalt powder as a supplementary cementitious material in cement paste for CCS wells: chemical and mechanical resistance of cement formulations for CO_2 geological storage sites, Int. J. Greenh. Gas Control 109 (2021) 103337, https://doi.org/10.1016/j.ijggc.2021.103337.
[148] G. Zheng, J. Sun, X. Guo, Z. Li, Research on the relationship between pore structure and the compressive strength of oil-well cement, Energies 16 (2023) 1–18, https://doi.org/10.3390/en16155650.
[149] S. Roussanaly, A. Aasen, R. Anantharaman, B. Danielsen, J. Jakobsen, L. Heme-De-Lacotte, G. Neji, A. Sødal, P.E. Wahl, T.K. Vrana, R. Dreux, Offshore power generation with carbon capture and storage to decarbonise mainland electricity and offshore oil and gas installations: a techno-economic analysis, Appl. Energy 233–234 (2019) 478–494, https://doi.org/10.1016/j.apenergy.2018.10.020.
[150] J. Beiron, F. Normann, F. Johnsson, A techno-economic assessment of CO_2 capture in biomass and waste-fired combined heat and power plants – a Swedish case study, Int. J. Greenh. Gas Control 118 (2022), https://doi.org/10.1016/j.ijggc.2022.103684.
[151] K.A. Titus, D. Dempsey, R.A.M. Peer, R. Archer, Techno-economic analysis of geothermal combined with direct and biomass-based carbon dioxide removal for

high-temperature hydrothermal systems, Geothermics 125 (2025), https://doi.org/10.1016/j.geothermics.2024.103159.
[152] W. Zhou, W. Fan, R. Lan, W. Su, J.L. Fan, Retrofitted CCS technologies enhance economy, security, and equity in achieving carbon zero in power sector, Appl. Energy 378 (2025), https://doi.org/10.1016/j.apenergy.2024.124803.
[153] J. Jakobsen, S. Roussanaly, R. Anantharaman, A techno-economic case study of CO_2 capture, transport and storage chain from a cement plant in Norway, J. Clean. Prod. 144 (2017) 523–539, https://doi.org/10.1016/j.jclepro.2016.12.120.
[154] T.T. Kashyap, R. Sharma, D. Paul, R. Hiremath, Techno-economic feasibility of CO_2 utilization for production of green urea by Indian cement industries, J. Clean. Prod. 476 (2024), https://doi.org/10.1016/j.jclepro.2024.143799.
[155] G. Skaugen, S. Roussanaly, J. Jakobsen, A. Brunsvold, Techno-economic evaluation of the effects of impurities on conditioning and transport of CO_2 by pipeline, Int. J. Greenh. Gas Control 54 (2016) 627–639, https://doi.org/10.1016/j.ijggc.2016.07.025.
[156] S. Roussanaly, G. Skaugen, A. Aasen, J. Jakobsen, L. Vesely, Techno-economic evaluation of CO_2 transport from a lignite-fired IGCC plant in the Czech Republic, Int. J. Greenh. Gas Control 65 (2017) 235–250, https://doi.org/10.1016/j.ijggc.2017.08.022.